Towards therapy for Batten disease

Mariana Catanho da Silva Vieira

MRC Laboratory for Molecular Cell Biology
University College London
PhD Supervisor: Dr Sara E Mole

A thesis submitted for the degree of
Doctor of Philosophy
University College London

September 2014

Declaration

I, Mariana Catanho da Silva Vieira, confirm that the work presented in this thesis is my own. Where information has been derived from other sources, I confirm that this has been indicated in the thesis.

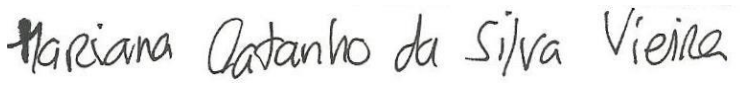

Abstract

The gene underlying the classic neurodegenerative lysosomal storage disorder (LSD) juvenile neuronal ceroid lipofuscinosis (JNCL) in humans, *CLN3*, encodes a polytopic membrane spanning protein of unknown function. Several studies using simpler models have been performed in order to further understand this protein and its pathological mechanism. *Schizosaccharomyces pombe* provides an ideal model organism for the study of CLN3 function, due to its simplicity, genetic tractability and the presence of a single orthologue of CLN3 (Btn1p), which exhibits a functional profile comparable to its human counterpart. In this study, this model was used to explore the effect of different mutations in *btn1* as well as phenotypes arising from complete deletion of the gene. Different *btn1* mutations have different effects on the protein function, underlining different phenotypes and affecting the levels of expression of Btn1p. So far, there is no cure for JNCL and therefore it is of great importance to identify novel lead compounds that can be developed for disease therapy. To identify these compounds, a drug screen with *btn1*Δ cells based on their sensitivity to cyclosporine A, was developed. Positive hits from the screen were validated and tested for their ability to rescue other specific phenotypes also associated with the loss of *btn1.* The same hits were also tested in JNCL patient fibroblasts and in a zebrafish model of the disease. Promising results were obtained for three compounds: alloxazine, prochlorperazine dimaleate and E-64, with the latest being the one with the most potential for developing therapeutic tools. Yeast models for other LSDs (Chédiak Higashi Syndrome, Niemann-Pick disease type C2 and congenital CLN10 disease) were also characterised in terms of cellular phenotypes and the compounds described above were also tested in these models. Overlapping phenotypes were observed on all the yeast models, suggesting at least one common pathway between these LSDs.

Acknowledgement

Firstly, I would like to thank my supervisor Dr Sara Mole for her continuous support and encouragement during this project. Secondly, I am very grateful for all the help other members of the lab gave me throughout: Dr Mike Bond, Davide Marotta, Rachel Brown, Sophia kleine-Holthaus and Varun Warrier; for all their moral support, coffee breaks, and post-work time. I would also like to thank my PhD committee for their guidance: Julie Pitcher, Jürg Bähler and Robin Ketteler. I am very grateful to all the work that was done by Dr Claire Russell and Dr Jamie Freeman, that was crucial to my project; all the support from the UCL Yeast Club, specially Rob de Bruin's and Jürg Bähler's lab, from the NCL community; and all the work of the support staff at the Laboratory for Molecular Cell Biology (LMCB), from the reception girls to the light microscopy unit.

I am very grateful to the entities that helped by funding my project: the NCL-Stiftung foundation (specially Frank Stehr, who was always very helpful), the BDFA association and the Medical Research Council.

I am incredibly grateful to my parents Ricardo and Carmo, my sisters Francisca and Mafalda, and the rest of my family (grandparents, uncles, aunts and cousins) for all their encouraging words and warm embraces. My friends have been very supporting and present through the good and bad moments, and for that I thank them. Finally, I want to thank my other half, Filipe, for that without him this journey would never be possible!

Table of contents

Table of figures

List of tables

Abbreviations

$5\text{-}HT_3$ - 5-hydroxytryptamine$_3$
ACh - acetylcholine
Ala – alanine
ANCL - adult neuronal ceroid lipofuscinosis
ANP - D-(-)-threo-2-amino-1-[p-nitrophenyl]-1,3-propanediol
(s)APP – (soluble) amyloid precursor protein
ATP – adenosine triphosphate
bp – base pairs
BSA – bovine serum albumin
CHS – Chédiak-Higashi syndrome
CI-MPR - cation-independent mannose 6-phosphate receptor
Cpy - carboxypeptidase Y
CsA – cyclosporine A
CSPα - cysteine-string protein α
DMEM - Dulbecco's modified eagle's medium
DMSO – dimethyl sulfoxide
DNA – deoxyribonucleic acid
dNTP – deoxyribonucleotide
E-64 - L-trans-Epoxysuccinyl-leucylamido(4-guanidino)butane
EDTA - ethylenediamine tetraacetic acid
EM – electron microscope
EPMR - epilepsy with mental retardation
ER – endoplasmic reticulum
FBS – foetal bovine serum
FDA – food and drug administration
FM4-64 - N-(3-triethylammoniumpropyl)-4-(6-(4-(diethylamino) phenyl) hexatrienyl) pyridinium dibromide
FOA – 5-fluoroorotic acid
G418 – geneticin
GDNF - glial cell line-derived neurotrophic factor

GFP – green fluorescent protein

Glu - glutamic acid

Gly – glycine

GROD(s) – granular osmiophilic deposit(s)

GTP – guanosine-5’-triphosphate

(dd) H_2O – (double distilled) water

Hoechst - bisBenzimide H33342 trihydrochloride

Hpf – hours post fertilization

JNCL – juvenile neuronal ceroid lipofuscinosis (or juvenile CLN3 disease)

JNK - jun N-terminal kinase

kan – kanamycin

LB - lysogeny broth

(c) (v) LINCL – (classic) (variant) late infantile neuronal ceroid lipofuscinosis

LMCB – Laboratory for Molecular Cell Biology

LoPac - library of pharmacologically active compounds

LSD(s) – lysosomal storage disorder(s)

Lys – lysine

LYST - lysosomal trafficking regulator protein

MFS(D8) - major facilitator superfamily (domain containing 8)

MM – minimal medium

NCL – neuronal ceroid lipofuscinosis

NECA - N-ethyl carboxamidoadenosine

NPC – Niemann-Pick disease type C

OD – optic density

ORF – open reading frame

rpm – rotations per minute

PBS – phosphate buffered saline

PCR – polymerase chain reaction

PEG – polyethylene glycol

PenStrep - Penicillin streptomycin

PFA - paraformaldehyde

PPT1 - palmitoyl-protein thiosterase 1

(si)RNA – (small interfering) ribonucleic acid

ROS – reactive oxygen species

SEM – standard error of the mean

TGN – trans-Golgi network

(m)TOR(C) – (mammalian) target of rapamycin (complex)

Ura – uracil

UTR – untranslated region

YE(S) - yeast extract (with supplements)

v-ATPase – vacuolar adenosine triphosphate ase complex

vps – vacuolar protein sorting

wt – wild-type

1 Introduction

Juvenile CLN3 disease is one type of a group of diseases known as the neuronal ceroid lipofuscinosis (NCL), and is caused by mutations in the *CLN3* gene. *CLN3* encodes a polytopic membrane spanning protein of unknown function. It is conserved and all evidence obtained so far suggests the same function in simple yeast as in human cells. Work done in fission yeast has shown that complete loss of the CLN3 orthologue, Btn1p, has multiple effects within the cell. Current therapeutic strategies for other types of NCL caused by enzyme defects are not applicable to juvenile CLN3 disease (JNCL), and new strategies or tools are urgently required for treatment of this disease.

This first chapter consists of an introductory description of different topics that are relevant for a better understanding of this project. First an overview of the lysosomal storage disorders (LSDs) group is presented, including a more detailed description of all types of NCL, particularly juvenile CLN3 disease. Descriptions of two other LSDs (Chédiak-Higashi Syndrome and Niemann Pick type C disease) are also included. Second, all previous work that has been done with fission yeast and the CLN3 orthologue, Btn1p, will be described. Last, the aims of this project will be presented.

1.1 Lysosomal storage disorders

In simple terms, lysosomal storage disorders (LSDs) are rare monogenic diseases characterised by biological defects that lead to the accumulation of unmetabolised compounds in lysosomes. Until the present date, 70 disorders have been identified as part of this group, with a collective prevalence varying between 1 in 5000 and 1 in 1000 live births (Aerts *et al.* 2011). Most LSDs are inborn errors of metabolism that originate from a defective catabolism and consequent intralysosomal accumulation of endogenous undegraded molecules. The majority of LSDs results from loss of activity of a lysosomal catabolic enzyme, which may be related to a defective protein synthesis or folding, enzyme activation or membrane protein defects (Jeyakumar *et al.* 2005). Niemman Pick type C and several NCL, among others, fall into this latter category. However, the broad clinical spectrum of LSDs are clearly not simply an effect of the intralysosomal compound storage, but a consequence of defects in signalling pathways that affect the cell far beyond the lysosome, both structurally and biochemically (Vellodi 2005). This is becoming more apparent as the lysosome is no longer considered to be a waste recycling centre but play a central role in several cellular functions such as energy metabolism, lipid homeostasis, membrane repair and defence against pathogens, among others (Settembre *et al.* 2012). The pathophysiology of LSDs varies between the different disorders depending on the underlying defect, the type of storage compound and how this storage affects the cell metabolism (Gieselmann 2006). The majority of affected individuals with any type of LSD often show abnormalities at a neurological level that can lead to neurodegeneration (Walkley 1998).

1.1.1 Neuronal ceroid lipofuscinosis

The neuronal ceroid lipofuscinosis (NCL) are neurodegenerative disorders grouped together on a clinical basis, with onset usually in childhood (Mole *et al.* 1999). Children with NCL can start manifesting symptoms at any age, even before birth. The order of onset of the symptoms varies between the different types of NCL, but the main symptoms are common to all types. These include seizures and blindness, as well as progressive decline of cognitive and motor functions, eventually leading to a premature death.

NCL are the most common of this type of diseases, with an incidence that can be as high as 7 in 100,000 births in some countries (Kyttälä *et al.* 2006). NCL are characterised by accumulation of autofluorescent ceroid and lipofuscin-like pigments in lysosomes. The ceroid pigment accumulates in disease, particularly in diseases caused by lysosomal dysfunction (Sulzer *et al.* 2008), whereas lipofuscin is an age-associated pigment that accumulates in the brains of all individuals as they get older, but in NCL cases this accumulation occurs much earlier (Seehafer & Pearce 2006). This storage material is not an obvious result of a defect in a single catabolic step. The major protein component of the storage material varies according to the NCL type, but in the majority of cases it is the subunit c of mitochondrial adenosine triphosphate (ATP) synthase (Haltia 2006). This storage material has a characteristic pattern when examined under the electron microscope (EM), which varies according to the type of NCL (e.g. a fingerprint-like pattern for juvenile CLN3 disease). Most patient cells show this accumulation, but characteristically this leads to death only in neurons. The reason why this happens is unknown, however it is thought that this is due to the increased energy and metabolism requirements of neurons, which may make them more sensitive to the accumulated material or other underlying molecular defects (Goebel & Lake 1998).

There are many types of NCL, traditionally classified according to the age of onset and the order of appearance of clinical symptoms, but recently modified according to the underlying genetic defect (Mole *et al.* 2011). The term Batten disease can be used to describe all forms of NCL, or more specifically, the

juvenile type. A brief description of each NCL is included below, and a table summarising all of these types is also presented (Table 1.1).

Congenital CLN10 disease

The congenital form of NCL, known as congenital CLN10 disease, is the most aggressive form of all NCLs and the one with the earliest onset. This disease was firstly identified in 1941 (Norman & Wood 1941) and has been described in 11 patients to date. CLN10 disease is a very rare form of NCL although many cases may be undiagnosed due to spontaneous abortions and stillborn unviable foetuses (Anderson *et al.* 2013). This disease is caused by at least seven different mutations in the *CTSD* gene, which encodes for cathepsin D (Warrier *et al.* 2013). Cathepsin D is a lysosomal protease of the pepsin family (Rawlings & Barrett 1995) that is involved in several biological processes such as apoptosis, cell invasion, proteolytic degradation and other brain biological functions such as aging or even homeostasis of neuronal structures (Koike *et al.* 2000; Steinfeld *et al.* 2006). It is suggested that the neuronal death seen in this form of NCL occurs due to defects in the macroautophagy-lysosomal degradation pathway (Kohan *et al.* 2011). More interestingly, CLN3 has been suggested to affect the transport and proteolytic maturation of cathepsin D, due to its effect on vesicular trafficking and in lysosomal pH, respectively (Golabek *et al.* 2000; Fossale *et al.* 2004). This establishes a link between these two proteins.

The protein constituents of the storage material in CLN10 disease are mainly saposins A and D, and the material has a granular ultrastructure resembling granular osmiophilic deposits (GRODs). Individuals with congenital onset show different phenotypes, such as microcephaly at time of birth, cerebral and cerebellar atrophy, seizures, spasticity, low set ears and broad nasal bridge in some cases, and have postnatal respiratory insufficiency, leading to death within hours to weeks after birth (Siintola *et al.* 2006). Missense mutations in *CTSD* can also cause a NCL disease with later ages of onset, where affected

individuals have a normal early development but start to manifest ataxia and visual defects in early childhood, with a progressive decline that will eventually lead to loss of psychomotor functions and death (Steinfeld *et al.* 2006). In these cases there is an evident reduction of the proteolytic activity of cathepsin D, and the amount of protein present in the cells is markedly reduced. It is therefore proposed that the level of residual enzyme activity in individuals with *CTSD* mutations is critical for the clinical manifestation of the CLN10 disease

Mutations in the cathepsin D gene are also present in other animals, where phenotypes associated with the CLN10 disease are evident: sheep, mice and fruit fly (*Drosophila melanogaster*) (Koike *et al.* 2000; Tyynelä *et al.* 2000; Myllykangas *et al.* 2005). The *CTSD* gene is also conserved in fission yeast (see below, section 1.2.2).

Infantile CLN1 disease

The gene underlying infantile CLN1 disease, *PPT1* (or *CLN1*) encodes for the palmitoyl-protein thiosterase protein (PPT1) and was identified in 1995 (Vesa *et al.* 1995). In individuals with the mutated gene, there is no detectable enzyme activity in the brain. PPT1 removes thioester-linked fatty acids from cysteine residues in proteins and facilitates their degradation and/or recycling in the lysosome (Das *et al.* 1998). Therefore cysteine-containing fatty acyl thioesters accumulate intracellularly in cells with defective PPT1. PPT1 has been associated with different cellular functions: cholesterol metabolism, neuronal maturation, calcium homeostasis, endocytosis, among other, and it also has an antiapoptotic effect by decreasing the rate of activation of Ras oncogenes (Cho & Dawson 2000; Ahtiainen *et al.* 2006; Ahtiainen *et al.* 2007). The neurodegeneration that occurs in the cases of infantile CLN1 disease was reported as being a result of neuronal apoptosis via endoplasmic reticulum (ER) stress-induced caspase-12 activation and high production of reactive oxygen species (ROS) (Kim *et al.* 2006). The *PPT1* gene is conserved in many eukaryotic species, such as *Caenorhabditis elegans*, *D. melanogaster* and

Schizosaccharomyces pombe (Korey & MacDonald 2003; Cho & Hofmann 2004; Porter *et al.* 2005).

Classic infantile CLN1 disease is a rare disorder, with an incidence of 1 in 100 000 births, but it is a devastating condition (Haltia *et al.* 1973). Symptoms appear before the age of 18 months and include: cerebellar atrophy, microcephaly, ataxia, blindness, seizures, frequent convulsions and a progressive psychomotor deterioration that starts at about 1 year of age. By 3 years of age they are diagnosed with brain death, which persists until death between 10-14 years of age (Haltia *et al.* 1973; Santavuori *et al.* 1973). Histologically, the storage material is similar to that of congenital CLN10 disease, with a GROD-like characteristic pattern and composition of mainly saposins A and D (Tyynelä *et al.* 1993).

Nonsense biallelic mutations in the *CLN1* gene result in infantile CLN1 disease; however, other type of mutations in this gene can cause forms of NCL with later onset. For instance, heterozygous mutations in the *PPT1* gene were reported to underlie a type of NCL clinically consistent with juvenile NCL but with an ultrastructural profile similar to the infantile form, granular deposits consisted of saposins (Mitchison *et al.* 1998; Kalviainen *et al.* 2007). Furthermore, some missense mutations in the *PPT1* gene result in phenotypes clinically similar to the late infantile and juvenile forms of NCL, with disease onset at 2-4 years and after 5 years of age, respectively. However, the storage material observed in these cases is once again GROD-like (Das *et al.* 1998). PPT1 deficiency can also be associated with adult-onset NCL where symptoms start occurring as late as in the third decade of life of the patients (van Diggelen *et al.* 2001; Ramadan *et al.* 2007). It is suggested that if there is sufficient enzyme function, even at low levels, this is enough to ameliorate the NCL phenotype and delay the onset of the disease. These findings are supportive for a therapeutic strategy that includes enzyme replacement therapy. In fact, recent work in *PPT1* knockout mice injected from birth with purified recombinant PPT1 showed that the treatment was well tolerated and resulted in significant improvements in survival, motor performance and brain pathology of the mice (Hu *et al.* 2012).

Late infantile NCL

There are different forms of late infantile NCL (LINCL), according to the gene that underlies the disease: *CLN2*, *CLN5*, *CLN6*, *CLN7* or *CLN8*.

Classic late infantile NCL (cLINCL, CLN2 disease) is caused by mutations in the *CLN2* gene (also known as tripeptidyl peptidase 1*, or TPP1*) (Sleat *et al.* 1997). TPP1 is a lysosomal peptidase, and mutations in the encoding gene lead to its retention in the ER and posterior degradation (Steinfeld *et al.* 2004). It is also thought that TPP1 may play a fundamental role in the degradation of subunit c of the mitochondrial ATP synthase, which accumulates in cLINCL as curvilinear bodies (Ezaki *et al.* 2000). The onset of symptoms in classic CLN2 disease is between 2 and 4 years of age, and death of patients occurs between 7 and 15 years of age (Sleat *et al.* 2008). Individuals show several symptoms, such as: speech impediments, epilepsy, mental deterioration and ataxia, followed by loss of vision and motor functions by the age of 10 years (Steinfeld *et al.* 2002). Mutations in *CLN2* have on occasions also caused infantile NCL with an earlier onset before the first year of age, or more commonly a protracted form, with a juvenile age of onset (Ju *et al.* 2002; Bessa *et al.* 2008).

A second type of LINCL is CLN5 disease, previously known as Finnish variant LINCL (vLINCL), and is caused by mutations in the *CLN5* gene (Savukoski *et al.* 1998). This gene encodes a lysosomal glycoprotein of unknown function which traffics through the ER and Golgi apparatus to the lysosomes, and although originally reported as a membrane associated form, is now thought to be soluble (Isosomppi *et al.* 2002; Vesa *et al.* 2002; Larkin *et al.* 2013). When mutated, the CLN5 protein may not traffic to lysosomes (Schmiedt *et al.* 2010). CLN5 was also shown to interact directly with two other NCL proteins, TPP1 and CLN3 (Vesa *et al.* 2002). In CLN5 disease, patients start manifesting symptoms at a slightly later age than in CLN2 disease (between 4 and 7 years of age) and the survival time is longer (up to 30 years of age) (Santavuori 1982; Moore *et al.* 2008). Symptoms vary between motor clumsiness, mental retardation, progressive visual failure, ataxia and myoclonic seizures (Savukoski *et al.* 1998). CLN5 disease patients can have mixed ultrastructural

patterns of inclusions: curvilinear, fingerprint and rectilinear; all containing subunit c of ATP synthase (Moore *et al.* 2008; Xin *et al.* 2010). Late infantile CLN5 disease is also manifested by Border Collie dogs (Melville *et al.* 2005). Certain mutations in *CLN5* have been reported to underlie later forms of NCL, such as juvenile and adult forms (Sleat *et al.* 2009; Xin *et al.* 2010).

Another variant form of LINCL is CLN6 disease, once known as Lake-Cavanagh disease. This type is caused by mutations in the *CLN6* gene, which encodes a putative transmembrane protein that localises to the ER (Gao *et al.* 2002; Wheeler *et al.* 2002; Mole *et al.* 2004). *CLN6* is highly conserved across vertebrates, with a orthologue in mice and in sheep (Broom & Zhou 2001; Gao *et al.* 2002; Tammen *et al.* 2006). Variant late infantile CLN6 disease is characterised by storage bodies containing subunit c of ATP synthase that can adopt a curvilinear, rectilinear or fingerprint profile (Moore *et al.* 2008). The disease course is similar to cLINCL; however, patients start manifesting symptoms slightly later, at 5 to 7 years of age, and survive until their second decade of life (Siintola *et al.* 2005; Moore *et al.* 2008). Symptoms include seizures and motor impairments in an early stage, and loss of vision later.

A third type of LINCL, late infantile CLN7 disease, was first recognised in Turkish patients (Topçu *et al.* 2004). This variant form is caused by mutations in the major facilitator superfamily domain containing 8 (*MFSD8* or *CLN7*) gene, which encodes a polytopic membrane protein with 12 membrane-spanning domains that is mainly localised in the lysosomes. MFSD8 belongs to a transporter superfamily and is conserved in vertebrates (Siintola *et al.* 2007). Compared to the classic form of CLN2 disease, patients with this variant show a slower but more severe course of the disease, with a higher frequency of seizures accompanied by a cerebral and cerebellar atrophy (Aiello *et al.* 2009). Other symptoms include motor impairment, ataxia, seizures and developmental regression (Topçu *et al.* 2004). Mutations in *CLN7* can also underlie juvenile NCL (Kousi *et al.* 2009).

The *CLN8* gene was initially identified as the gene underlying progressive epilepsy with mental retardation (EPMR) (Ranta *et al.* 1999). It is now known

that EPMR (or Northern epilepsy) is a form of LINCL (more specifically a mutation-specific phenotype) with a more protracted course. The age of onset is between 5 and 10 years of age, when patients start manifesting seizures followed by a slow deterioration of mental capacities (Herva *et al.* 2000). Other mutations cause a more typical late infantile CLN8 disease. EM studies show that the storage bodies contain subunit c of ATP synthase and can have a fingerprint, curvilinear or rectilinear ultrastructural profile (Allen *et al.* 2012). CLN8 is a predicted transmembrane protein, which is located in the ER and traffics between the ER and the ER-Golgi intermediate compartments (Lonka *et al.* 2000). The function of CLN8 remains elusive but it has been associated with an indirect role of in protecting neurons from damage (Vantaggiato *et al.* 2009). Furthermore, a mutation in *CLN8* underlies a NCL-like phenotype in English Setter dogs (Katz *et al.* 2005).

Adult NCL

The basis of adult-onset NCL is quite complex, since genes with different effects on the disease phenotype have been identified, all leading to an adult onset form of NCL (or ANCL). In general, the term adult NCL comprises a group of rare and genetically heterogeneous disorders with disease onset varying from 10 to 50 years of age (Berkovic *et al.* 1988). There are cases of ANCL where the genetic cause is still unknown.

The form entitled adult CLN6 disease (or Kufs disease type A) is an autosomal recessive disease caused by mild mutations in the *CLN6* gene, the same gene that is associated with disease onset in late infancy (Arsov *et al.* 2011). This form of NCL is characterised by progressive myoclonic epilepsy and ataxia, which start around the third decade of life, and no retinal degeneration (Berkovic *et al.* 1988). Storage material is mainly located in the neurons and can have three different profiles: fingerprint, rectilinear and GROD-like (Burneo *et al.* 2003).

Kufs type B disease is another type of ANCL. This type of Kufs disease differs from type A because it is mainly characterised by dementia, cerebellar signs, several motor deficiencies and behavioural disturbances, rather than epilepsy (Burneo *et al.* 2003). One gene, underlying the adult CLN13 disease, *CTSF* (or *CLN13*), was recently identified in some of these cases. *CTSF* encodes cathepsin F, a lysosomal protease (Smith *et al.* 2013).

Another form of ANCL is known as adult CLN4 disease or Parry disease. It is autosomal dominant and caused by mutations in the deoxyribonucleic acid (DNA) J homologue subfamily C member 5 (*DNAJC5* or *CLN4*) gene that encodes for cysteine-string protein α (CSPα), a highly conserved protein that is involved in the rescue of unfolded synaptic proteins (Cadieux-Dion *et al.* 2013). Mutations in *DNAJC5* reduce the amount of functional CSPα affecting its location in neuronal cells, which might lead to dysfunction at a presynaptic level and to the neurodegeneration seen in affected individuals. There is also accumulation of misfolded proteins that are resistant to proteolysis in the neurons' lysosomes (Noskova *et al.* 2011). The age of onset of symptoms in the affected individuals varies between 25 and 46 years of age and includes seizures, cognitive deterioration with loss of speech, cerebral atrophy, motor deficiencies (including Parkinsonism in some cases) and predominantly dementia, with no retinal degeneration (Nijssen *et al.* 2002; Burneo *et al.* 2003; Noskova *et al.* 2011). The storage material is arranged in three different ultrastructural profiles: fingerprint, rectilinear and GROD-like (Josephson *et al.* 2001).

Other more rare types of ANCL have been described. For instance, a homozygous mutation in the *GRN* gene (also known as *CLN11*), which encodes progranulin, has been identified in ANCL patients (Smith *et al.* 2012). Progranulin has been associated with several roles, such as inflammation, tumourigenesis and tissue repair (Bateman & Bennett 2009). Heterozygous mutations in this same gene are better known to cause frontotemporal lobar degeneration, the second most common early-onset dementia (Yu *et al.* 2010). In this CLN11 disease, affected individuals show visual failure and convulsions

in the second decade of life, followed by ataxia, cerebellar atrophy and early deterioration of cognitive capacities (Smith *et al.* 2012). Storage material with a rectilinear profile was identified in a progranulin-deficient mouse model (Petkau *et al.* 2012).

In a mass spectrometry-based assay, mutations in further genes were shown to cause adult forms of NCL: two missense mutations in the *CLN5* gene and a missense mutation in the N-sulphoglucosamine sulphohydrolase (*SGSH*) gene, which more usually underlies mucopolysaccharidoses III A (Sleat *et al.* 2009). Another study also showed that mutations in *CLN5* cause ANCL (Xin *et al.* 2010).

1.1.2 Juvenile CLN3 disease

The juvenile form of NCL (JNCL), now known as juvenile CLN3 disease, is the most common form of NCL accounting for about 50% of all known NCL cases. The incidence of juvenile CLN3 disease can be as high as 7 births per 100,000 in Scandinavia (Uvebrant & Hagberg 1997).

Children with juvenile CLN3 disease start manifesting symptoms between the ages of 4 to 10 years. Symptoms start with visual impairment, followed by seizures and cognitive, speech and motor decline, progressively leading to death, usually in the second or third decade of life (Consortium 1995). Most patients also show behavioural problems with angry outbursts, physical violence, and features of depression. Magnetic resonance imaging examinations show cerebral and cerebellar atrophy (Mole *et al.* 2005).

The juvenile CLN3 disease is characterised by the presence of lipofuscin with a fingerprint ultrastructural pattern (Palmer *et al.* 1992). These fingerprint profiles are often seen within large membrane-bound lysosomal vacuoles in the patients' blood lymphocytes, but they are also found in neuronal tissues. Subunit c of ATP synthase complex is found in high concentrations in patients' lysosomes, being the main protein component of the accumulated material in juvenile NCL.

Juvenile CLN3 disease, like the majority of NCL disorders, is an autosomal recessive inherited condition, caused by mutations in the human gene *CLN3* (Consortium 1995). *CLN3* encodes a polytopic membrane protein with 438 amino acids. The proposed topology of the CLN3 protein consists of six transmembrane domains and a lumenal amphipathic helix (Nugent *et al.* 2008; Ratajczak *et al.* 2014) (Figure 1.1.1).

Figure 1.1.1 Proposed topologies of Btn1p showing the position of different mutations

Proposed topology of Btn1p according to (A) Nugent *et al* and (B) Ratjaczak *et al*. Positions E295 and G187, where p.E295K and p.G187A mutations occur, are shown in the diagram by oval shapes. The region deleted in the 1-kb deletion is represented in light grey (Nugent *et al.* 2008; Ratajczak *et al.* 2014).

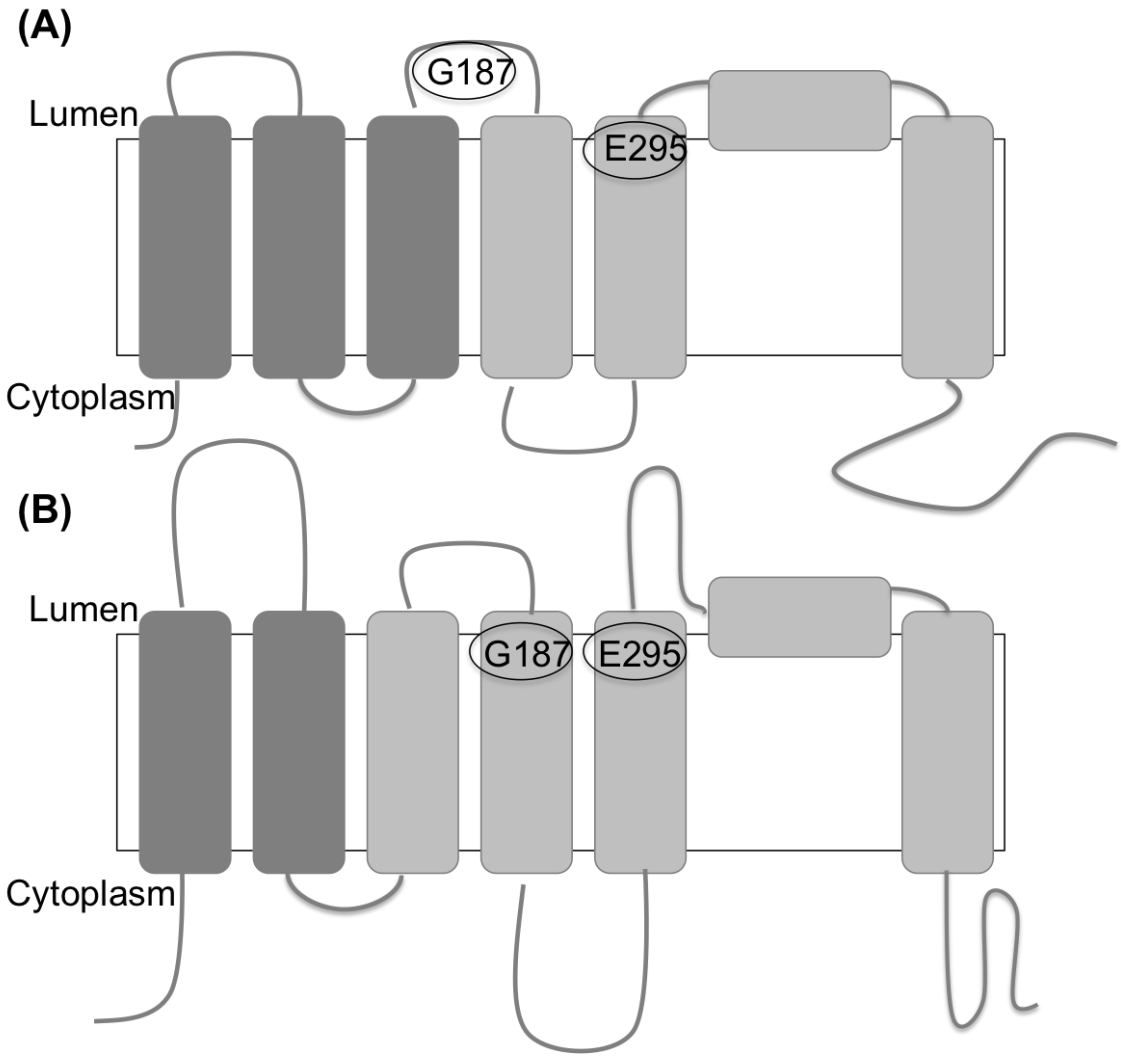

Over 50 mutations have been described in *CLN3* to date (NCL resource mutation database - http://www.ucl.ac.uk/ncl). The most common mutation, present in almost all patients, is a 1-kb intragenic deletion that removes two internal exons within the *CLN3* gene, and that can be found on both disease alleles or in compound heterozygosity with a different mutation (Consortium 1995; Munroe *et al.* 1997). This deletion is known to result in at least two different transcripts: one predicted to encode a truncated protein of just over 100 amino acids and another lacking three internal exons. Thus, two mutant proteins may be expressed in cells of juvenile CLN3 disease patients (Kitzmuller *et al.* 2008). Previously it had been thought that these patients had lost all function of CLN3; however it was later shown that patients with this mutation have a mutation-specific phenotype since partial function of CLN3 remains in all cells (Haines *et al.* 2009). Moreover, the mutant protein is able to rescue the enlarged lysosomes that arise from complete or severe loss of CLN3 function (Kitzmuller *et al.* 2008). Furthermore, the existence of subclinical eye features was reported in healthy carriers of the 1-kb deletion (Gottlob *et al.* 1988).

Other mutations have been detected in *CLN3*. These mutations can be in compound heterozygosity with the 1-kb deletion. The majority are missense mutations, but other types have also been found: nonsense mutations, small deletions, small insertions, intronic and splice-site mutations (Munroe *et al.* 1997). Approximately 80% of mutations in *CLN3* cause truncation of the protein resulting in prematurely truncated products (Kousi *et al.* 2012). The p.Glu295Lys is one of the mutations associated with the mildest form of juvenile CLN3 disease in patients also carrying the 1-kb disease allele, with blindness as a clinical symptom for several decades, before the remaining symptoms start to manifest (Wisniewski *et al.* 1998; Aberg *et al.* 2009). Another mutation, p.Gly187Ala, is predicted to cause complete loss of CLN3 function, perhaps through disruption of protein folding and eventual degradation (Haines *et al.* 2009). There is evidence of correlation between genotype and phenotype in the CLN3 disease. For example, it has been reported that mutations in the lumenal regions, including the amphipathic helix, have the most significant impact on the

CLN3 function (Haines *et al.* 2009). Similarly, any mutation that will affect the protein structure will give rise to a classic juvenile NCL phenotype, whereas a more protracted disease course will be underlined by other mutations, presumably affecting less important CLN3 residues (Mole *et al.* 2005). Remarkably, several individuals whose only symptoms are visual failure, even in late adulthood, have recently been shown to harbour mutations in *CLN3* (Coppieters *et al.* 2014; Wang *et al.* 2014). This relationship between disease severity and the underlying mutation suggests that certain protein regions are more important for its activity than others. This makes it very important to further elucidate the protein function and predict which are the important regions, in order to reach a therapeutic goal. This will be further discussed later in the Discussion Chapter.

CLN3 is the most highly conserved of the NCL genes, and it has been described in all eukaryotic species, except plants (Mole *et al.* 2005) (Figure 1.1.2). This high conservation between species suggests an important role for this protein at the cellular level. The fact that the protein is greatly conserved also provides several simpler models for juvenile CLN3 disease. Organisms that have been used as models for the study of CLN3 include: the budding yeast *Saccharomyces cerevisiae*, fission yeast *Schizosaccharomyces pombe*, the nematode worm *Caenorhabditis elegans,* fruit fly *Drosophila melanogaster*, zebrafish *Danio rerio* and at least four different mouse models. In budding yeast, the orthologue of CLN3 is Btn1p. Btn1p is composed of 408 amino acids, and is 59% similar and 39% identical to the human protein (Pearce & Sherman 1997). The fission yeast orthologue has the same denomination, Btn1p, but is slightly smaller, with 396 amino acids, and is 48% similar and 30% identical to its human orthologue (Gachet *et al.* 2005). *C. elegans* has three *CLN3* gene orthologues: *cln-3.1*, *cln-3.2*, and *cln-3.3,* all with distinct expression patterns (de Voer *et al.* 2001). The fruit fly model of juvenile CLN3 disease is a gain-of-function system, and the *Drosophila cln3* is 60% similar to the human gene. Overexpression of *cln3* causes degeneration and roughening of the fly eyes, duplicated macrochaetae on the thorax, thickening of wing veins and increased apoptosis in the wings (Tuxworth *et al.* 2009). A zebrafish model of CLN3

disease was generated by a *Cln3*-targeted morpholino approach. These fish show a spontaneous tail flicking phenotype, locomotion impairments with no movement, smaller eyes and premature death (Claire Russell and Kim Wager; personal communication). Finally, there are four mouse models with different deletions and insertions in the *Cln3* gene. The first one was generated by targeted disruption of exons 1 to 6 of *Cln3*. These mice show accumulation of autofluorescent material in neurons, cortical atrophy and neurodegeneration (Mitchison *et al.* 1999). The second mouse model is also a knockout model, created by disruption of exons 7 and 8 of *Cln3,* and they also show storage material and neurodegeneration (Katz *et al.* 1999). The other two models are knock-in mice. One is a $Cln3^{\Delta ex7\text{-}8}$ knock-in mouse, a genetic model of the common 1-kb deletion found in juvenile NCL patients, where exons 7 and 8 have been deleted. This mouse shows degeneration in the retina, cerebral cortex and cerebellum, neurological problems and suffers from a premature death (Cotman *et al.* 2002). The last mouse is another knock-in reporter model of the disease, where exons 1 to 8 of *Cln3* are replaced with β-galactosidase reporter. These mice show autofluorescent inclusions and neurological impairment, such as tremors, susceptibility to seizures and deficient motor functions (Eliason *et al.* 2007). All of these models contributed to important findings regarding the function of CLN3, and this is discussed below.

Figure 1.1.2 Conservation of CLN3 between several species

Diagram of CLN3 amino acid conservation between human, mouse, *Danio rerio* (zebrafish), *Drosophila melanogaster* (fruit fly) and *Schizosaccharomyces pombe* (fission yeast). Each amino acid is represented by a letter and '-' represents the lack of those amino acids in the organism. Asterisks and grey rectangles represent residues that are known to be mutated in the human CLN3. The regions in black are regions that are exactly the same between the species; regions in grey correspond to regions where the amino acids are very similar respective to their properties. Lines above the amino acids correspond to the predicted transmembrane domains domains of the CLN3 protein according to the topology proposed by Nugent *et al.*. All mutated residues are highly conserved between species, as well as the transmembrane regions.

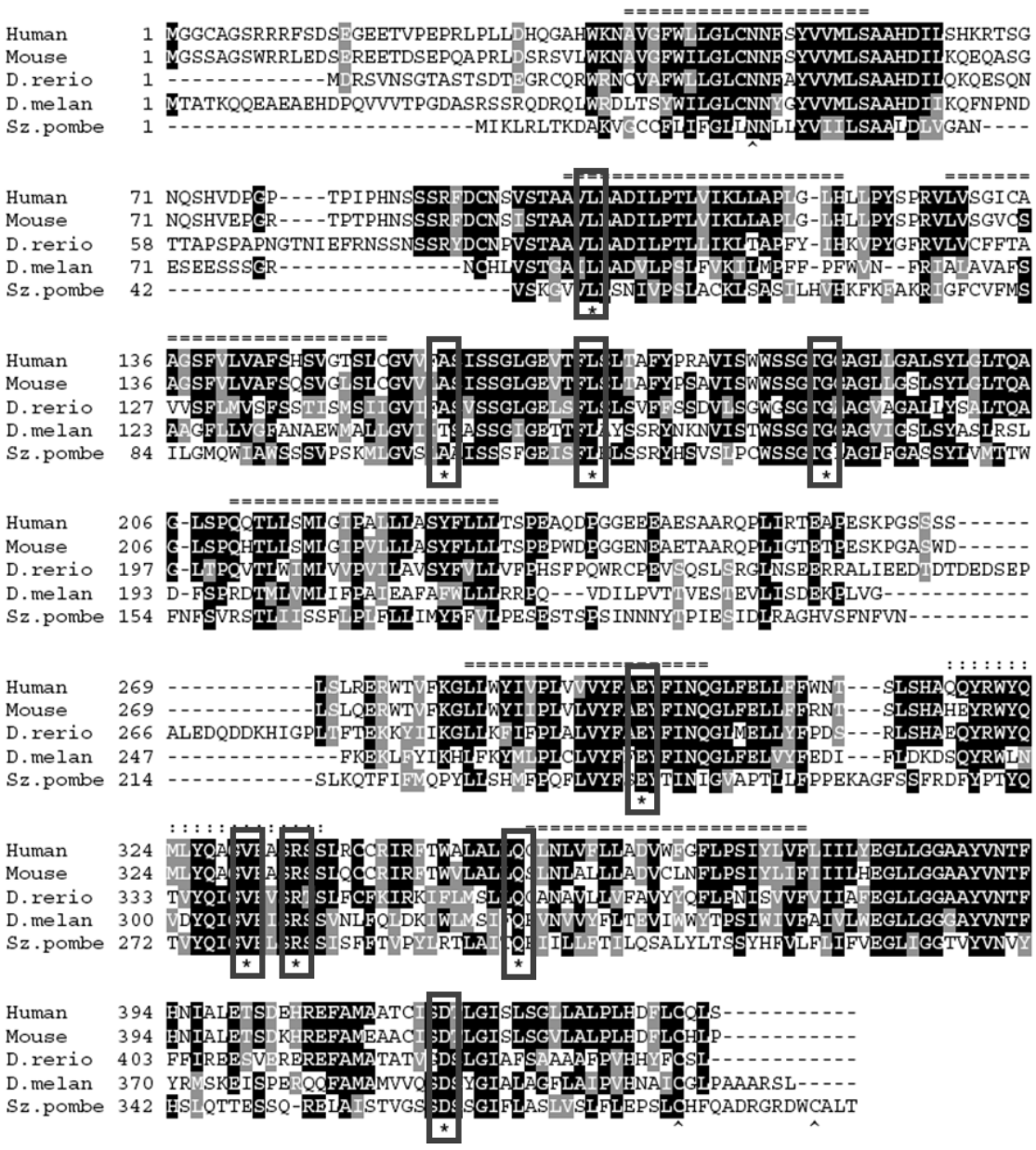

Table 1.1 Summary of different types of NCL

NCL type	Gene / Protein	Protein function
Congenital CLN10 disease	*CTSD* / cathepsin D	Lysosomal protease
Infantile CLN1 disease	*CLN1* / PPT1	Lysosomal thioesterase
Late infantile CLN2 disease	*CLN2* / TPP1	Lysosomal peptidase
Late infantile CLN5 disease	CLN5	Lysosomal glycoprotein
Late infantile CLN6 disease	CLN6	ER transmembrane protein
Late infantile CLN7 disease	*CLN7* / MFSD8	Membrane transporter protein
Late infantile CLN8 disease or EPMR	CLN8	Predicted transmembrane protein
Juvenile CLN3 disease	CLN3	Predicted transmembrane protein
Adult CLN6 disease or Kufs disease type A	CLN6	ER transmembrane protein
Adult CLN13 disease or Kufs disease type B	*CTSF* / cathepsin F	Lysosomal protease
Adult CLN4 disease or Parry disease	*DNAJC5* / CSPα	Involved in protein folding
Adult CLN11 disease	*GRN* / progranulin	Cell growth regulator

CLN3 function

The exact function of CLN3 is still unknown and thought to be complex. Over the years, several important cellular roles have been associated with this protein such as autophagy, cytoskeletal organization, lysosomal homeostasis, lipid modification, apoptosis, trafficking, amino acid transport and metabolism. All of these functions are discussed below, together with a summary of the current information available on the CLN3 localisation and trafficking.

CLN3 localisation and trafficking

CLN3 has been reported at different locations in mammalian cells. These different locations include lysosomal or late endosomal compartments (Järvelä *et al.* 1998; Järvelä *et al.* 1999; Kida *et al.* 1999; Kyttälä *et al.* 2004) including the lysosomal membrane (Ezaki *et al.* 2003), the Golgi apparatus (Kida *et al.* 1999; Kremmidiotis *et al.* 1999; Getty *et al.* 2013), the trans-Golgi network (TGN) (Tecedor *et al.* 2013), the endoplasmic reticulum (Kida *et al.* 1999), the nucleus (Margraf *et al.* 1999), the mitochondria (Katz *et al.* 1997) and in membrane lipid rafts (Rakheja *et al.* 2004). CLN3 has also been located in synaptosomes (Luiro *et al.* 2001). These studies were all done with overexpressed CLN3 as the amount of endogenous protein is too low to be detected using antibodies.

Further work concerning CLN3 localisation was carried out in simpler disease models, again by studying ectopic expression with a GFP tag. Btn1p, the yeast orthologue of CLN3, is located in the perimeter membrane of vacuoles (the yeast organelles equivalent to mammalian lysosomes) and prevacuolar compartments, both in *S. cerevisiae* and *S. pombe* (Croopnick *et al.* 1998; Pearce *et al.* 1999b; Gachet *et al.* 2005). Additionally, Btn1p was observed in the Golgi apparatus at steady state with trafficking via the endocytic system to the vacuoles, in *S. pombe* (Gachet *et al.* 2005; Codlin & Mole 2009) and *S. cerevisiae* (Kama *et al*. 2011).

The effect of different mutations on the localisation of CLN3 has been reported in several studies. The presence of the common deletion in CLN3 has been shown to prevent exit of the protein from the ER and subsequent targeting to the endosomal/lysosomal compartments (Järvelä *et al.* 1999). Similarly, work done in the fission yeast model of juvenile CLN3 disease, showed that the missense mutation p.Gly187Ala (or p.Gly136Ala in Btn1p) and other mutations in the predicted second lumenal loop of Btn1p (according to (Nugent *et al.* 2008) affect trafficking to the vacuoles and retain Btn1p in the ER (Codlin & Mole 2009; Haines *et al.* 2009). Other missense mutations in *CLN3* were also studied. Work using mammalian cells showed that these mutations do not seem to affect CLN3 trafficking, since mutant CLN3 was observed in the same compartments as the wild-type protein, in the endosomal-lysosomal pathway (Järvelä *et al.* 1999; Haskell *et al.* 2000). However, recent work done in our group with fission yeast showed different results. In this study, mutations in the Btn1p C-terminal cysteine residues led to internalisation of the protein into the vacuoles (Haines *et al.* 2009).

CLN3 undergoes several post-translational modifications. CLN3 is N-glycosylated in two sites (asparagine residues 71 and 85) that are not essential for targeting CLN3 to the lysosomes, since the presence of mutations in these sites does not affect the lysosomal sorting of CLN3 (Storch *et al.* 2007). The C-terminal of CLN3 contains a farnesylation motif (Pullarkat & Morris 1997). The inhibition of farnesylation in this motif appears to impair the sorting efficiency of CLN3 in early endosomes and subsequently increases the amount of CLN3 in the plasma membrane (Storch *et al.* 2007). Two other motifs are essential for CLN3 sorting to the lysosome both in neuronal and non-neuronal cells: one is located in the C-terminal and consists of a methionine and a glycine separated by nine amino acids [$M(X)_9G$] (from 409 to 419), and the other is a dileucine motif (in hydrophobic amino acids 253 and 254) that resembles classic lysosomal targeting motifs in the second cytosolic loop domain of CLN3, LI (Kyttälä *et al.* 2004).

Lysosome homeostasis

As mentioned above, CLN3 is localised in the membrane of late endosomes and lysosomes. Therefore, it is plausible that it exerts some functional roles in these organelles. Evidence of CLN3 function in lysosomal homeostasis has been reported in several studies. The lysosomal pH in fibroblasts is increased in several NCL, including the juvenile form (Holopainen *et al.* 2001). This is thought to result from a decrease in the vacuolar H+ ATPase complex (v-ATPase) activity, reported in other study (Ramirez-Montealegre & Pearce 2005). It is also thought that this decreased activity in the lysosomes disturbs the catalytic activity of lysosomal proteins and subsequently leads to accumulation of lipopigments, characteristically seen in NCL (Holopainen *et al.* 2001).

It was reported that the activities of several lysosomal enzymes are increased in Juvenile NCL patients (Sleat *et al.* 1998). Similarly, work done in a knockout mouse model of this disease showed that the activity of the lysosomal acid phosphatase LAP/ACP2 was significantly increased in the mice brain (Pohl *et al.* 2007). In the same study, this lysosomal phosphatase was reported as being present at high levels in juvenile NCL patient fibroblasts. This may reflect compensatory effects occurring in the cell that are initiated at the lysosome.

The level of expression of *CLN3* is thought to influence lysosome size in mammalian and yeast cells: in HeLa cells depleted for *CLN3* by the action of small interfering ribonucleic acid (siRNA) lysosomes are larger than in control cells and overexpression of *CLN3* decreases their size (Kitzmuller *et al.* 2008). Similar effects were seen in induced pluripotent stem cells derived from patient fibroblasts and in *S. pombe* (Gachet *et al.* 2005; Lojewski *et al.* 2014). Additionally, fibroblasts from patients containing the 1-kb common deletion when treated with siRNA against *CLN3* showed an increase in lysosomes size. This result corroborates the finding that the 1-kb deletion retains some function and is not a null mutation (Kitzmuller *et al.* 2008).

Alterations in lysosomal pH have also been reported in both yeast models of

juvenile CLN3 disease (*S. cerevisiae* and *S. pombe*), but with contradictory effects. Fission yeast cells show the same phenotype as mammalian cells: when *btn1* is deleted vacuoles are larger and less acidic than in wild-type cells, and overexpression of *btn1* increases acidity (Gachet *et al.* 2005). In contrast, in budding yeast, cells deleted for *BTN1* have more acidic vacuoles, thought to be due to an increase in v-ATPase activity (Chattopadhyay *et al.* 2000). In fission yeast, ectopic expression of *btn1* is able to compensate for v-ATPase function in cells deleted for genes encoding v-ATPase subunits, suggesting that its contribution to vacuole acidification is not only via an effect on the v-ATPase activity (see more details below, section 1.2.3) (Codlin *et al.* 2008a). This rescue may be due to an effect that Btn1p exerts on the activity of other ion transporters or channels, or as a direct consequence of its own activity.

Trafficking, endocytosis and autophagy

CLN3 dysfunction has been associated with defects in membrane trafficking routes and endocytosis. HeLa cells treated with *CLN3* siRNA show a defect in trafficking of the cation-independent mannose 6-phosphate receptor (CI-MPR). This defect results in an impediment in the ability of CI-MPR to exit the TGN, where it accumulates (Metcalf *et al.* 2008). Furthermore, there was a reduction in the maturation rate and cellular activity of lysosomal cathepsins B and D, which suggests that CLN3 plays an essential role in trafficking and delivery of lysosomal enzymes, affecting the ability of lysosomes to perform their functions. Another study performed in cultured human embryonal kidney cells confirmed that the maturation process of cathepsin D is deficient when CLN3 function is inhibited (Golabek *et al.* 2000). The lysosomal degradation of the amyloid-β protein precursor was also affected in the absence of CLN3. Furthermore, processing and transport of cathepsin D are also disrupted in a knock-in mouse model of juvenile CLN3 disease (Fossale *et al.* 2004). However, these effects on cathepsin D activity are not as low as the levels required to directly induce disease resembling CLN10 disease.

In *S. pombe*, it was found that the post-Golgi trafficking of vacuolar protein sorting 10 protein (Vps10p), the sorting receptor of the vacuole hydrolase carboxypeptidase Y (Cpy1p), is impaired in *btn1*Δ cells (where *btn1* is deleted). This leads to a defect in the sorting of Cpy1p so that it is secreted from the cell. The fact that Vps10p is not able to traffic from the Golgi to the TGN might be due to a direct effect that Btn1p exerts on the Golgi compartment, where it is located at steady state and which undergoes striking morphological changes in the absence of Btn1p (Codlin & Mole 2009).

Studies in different CLN3 models reported defects in the endocytic process: *S. pombe btn1*Δ cells (Codlin *et al.* 2008b), knock-in mice neuronal precursor cells (Fossale *et al.* 2004) and juvenile NCL patient fibroblasts (Luiro *et al.* 2004). In a recent study with brain endothelial cells, CLN3 was reported to mediate the transport of microdomain-associated proteins, caveolin-1 and multidrug resistance protein 1, MDR1, from the TGN to the plasma membrane. Therefore, all functions associated with these proteins such as drug efflux, endocytosis and regulation of cell volume, were impaired in *CLN3*-null cells (Tecedor *et al.* 2013). Another recent study performed in endothelial brain cells from a knock-in juvenile NCL mouse model revealed that these cells have defects in the ADP-ribosylation factor 1-cell division control protein 42 homologue (ARF1-Cdc42) pathway (Schultz *et al.* 2014). These defects have a direct impact on the fluid-phase endocytic process and other cellular processes such as filopodia formation and cell migration.

In a study with the *S. cerevisiae* model of juvenile CLN3 disease, it was revealed that the expression of *BTN2* (orthologue of the human *Hook1*) is elevated in *BTN1*Δ cells (Pearce *et al.* 1999b). Furthermore, Btn2p is involved in the regulation of the endocytic SNARE complex in yeast and mediates retrograde sorting of proteins from late endosomes back to Golgi compartments (Kama *et al.* 2007; Kama *et al.* 2011). The orthologue of Hook1 in *Drosophila* regulates endocytosis of surface ligands (Kramer & Phistry 1996, 1999) In fibroblasts from juvenile NCL patients; *CLN3* overexpression induces aggregation of Hook1 and a weak interaction between these two proteins was

found (Luiro *et al.* 2004). Additionally, Hook1 has been shown to physically interact with endocytic Rab7, Rab9 and Rab11, suggesting a role for Hook1 in membrane trafficking.

There is also evidence of autophagy disruption in a knock-in mouse model of juvenile CLN3 disease at the level of autophagic vacuole maturation. In these murine cells the levels of the autophagy marker LC3-II were increased, lysosomes and autophagic vacuoles were less mature than in wild-type mice, and there was accumulation of subunit c of mitochondrial ATP synthase in vacuoles (Cao *et al.* 2006). Another recent study showed an upregulation of the Akt-mTOR (mammalian target of rapamycin) signalling pathway and decreased acidity in juvenile NCL patient fibroblasts, both leading to macroautophagy and disrupted endocytosis (Vidal-Donet *et al.* 2013). The increased lysosomal pH affects the maturation of autophagosomes and impairs endocytosis.

Cytoskeletal organization

Since CLN3 and Hook1 may interact (see above), and Hook1 interacts with microtubules (Walenta *et al.* 2001), it is plausible that CLN3 function may be related to cytoskeletal organization (Luiro *et al.* 2004). In fact, gene expression profiling of embryonic cortical neurons of a knockout mouse model revealed a downregulation of dynactin (Luiro *et al.* 2006). Dynactin interacts with microtubules, suggesting a microtubule-related defect in this mouse model. In other studies, an interaction between CLN3 and the plasma membrane fodrin cytoskeleton was reported, since this structure has an abnormal appearance in patient fibroblasts and in brain cells from a knockout mouse model (Uusi-Rauva *et al.* 2008; Getty *et al.* 2011). A recent study showed that cells from a knockout mouse model have defects at a cytoskeletal level, due to alterations in the cytoskeleton-associated nonmuscle myosin-IIB activity (Getty *et al.* 2011). These mice fibroblasts appeared longer and thinner than those from wild-type mice.

Work using the *S. pombe* model of juvenile CLN3 disease also contributes to this idea that CLN3 (or Btn1p) function is linked to the cytoskeleton. Severe defects in the F-actin cytoskeleton were reported in yeast *btn1*Δ cells at a high temperature of growth (Codlin *et al.* 2008b). F-actin is depolarized which leads to an abnormal cell morphology. Moreover, at the same temperature, *btn1*Δ yeast cells adopt a curved morphology and show bundling of microtubules (Haines *et al.* 2009).

Amino acid transport

Lysosomes isolated from lymphoblasts of juvenile NCL patients show defective transport of arginine, leading to a depletion of arginine in patient lysosomes (Ramirez-Montealegre & Pearce 2005). Arginine transport into the lysosomes is v-ATPase-dependent. Therefore, it is proposed that CLN3 has a role in the regulation of intracellular levels of arginine possibly due to decreased v-ATPase activity. The same phenotype was also seen in *S. cerevisiae* cells deleted for *BTN1* (Kim *et al.* 2003). In these cells transport of arginine into vacuoles also requires a functional v-ATPase. Levels of vacuolar arginine are depleted and there is no transport of this amino acid into the vacuole. These defects are rescued by expression of Btn1p and human CLN3, suggesting a potential role of CLN3 (and Btn1p) in the transport and/or regulation of the transport of amino acids into the lysosome (or vacuole). However, more recently it was shown that mutations in *CLN3* (and *BTN1*) predispose cells to keep low levels of arginine, since high levels are toxic to cells with no *BTN1* (Vitiello *et al.* 2007). Additionally, in the same study, it was also shown that the decreased level of intracellular arginine is not a result of altered arginine uptake, arginine efflux or incorporation into peptides. The altered metabolism of arginine was also studied in brains of a knockout mouse model of juvenile CLN3 disease. In this study, no differences in brain arginine levels were observed between wild-type and knockout mouse (Chan *et al.* 2009). However, a decrease in arginine transport into cerebellar granule cells was observed. Additionally, there was an alteration

in the production of nitric oxide, which is synthesized from arginine and therefore dependent on its availability. Nitric oxide is involved in many physiological processes in the brain, suggesting that imbalances in arginine (and consequently nitric oxide) brain levels can have great implications in neuronal function and survival.

Another study in *S. pombe* showed several metabolic abnormalities in the *btn1*Δ strain: increased glycolytic flux and glycolysis and amino acid changes (Pears *et al.* 2010). These phenotypes suggest that Btn1p has a role in the control of glycolytic rate and that vacuolar dysfunction may reflect the concentration of amino acids. This hypothesis is corroborated by the observation of high levels of glycogen storage in mammalian cells depleted for *CLN3*. In yeast cells, the increase in glycolytic flux may originate from increased activity of the v-ATPase as a compensatory mechanism for the increased vacuole pH in *btn1*Δ cells (mentioned above); or simply to meet energy demands of *btn1*Δ cells in which oxidative phosphorylation is suppressed.

Other functions

Another proposed function for CLN3 is an anti-apoptotic activity, reported in several studies. Overexpression of *CLN3* reduced drug-mediated apoptosis in at least three studies (Puranam *et al.* 1999; Persaud-Sawin *et al.* 2002; Narayan *et al.* 2006a). However, in a more recent study the ectopic overexpression of *cln3* in the wing of *Drosophila* increased apoptosis, opposing the previous idea of a CLN3 anti-apoptotic activity (Tuxworth *et al.* 2009). In the same study, it was revealed that *cln3* expression activates the Jun N-terminal kinase (JNK) signalling pathway and inhibits the Notch signalling pathway.

Several studies proposed that CLN3 confers resistance to oxidative stress. Cells from the knock-in $Cln3^{\Delta ex7/8}$ mouse showed abnormally elongated mitochondria and a reduced survival rate after being exposed to hydrogen peroxide, implying an increased sensitivity to oxidative stress and a defective

energy metabolism in these cells (Fossale *et al.* 2004). Similarly, the fruit fly model of juvenile CLN3 disease was reported as being hypersensitive to oxidative stress generated by hydrogen peroxide, diethylmaleate and paraquat (Tuxworth *et al.* 2011). Overexpression of *cln3* in this model conferred resistance to this type of stress. In the same study, CLN3 was also shown to interact with JNK and FOXO stress signalling pathways, promoting stress resistance. Additionally, a study in SH-SY5Y neuroblastoma cells revealed that overexpressed *CLN3* confers resistance to ER stress induced by treatment with tunicamycin (Wu *et al.* 2014). In another recent study, mitochondrial abnormalities such as increased distension, disruption of the internal architecture and loss of cristae were observed in neural progenitor cells from juvenile NCL patients (Lojewski *et al.* 2014). In an older study, other mitochondrial defects were reported in a knockout mouse model: lower mitochondrial oxygen consumption due to reduced activities of respiratory chain complexes in this organelle and a larger mitochondrial size when compared to wild-type mice (Luiro *et al.* 2006).

Another proposed function of CLN3 is as a lipid catalyst or modifier. CLN3 was proposed to be a palmitoyl-protein Δ-9 desaturase, since a possible fatty acid desaturase domain was identified in a study using the Pfam server (Narayan *et al.* 2006b). This enzymatic activity is deficient in a knockout mouse model of juvenile CLN3 disease and in cultured SH-SY5Y neuroblastoma cells treated with *Cln3* siRNA. However the motif is not conserved in yeast *btn1* (Kitzmuller *et al.* 2008). CLN3 has been related to the production of the bis(monoacylglycerol)phosphate phospholipid, since it is reduced in extracts from juvenile NCL patient brains (Hobert & Dawson 2007).

Finally, CLN3 interacts with a neuronal calcium-binding protein, Calsenilin, *in vitro,* and regulates intracellular levels of free calcium (Ca^{2+}) in SH-SY5Y cells (Chang *et al.* 2007). This interaction was reported as being essential for supressing Ca^{2+}-induced cell death in neurons. In fact, the level of intracellular calcium is increased in SH-SY5Y cells treated with *CLN3* siRNA (An Haack *et al.* 2011); and a calcium channel antagonist, amlodipine, was reported as being

able to reverse elevated calcium levels in rat cortical neurons treated with siRNA against *CLN3* (Warnock *et al.* 2013).

1.1.3 Chédiak-Higashi syndrome and Niemann-Pick type C disease

Two further lysosomal storage disorders will be briefly described: the Chédiak-Higashi syndrome (CHS) and the Niemann-Pick type C disease (NPC). Yeast strains for both of these diseases were characterised during this study (Results Chapter 4).

Chédiak-Higashi syndrome (CHS) is a rare autosomal recessive disorder caused by mutations in the lysosomal trafficking regulator protein (LYST). Human *LYST* gene (also known as *CHS1*) was identified following identification of its murine orthologue, *beige* (Barbosa et al. 1996). LYST is known to be a large cytosolic- and microtubule-associated protein, however its exact function remains unknown. LYST has been associated with lysosomal homeostasis, more specifically fission and/or fusion of lysosomes (Holland *et al.* 2014).

Symptoms of CHS include partial albinism of hair and eyes, progressive neurologic defects, severe immunodeficiency with impaired activity of natural killer cells and increasing susceptibility to infections (Higashi 1954; Barrat *et al.* 1996). Death typically occurs in childhood, in the first decade of life, in a disease stage denominated 'accelerated phase', characterised by lymphocytic infiltration of various body organs. However, some patients with a mild disease course can survive until adulthood (Karim *et al.* 2002). The hallmark of CHS is the presence of abnormally large organelles (including lysosomes) and vesicles in different types of cells, such as granulocytes (Burkhardt *et al.* 1993; Karim *et al.* 1997). These defects may result from a defective trafficking of proteins involved in the genesis of these components (Faigle *et al.* 1998) or a problem in membrane remodelling. CHS can be treated by bone marrow transplantation, but since this does not apply to the central nervous system, patients eventually develop neurologic defects (Kaplan *et al.* 2008).

There is a orthologue of *LYST* in fission yeast, *lvs1* (large vacuoles size). This gene was identified after a BLAST (Basic Local Alignment Search Tool) search, as a protein containing a single BEACH domain, similar to the human

counterpart (Fred Chang, unpublished data). Other phenotypes observed in this yeast strain are discussed in this study (Results Chapter 4).

Niemann-Pick disease type C (NPC) is one of the three Niemann-Pick diseases (types A-C) and has a prevalence as high as 1/120,000 live births in Western Europe (Vanier & Millat 2003). It is an autosomal recessive LSD with a highly variable clinical phenotype. NPC can be caused by mutations in two genes: *NPC1*, in approximately 95% of cases, and *NPC2* (or *HE1*) (Carstea *et al.* 1997; Naureckiene *et al.* 2000). NPC1 is predicted to be a glycoprotein that localises to the limiting membrane of late endosomes and can be transiently associated with lysosomes and TGN (Higgins *et al.* 1999). NPC2 is a soluble glycoprotein present in the lumen of lysosomes that binds to mannose-6-phosphate receptor and to cholesterol, regulating their levels in the lysosomes (Ko *et al.* 2003; Vance 2006).

The exact functions of NPC1 and NPC2 proteins are still unknown, but different studies have reported their involvement in the transport of cholesterol and other cargo in the late endosomes and lysosomes. In a recent study, a model of “hydrophobic handoff” of cholesterol between NPC1 and NPC2 was proposed (Wang *et al.* 2010). In this model, NPC2 accepts cholesterol in the lysosomal lumen, binds it and then directly transfers it to membrane-bound NPC1, for a consequent export from the lysosome membrane. Low density lipoprotein (LDL)-derived cholesterol is exported from lysosomes (or late endosomes) to the TGN for esterification or to the plasma membrane for efflux (Ioannou 2000). However, the mechanism responsible for this efflux is still unknown: NPC1 may act as a molecular pump, directly responsible for cholesterol efflux, or it may promote this trafficking process via membrane vesicles or sterol carrier proteins, such as oxysterol-binding protein (Yu *et al.* 2014). Cells with mutant NPC1 have been shown to have low levels of calcium in their lysosomes, caused by sphingosine storage and preceding cholesterol storage (Lloyd-Evans *et al.* 2008). Therefore, it is possible that NPC1 is involved in the efflux of sphingosine from lysosomes.

The clinical presentation of NPC is highly variable, with age of onset varying from the perinatal period to adulthood. Symptoms can be hepatic, psychiatric or neurologic (Vanier & Millat 2003). Patients with the 'classic' late-infantile/juvenile form of NPC start manifesting symptoms between 3 and 5 years of age. They progressively develop neurologic abnormalities, such as: ataxia, seizures, spasticity, and loss of speech and other intellectual abilities. Death usually occurs in their teenage years but they can survive until their thirties (Vanier & Millat 2003). At a cellular level, NPC patients present excessive storage of endocytosed unesterified cholesterol, sphingomyelin and glycolipids in the lysosomal/late endosomal system, accumulated due to impaired cholesterol intracellular transport (Pentchev *et al.* 1985). This accumulation occurs in all tissues except the brain (Vance 2006).

The *S. cerevisiae* orthologue of NPC1 is Ncr1p. Yeast cells lacking Ncr1p have mitochondrial dysfunctions such as sensitivity to oxidative stress, and a reduced chronological lifespan (survival of non-dividing stationary cells) (Vilaca *et al.* 2014). *S. pombe* has a predicted orthologue of *NPC2,* but not *NPC1*. The *npc2*Δ strain had not been characterised prior to this study (Results Chapter 4).

1.2 Fission yeast: a model for juvenile CLN3 disease

Schizosaccharomyces pombe is a genetically tractable unicellular eukaryote with only 5123 genes arranged in 3 chromosomes (Robinow 1977; Wood *et al.* 2002) (http://www.pombase.org/). Fission yeast has a rod-like shape, grows by increasing its length and divides via the formation of a septum in the medial region of the region of the cell, where the division in two daughter cells occur (Forsburg & Rhind 2006) (see Figure 1.2.1 for examples of fission yeast cells with and without septa). These cells have a short generation time, with each cycle lasting 2 to 4 hours (Moreno *et al.* 1991). Together these characteristics make *S. pombe* an ideal model for the study of eukaryotic cell biology and gene function. Furthermore, fission yeast genes can be easily tagged, mutated and deleted.

S. pombe cells are usually haploid and can have two mating types: *h*+ and *h*-. *h+/h-* heterozygous diploid zygotes can be created when a pair of haploid cells of opposite mating types mate after a period of starvation (Moreno *et al.* 1991). These zygotes undergo meiosis forming haploid spores that only germinate when in adequate nutritional conditions. Haploid fission yeast cells are commonly used as models in laboratory since only one copy of the gene is present in this organism, and this excludes any issue regarding dominant or recessive alleles or mutations expressed in diploid organisms.

S. pombe and Saccharomyces cerevisiae are not closely related despite being from the same fungi division (Hedges 2002). *S. pombe* is functionally and genetically more similar to mammalian cells than *S. cerevisiae,* making it the favourite yeast to study processes such as the cell cycle, genetic recombination, chromosome structure, translation, meiosis, mitosis and RNA splicing (Moreno *et al.* 1991; Wood *et al.* 2002; Forsburg & Rhind 2006). The use of fission yeast in this project, instead of budding yeast, is mainly due to the fact that several phenotypes, associated with vacuole function and cell morphology, have already been described and developed in *S. pombe* (see below, section 1.2.3). Furthermore, it has numerous dynamic vacuoles making it a better model

system to study LSDs. Therefore those phenotypes can be used in this project in order to further elucidate the molecular mechanisms of Btn1p, CLN3 and juvenile CLN3 disease.

1.2.1 Function of yeast vacuoles

S. pombe contains many small circular vacuoles (around 50 to 80 per cell), contrary to budding yeast (with 2 to 4 large vacuoles) (Bone *et al.* 1998) (see Figure 1.2.1). However, vacuole function is the same in both strains. Therefore, much of what is known about the vacuoles in fission yeast was predicted from studies in *S. cerevisiae* and then confirmed in *S. pombe*.

Vacuoles, like lysosomes, are acidic compartments containing several hydrolytic enzymes. They are responsible for degradation of macromolecules, and are also involved in osmoregulation, pH homeostasis and act as storage reservoirs for metabolites and amino acids (Klionsky *et al.* 1990). When *S. pombe* is placed in an aqueous environment, its vacuoles fuse with each other creating larger structures that occupy a great portion of the cell's volume (Bone *et al.* 1998). *S. cerevisiae YPT7* gene, encoding for a guanosine-5'-triphosphate(GTP)ase protein of the Rab family, initiates vacuoles fusion, in a process called docking (Price *et al.* 2000). Similarly, the *S. pombe* Ypt7p is also responsible for the vacuolar fusion in these cells (Bone *et al.* 1998). *ypt7*Δ fission yeast cells have much smaller vacuoles than wild-type cells. Other factors can also influence vacuole size in fission yeast. Mutations in genes involved in vacuolar H^+ ATPase function and in *vps34* (a phosphoinositide-3-Kinase) cause an increase in vacuole size (Iwaki *et al.* 2004). The same phenotype is observed in *btn1*Δ (see above, section 1.1.2). Vacuole size can be measured after labelling the vacuole membrane with the lipophilic dye N-(3-triethylammoniumpropyl)-4-(6-(4-(diethylamino) phenyl) hexatrienyl) pyridinium dibromide (FM4-64). The presence of multiple vacuoles in *S. pombe* makes it a suitable organism for the study of NCLs, since lysosomes play a pivotal role in these disorders.

Figure 1.2.1 Fission yeast

Schizosaccharomyces pombe cells stained with calcofluor in the left panel and with FM4-64 in the right panel, showing their cell walls/septa and vacuoles, respectively. Bold arrows indicate septated yeast cells. Scale bars – 10µm.

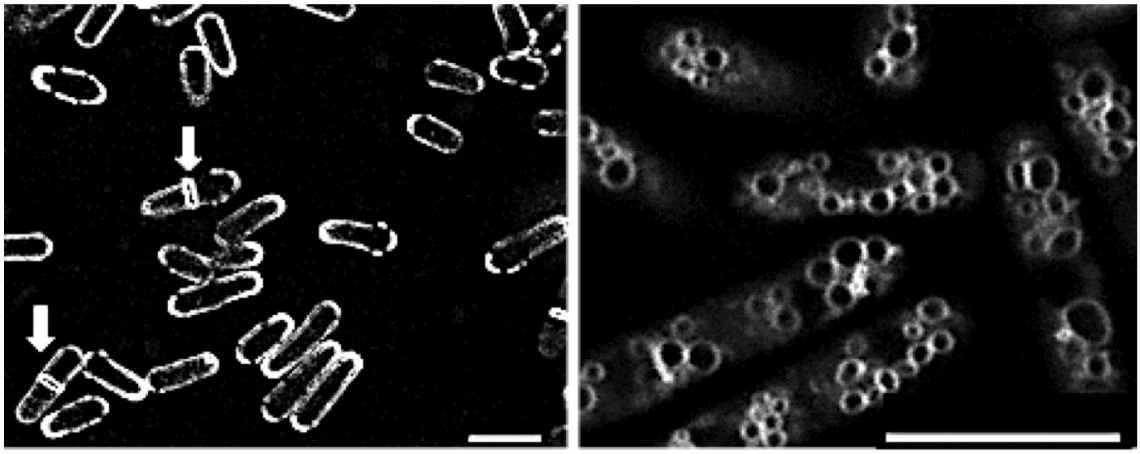

1.2.2 NCL genes in *S. pombe*

At least three NCL genes have predicted orthologues in *S. pombe*: *CLN1*, *CLN3* and *CLN10*.

The *S. pombe CLN1* orthologue is called *pdf1* (palmitoyl protein thioesterase-dolichol pyrophosphate phosphatase fusion 1) and encodes the orthologue of Ppt1p fused to dolichol pyrophosphate phosphatase 1 (Dolpp1p). The deletion of the entire open reading frame of *pdf1* is nonviable for the cells. However, cells with mutations in the *ppt1* domain are viable, but sensitive to growth in the presence of sodium orthovanadate and elevated pH (Cho & Hofmann 2004). These phenotypes can be rescued by the ectopic expression of human *PPT1* indicating that these proteins are functional orthologues.

The orthologue of *CLN10/CTSD* in *S. pombe* is *sxa1*. This gene encodes for an aspartyl protease that is 40% identical and 22% similar to the human protein. Little is known about this yeast protein, except that it is involved in the mating response (Imai & Yamamoto 1992). Phenotypes of the *sxa1*Δ strain were characterised in this study and are described in Results Chapter 4.

Finally, the fission yeast orthologue of *CLN3* is *btn1*. As previously mentioned, Btn1p is 30% identical and 48% similar to human CLN3. Several phenotypes have been associated to the loss of *btn1* (or mutant Btn1p) in yeast cells. This is discussed in the section below.

1.2.3 Btn1p, the orthologue of CLN3

All evidence supports the same function of CLN3 and its yeast orthologue Btn1p. Ectopic expression of the human *CLN3* gene can rescue all tested phenotypes that arise in *btn1*Δ yeast cells that are deleted for *btn1* (see below). Moreover, there are several highly conserved regions between CLN3 and Btn1p, and the hydropathy profiles of these proteins are similar (Nugent *et al.* 2008). The majority of amino acids that are affected by the described missense mutations in *CLN3* are also conserved in *S. pombe* (Gachet *et al.* 2005; Kitzmuller *et al.* 2008).

Several studies in fission yeast have shown multiple effects of complete loss of Btn1p function in *btn1*Δ cells. Btn1p is thought to be involved in vacuole homeostasis, cytokinesis, cell wall arrangement, cytoskeletal organisation, endocytosis, growth regulation, response to stress and trafficking. Some of these phenotypes were described above (section 1.1.2) and others are discussed below. A diagram representing the complexity of localisation of BTn1p and *btn1*Δ phenotypes is shown at the end of this subchapter *(*Figure 1.2.2).

Localisation and trafficking of Btn1p

Ectopically expressed Btn1p tagged with green fluorescent protein (GFP) was first shown to be located in vacuoles of fission yeast cells, more specifically in the membrane of these organelles. Tagged Btn1p was tracked and observed to follow a trafficking route through small pre-vacuolar and endosomal compartments to the vacuolar membrane, within 3 hours of promoter repression, in a Ypt7p-dependent manner (Gachet *et al.* 2005). It was also shown that Btn1p exerts some function in its pre-vacuolar localisation, since in *ypt7*Δ cells that are also deleted for *btn1,* the vacuoles were still larger and more alkaline than those of *ypt7*Δ cells, where Btn1p is unable to traffic to the vacuoles. More recently, at steady-state, Btn1p was found to be located in the

Golgi complex and its loss showed a striking effect on the number of the Golgi compartments, their morphology and location within the cell (Codlin & Mole 2009). The absence of Btn1p also affected trafficking through the Golgi. Thus, Btn1p protein, in *S. pombe*, is required for correct sorting and trafficking of molecules to or through the Golgi. The fact that Btn1p affects the Golgi, which is important for the correct trafficking and sorting of proteins and molecules, can explain the wide diversity of phenotypes that occur in *btn1*Δ cells.

Defective vacuole homeostasis

As mentioned before, *btn1*Δ cells have larger and less acidic vacuoles than wild-type cells, suggesting an imbalance in vacuole homeostasis. Growth of *btn1*Δ cells in acidic media led to a reduction in vacuole size, establishing a link between size and pH in these organelles (Gachet *et al.* 2005). Defects affecting vacuolar (and lysosomal) function will probably affect the autophagic process and/or the trafficking of proteins that may be involved in neurotransmission in humans (Kim *et al.* 2003; Gachet *et al.* 2005).

Cytokinesis delay and cell wall defects

*btn1*Δ cells are longer at division, have a slower growing rate and a higher septation index than wild-type cells (Gachet *et al.* 2005). This leads to a higher number of binucleate cells and suggests an abnormal cell cycle and a delay in the cytokinesis process in these cells. The secondary septum seen in some *btn1*Δ cells is significantly thicker than in wild-type cells, as are other regions of the cell wall on the sides of the cells (Codlin *et al.* 2008a). *btn1*Δ cells show defects in the cell wall glucan composition, noticeable by sensitivity to β-glucanase zymolyase-20T. A similar defect was observed in cells containing v-ATPase mutants, *vma1*Δ or *vma3*Δ. Growth in acidic media was sufficient to rescue the zymolase sensitivity in all of these strains (*btn1*Δ, *vma1*Δ and

*vma3*Δ) suggesting that this phenotype is pH-dependent and that defects in the vacuole homeostasis and cell wall composition are linked. On the other hand, the cytokinesis delay phenotype is pH-independent (it is not rescued by growth in acidic media) indicating that Btn1p acts in at least two different and independent pathways.

Defective growth at 37ºC, cytoskeletal organization and endocytosis

In a study of Codlin *et al* (2008), it was shown that the presence of Btn1p is essential for growth of yeast cells at 37°C (Codlin *et al.* 2008b). At this temperature, *btn1*Δ cells have a pear-like shape, swell and eventually lyse after 2 to 3 cell cycles. Phenotypes such as cytokinesis delay and zymolase sensitivity become more severe in *btn1*Δ cells grown at 37°C. Moreover, their normal bipolarized growth is disturbed after 7 hours of growth, with an inability to set up growth at a new end following division, and with deposition of the cell wall being position and structurally affected. Therefore, *btn1*Δ cells grow in a monopolar manner from one tip only. This defect was shown to be due to a failure in the polarization of sterol-rich membrane domains and the formation and polarization of F-actin patches to the cell tips after cytokinesis. The localisation of Btn1p is dependent on the actin cytoskeleton and is altered at 37ºC, where it localises near the cell tips and the septum. The defect that *btn1*Δ cells show in the actin cytoskeleton may affect the trafficking and activity of the membrane v-ATPase. Since this protein is crucial for maintaining the vacuole pH, the actin phenotype may be linked and modulate the acidification of vacuoles, as seen in these *btn1*Δ cells.

In the same study, it was also shown that the endocytosis process is defective in *btn1*Δ cells grown at high temperature, both in material uptake and in trafficking to the vacuole (Codlin *et al.* 2008b). In this case, the uptake of FM4-64 was severely reduced after 7 hours at 37ºC. A similar defect in neurons could affect the movement, release and uptake of neurotransmitters, leading to

neurodegeneration.

Effects of different mutations in Btn1p function

In a recent study, four different phenotypes that have been characterised in *btn1*Δ cells were selected as marker phenotypes to further understand the effect of mutations in Btn1p (Haines *et al.* 2009). These phenotypes were: enlarged vacuoles and cytokinesis delay with an increased septation index at 25°C, and monopolar growth and cell curving at 37°C. All of these phenotypes were rescued by expression of Btn1p and CLN3. Only the enlarged vacuoles phenotype was rescued by ectopic expression of the mutant *btn1* containing the equivalent to the human 1-kb common deletion. This corroborated the fact that this mutation does not completely abolish CLN3/Btn1p function. On the other hand, the cell curving phenotype was rescued only by a mutant protein carrying the equivalent to the p.Glu295Lys human mutation, which was found in patients with a very mild form of juvenile NCL (Wisniewski *et al.* 1998; Aberg *et al.* 2009), as previously mentioned. This suggests that further studies of the molecular basis of this mutation may reveal a novel target for therapies to delay onset of symptoms in juvenile CLN3 disease. Three of these phenotypes (enlarged vacuoles, increased septation index and cell curving at 37°C) were investigated again in this study and are discussed in Results Chapter 1.

Summary

Taken together, all of the phenotypes described in *btn1*Δ cells, associated with the high degree of sequence identity between the human gene *CLN3* and the yeast *btn1*, and the fact that CLN3 can compensate for loss of Btn1p, makes *S. pombe* a good candidate for the elucidation of the still unknown function of CLN3. Therefore, instead of using human or mammalian cells, one can use a simple model as fission yeast to overexpress, delete and model the effect of disease-causing or targeted mutations in *btn1*. This study of ectopic and

variable expression of Btn1p will be directly relevant to comprehend the function of human CLN3. Furthermore, therapeutic approaches for CLN3 disease can also be studied in *S. pombe* in the first instance before translation to higher eukaryotic organisms.

Figure 1.2.2 Complex picture of Btn1p localisation and function in a fission yeast cell

Diagram of a fission yeast cell summarising the complexity of Btn1p, with regard to its localisation and function(s). Btn1p/CLN3 has been proposed to be localised in the Golgi apparatus, and/or in the endolysosomal pathway including the vacuole (both represented in the picture in blue boxes). This protein has also been reported to have multiple effects in the cell: it affects the vacuolar pH and size, probably when it is localised in this organelle; on the other hand, it affects the Golgi complex size, structure and number and the cellular post-Golgi trafficking, probably when Btn1p is localised here. Other phenotypes may be affected from both locations or one of them: increased septation index, cell wall integrity and morphology, heat tolerance, glycolytic process, and others not represented in this figure. GA – Golgi apparatus: VAC – vacuole. This diagram was adapted from (Bond *et al.* 2013).

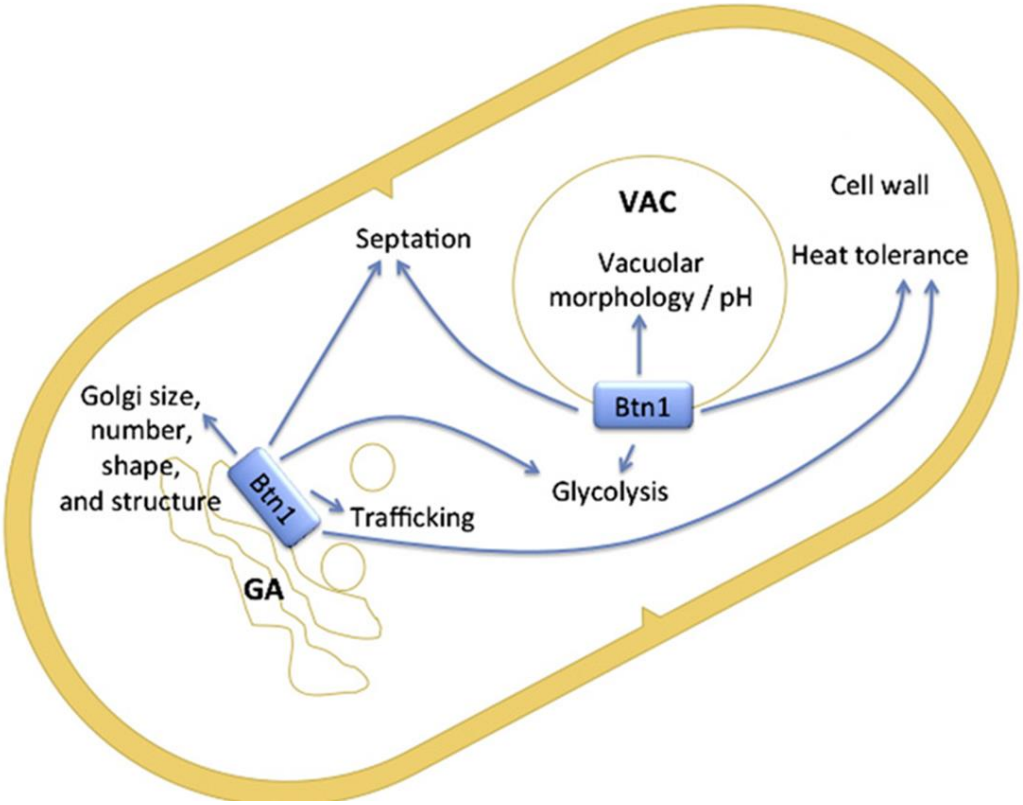

1.3 Project aims

So far, there is no cure for juvenile CLN3 disease and there is no available treatment for people manifesting the disease, mainly due to the fact that CLN3 is an intracellular membrane protein, not suitable for enzyme replacement therapy. However, the fact that most patients retain some function of CLN3 suggests that therapeutic methods that mimic the missing function, or improve the existing one, could be used to increase the quality of life of these patients and prevent or even halt the disease progression(Kitzmuller *et al.* 2008). Therefore, it is of great interest to identify novel lead compounds that revert phenotypes associated with juvenile CLN3 disease and that can be developed to treat the disease. However, screening for compounds in mammalian cells is not yet feasible, since no robust cellular phenotypes associated with juvenile NCL have been described to date. Therefore, in this study the identification of these compounds was done in a simple eukaryotic model, *S. pombe*, to simplify and accelerate the process. Although the work done in fission yeast is complementary, it is undoubtedly more far-reaching than candidate approaches in mammalian cells or other model systems.

The aims of this project were:

- To create yeast strains carrying endogenously expressed *btn1* and *btn1* containing the equivalent of disease-causing mutations, and investigate the localisation and the impact of these mutations on Btn1p function.

- To find a robust and striking phenotype in the *btn1*Δ strain suitable for a high-throughput screening approach.

- To identify potential therapeutic compounds in a library of 1280 Food and Drug Administration (FDA)-approved compounds, and test their ability to rescue phenotypes of *S. pombe btn1*Δ cells, juvenile CLN3 disease patient fibroblasts and a zebrafish model of the disease.

- To characterise yeast strains modelling three other lysosomal storage disorders (Chédiak-Higashi syndrome, Niemann-Pick disease type C2 and congenital CLN10 disease) in terms of phenotypes and investigate the efficacy of potential therapeutic compounds in these strains.

2 Materials & Methods

2.1 List of reagents

All the reagents used in this work, are summarised below, with details of the respective manufacturers:

Adenine : Sigma Aldrich
Agar : Formedium
Agarose : Sigma Aldrich
Alloxazine : Sigma Aldrich
Amino acid supplements : Formedium
Ammonium chloride (NH_4Cl) : Sigma Aldrich
Ammonium sulfate : Sigma Aldrich
Ampicillin : Sigma Aldrich
D-(-)-threo-2-amino-1-[p-nitrophenyl]-1,3-propanediol (ANP) : Sigma Aldrich
Biotin : Sigma Aldrich
BisBenzimide H33342 trihydrochloride (Hoechst) : Sigma-Aldrich
Bovine serum albumin (BSA) : VWR
Calcium chloride dihydrate ($CaCl_2.2H_2O$) : Sigma Aldrich
Calcofluor : Sigma Aldrich
Chloroquine diphosphate salt : Sigma Aldrich
Citric acid : Sigma Aldrich
Copper (II) sulfate pentahydrate ($CuSO_4{\cdot}5H_2O$) : Sigma Aldrich
Cyclosporine A (CsA) : Sigma Aldrich
Dimethyl sulfoxide (DMSO) : Sigma Aldrich
DNA 1kb ladder : Molecular Probes, Invitrogen
Dropout mix : Formedium
Dulbecco's modified eagle's medium (DMEM) : LMCB
E-64 : Sigma Aldrich
Ethidium bromide : Sigma Aldrich
Ethylenediamine tetraacetic acid (EDTA) : Sigma Aldrich
Foetal bovine serum (FBS) : Sigma Aldrich
5-fluoroorotic acid (FOA) : Formedium

FM4-64 : Molecular Probes, Invitrogen

Geneticin (G418) : Sigma Aldrich

Glucose : Formedium

Glycerol : BDH Prolabo, VWR

Herring sperm DNA : Sigma Aldrich

Histidine : Sigma Aldrich

Hydrogen chloride (HCl) : Sigma Aldrich

Inositol : Sigma Aldrich

Iron (III) chloride hexahydrate ($FeCl_3 \cdot 6H_2O$) : Sigma Aldrich

Leucine : Formedium

Lithium acetate : Sigma Aldrich

Lysogeny broth (LB) : LMCB

LysoSensor yellow/blue dextran : Molecular Probes, Invitrogen

Magnesium chloride ($MgCl_2$) : Sigma Aldrich

Magnesium chloride hexahydrate ($MgCl_2 \cdot 6H_2O$) : Sigma Aldrich

Manganese sulfate ($MnSO_4$) : Sigma Aldrich

Molybdate dihydrate ($MoO_4 \cdot 2H_2O$) : Sigma Aldrich

Nicotinic acid : Sigma Aldrich

Deoxyribonucleotide (dNTP) mix : Promega

Orthoboric acid (H_3BO_3) : BDH GPR

Pantothenic acid : Sigma Aldrich

Paraformaldehyde (PFA) : Sigma Aldrich

Penicillin streptomycin (PenStrap) : Sigma Aldrich

Polyethylene glycol (PEG) 4000 : Sigma Aldrich

Phosphate buffered saline (PBS) : LMCB

Potassium chloride : Sigma Aldrich

Potassium hydrogen phthalate : Sigma Aldrich

Potassium iodide : Sigma Aldrich

Prochlorperazine dimaleate : Sigma Aldrich

Propidium iodide : Sigma Aldrich

N-propyl-galate : Sigma Aldrich

RNase : Sigma Aldrich

Saponin : Sigma Aldrich

di-Sodium hydrogen phosphate (Na_2HPO_4) : Sigma Aldrich

Sodium sulfate (Na_2SO_4) : Sigma Aldrich

T4 DNA ligase : Promega

Tris : Sigma Aldrich

Triton X-100 : BDH Prolabo, VWR

Trypsin : Sigma Aldrich

Uracil : Formedium

Yeast extract (YE) : Formedium

Yeast nitrogen base : Formedium

Zinc sulphate heptahydrate ($ZnSO_4.7H_2O$) : Sigma Aldrich

2.2 Table of yeast strains

Table 2.1. Table of yeast strains

Strain	Genotype	Source
wild-type (wt) 972	*h*$^-$	Laboratory stock
*btn1*Δ	*h*$^-$, *btn1*::*NatMx, leu1*-32, *ura4*D18, *his3*$^-$, *ade6*-210,	This study
btn1::ura	*h*$^-$, *btn1*::*ura4*, *leu1*-32, *ura4*D18, *his3*$^-$, *ade6*-210	Laboratory stock
nmt3	*h*$^-$, *btn1*::*nmt3 gfp-btn1*	This study
nmt41	*h*$^-$, *btn1*::*nmt41 gfp-btn1*	This study
GFP-*btn1*	*h*$^-$, *btn1*::*gfp-btn1*, *leu1*-32, *ura4*D18, *his3*$^-$, *ade6*-210	This study
1kbΔ	*h*$^-$, *btn1*::*gfp-btn1*(1kbD), *leu1*-32, *ura4*D18, *his3*$^-$, *ade6*-210	This study
E240K	*h*$^-$, *btn1*::*gfp-btn1*(E240K), *leu1*-32, *ura4*D18, *his3*$^-$, *ade6*-210	This study
G136A	*h*$^-$, *btn1*::*gfp-btn1*(G136A), *leu1*-32, *ura4*D18, *his3*$^-$, *ade6*-210	This study
*btn1*Δ+prep42GFPbtn1	*h*$^-$, *btn1*::*NatMx*, *leu1*-32, *ura4*D18, *his3*$^-$, *ade6*-210	Laboratory stock
*btn1*Δ+prep42	*h*$^-$, *btn1*::*NatMx*, *leu1*-32, *ura4*D18, *his3*$^-$, *ade6*-210	Laboratory stock
*lvs1*Δ	*h*$^-$, *lvs1*::*kanMX6*, *leu1*-32, *ura4*D18, *his3*$^-$, *ade6*-210	Fred Chang laboratory
*sxa1*Δ	SPAC26A3.01, *sxa1*::*kanMX*	Bioneer library
*npc2*Δ	SPAPB8E5.04c, *npc2*::*kanMX*	Bioneer library

2.3 Fission yeast methods

The majority of yeast methods was done according to (Moreno *et al.* 1991).

2.3.1 Media

Yeast extract with supplements (YES)

Yeast extract	5g
Glucose	30g
Supplements stock (50X)	2ml
Agar (for solid medium)	20g
H_2O	to 1 l

Autoclaved.

For experiments with CsA, this chemical was added to a final concentration of 0.1 mg/ml in 1% DMSO as a carrier. (CsA stocks were prepared in DMSO in 100 mg/ml, and stored at -20ºC until use). For experiments with G418, the chemical was added to a final concentration of 100 mg/L. (G418 stock was prepared in 1 M Tris.HCl, pH 8, in a final concentration of 50mg/ml, and stored at -20ºC until use).

Supplements stock (500X)

Adenine	1.875g
Histidine	1.875g
Leucine	1.875g
Uracil	1.875g
H_2O	to 50ml

Diluted to 50X stock in sterile H_2O, filter sterilised and stored at 4ºC until use.

Minimal media (MM)

Ammonium Chloride (NH_4Cl)	5g
Potassium hydrogen phtalate	3g
Na_2HPO_4	2.2g
Adenine	500mg
Uracil	250mg
Leucine (if required)	250mg
Histidine	250mg
Agar (for solid medium)	20g
H_2O	to 0.9 l

Autoclaved.

Before use, the following were added to the initial solution:

20% Glucose	100ml
Salts stock (50X)	20ml
Vitamins stock (1000X)	1ml
Minerals stock (10.000X)	0.1ml

In the experiments with compounds, they were added to the MM or YES medium to a final concentration of 10 μM diluted in DMSO at the appropriate concentration (according to manufacturer's instructions).

For spot assays, ANP and chloroquine were added to a final concentration of 0.75 or 1 mM, and 0.1 mM, respectively. Stocks were prepared as following:

ANP (100 mM)	2.122g (in 20ml of DMSO)
Chloroquine diphospate salt (10 mM)	0.26g (in 50ml H_2O)

Both stored at -20ºC until use.

Salts stock (50X)

$MgCl_2.6H_2O$	53.3g
$CaCl_2.2H_2O$	0.735g
KCl	50g
Na_2SO_4	2g
H_2O	to 1 l

Filter sterilised and stored at 4ºC until use.

Vitamins stock (1000X)

Nicotinic acid	1g
Inositol	1g
Biotin	1mg
Pantothenic acid	0.1g
H_2O	to 100ml

Filter sterilised and stored at 4ºC until use.

Minerals stock (10.000X)

H_3BO_3	0.5g
$MnSO_4$	0.4g
$ZnSO_4.7H_2O$	0.4g
$FeCl_3.6H_2O$	0.2g
$MoO_4.2H_2O$	0.16g
KI	0.1g
$CuSO_4.5H_2O$	0.04g
Citric acid	1g
H_2O	to 100ml

Filter sterilised and stored at 4ºC until use.

5-fluoroorotic acid (FOA) media

Bottle 1:	FOA	437mg
	Uracil	50mg
	Dropout Mix	750mg
	Aminoacid supplements (-ura)	250mg
	Yeast Nitrogen Base	850mg
	Ammonium sulphate	2.5g
	H_2O	to 250ml

Sonicated and warmed to 50ºC.

Bottle 2:	Glucose	8.5g
	Bacto Agar	12g
	H_2O	to 300ml

Autoclaved immediately and poured to 250ml.

Contents of Bottle 2 were added to Bottle 1, mixed and poured onto plates.

2.3.2 Growth of yeast cells

To create *stock collections* of strains these were frozen at -80ºC. Cells were scraped from solid media after growth for 1 or 2 days, and mixed in 1ml of YES containing 20% (v/v) glycerol in a sterile cryotube. Tubes were briefly vortexed and stored at -80ºC. To re-isolate strains, a small amount of frozen stock was scraped and streaked onto a suitable plate and then incubated at 30°C for 1 to 4 days.

For yeast cells to grow they were incubated on YES or MM plates at 30°C for 1 to 4 days. Plates were also stored at 4°C for a maximum period of 3 weeks.
Cells were grown until the desired density, measured by spectrophotometry. Cell concentration measurements were based on optical density readings at 600nm (OD_{600}) using a Ultrospec 2000 spectrophotometer (Pharmacia Biotech) and adjusted for a 1:10 dilution in water. An OD_{600} of 0.1 was taken to correspond to 2×10^6 cells/ml.
Liquid cultures were prepared by inoculating colonies from plates. The majority of experiments were carried out with cells in mid log phase growth (1×10^6 - 5×10^6 cells/ml). These cultures were grown in 15ml in 50ml flasks and incubated at 30ºC with shaking (200 rpm).
For plasmid selection, strains containing plasmids were grown on medium containing appropriate supplements (adenine, leucine, histidine and uracil). The same was done for viability assays where cyclosporine A was added to the liquid medium at a final concentration of 0.1 mg/ml, and this was used to inoculate cells previously grown to log phase.

2.3.3 Transformation of yeast cells

btn1::ura strain (Table 2.1) was grown in 20ml of MM medium overnight at 30ºC to a density of approximately 1 x 10^7 cells/ml. The cell suspension was centrifuged in a Sigma 2-16K centrifuge (SciQuip, UK) at 2000 rpm for 5 minutes and washed with sterile water. Cell pellet was resuspended in 1ml of 0.1 M lithium acetate and 100μl aliquoted in eppendorf tubes, one for each transformation. The adequate amount of DNA and 2μl of herring sperm DNA (from 9-12 mg/ml stock) were added to the cells and incubated at room temperature for 5 minutes. 280μl of PEG solution (50% PEG 4000, 0.1 M lithium acetate, 0.01 M Tris.HCl) were added, mixed gently and suspensions incubated for 60 minutes at 30ºC. 43μL of DMSO were added and solutions heat shocked at 42ºC for 5 minutes.

In case of cells with a kanamycin-resistance (kan^R) marker, cells were centrifuged in a Sorvall Pico centrifuge at 5000 rpm for 2 minutes, resuspended in 500μl of H_2O and 250μl of suspension plated onto YES plates. Plates were incubated for approximately 20 hours at 30ºC, replica plated onto YES plates with 100mg/L G418. Replica plates were incubated for 2 to 3 days at 30ºC and large colonies restreaked onto fresh YES plates with G418. Colonies were checked for homologous recombination by colony PCR and by sequencing with the appropriate primers (Table 2.2).

In case of FOA selection, heat shocked cells were immediately incubated in 500ml of YES and incubated at 30ºC with shaking (200 rpm) for 2 to 3 days. 1ml was taken from each suspension, centrifuged and resuspended in 1ml of H_2O. 100 μl were plated onto FOA plates and incubated at 30ºC until colonies were visible. Colonies were checked for homologous recombination by colony PCR and by sequencing with the appropriate primers (Table 2.2).

2.3.4 Labelling vacuoles with FM4-64 and LysoSensor

For labelling of vacuoles with the FM4-64 dye, cells were grown in MM overnight to mid-log phase. 1ml of cells was centrifuged for 5 minutes at 2000 rpm. Cell pellets were resuspended in 50µl of YES with 1µl of FM4-64 and incubated in a 30ºC water bath for 20 minutes. 1ml of YES was added to each suspension and these were centrifuged at 2000 rpm for 5 minutes. Cell pellets were resuspended in 1ml of YES, 4ml of YES were added and cultures were incubated at 30ºC with shaking for 120 minutes. Cells were spun at 2000 rpm for 5 minutes and pellets were resuspended in 25µl of MM. 7µl of each sample were spotted onto microscope slides to be visualized.

In order to measure the vacuole pH, vacuoles were labelled with LysoSensor dye. Cells were grown overnight to mig-log phase. 1ml of each culture was mixed by inversion with 5µl of LysoSensor. Suspensions were incubated in the dark at room temperature for 10 minutes. Tubes were spun for 3 minutes at 2000 rpm, and cells were washed twice with MM. Cell pellets were resuspended in 50µl of MM and 5µl were spotted onto microscope slides to be visualized.

2.3.5 Calcofluor staining

For the septation index and cell curving assays, cells were grown overnight in MM to mid-log phase. For the cell curving assay, cells were grown for an additional 4 hours at 37ºC. Septation index corresponds to the number of cells with a clear septum stained with calcofluor (septated cells) divided by the total number of cells, in percentage. Septation index is an indication of the amount of cells that are halted in the cytokinesis process, and therefore, when this value is higher than normal it suggests a delay in the cell cycle. Cell curving is the percentage of cells with a curved or bent shape (instead of the normal rod shape) in the total number of cells. 5µl of each culture were spread onto a

microscope slide, 1 μl Calcofluor (50 μg/ml) was pipetted onto a coverslip, which was then used to cover the cells. Cells were visualized immediately.

2.3.6 Viability assays

For all the viability assays, cells were grown overnight in MM to mid-log phase. Cells were washed in sterile water, transferred to 20ml of YES medium (with or without 0.1mg/ml CsA) in a final density of 1 x10^8 cells/ml and incubated at 37ºC for 24 hours. Afterwards, 1ml of each culture was mixed by inversion with 15μl of propidium iodide (1 mg/ml) and 10μl of calcofluor (50 μg/ml). Cells were incubated in the dark at room temperature for 10 minutes. Suspensions were spun for 5 min at 2000 rpm and washed with 1X PBS. Pellets were resuspended in residual PBS and 5μl were spotted onto microscope slides, in order to be visualized.

2.3.7 Spot assays

Spot assays were performed in order to evaluate the cell growth rate of yeast strains in a range of different conditions. For all the spot assays, cells were grown overnight in MM to mid-log phase. Cultures were washed and diluted in sterile water to a final density of 1 x 10^6 cells/ml and four serial dilutions were prepared. 10μl of each dilution were spotted onto the appropriate plates. Plates were incubated at 37ºC for 1 to 5 days. In addition to the plates with chemicals used to test sensitivity, strains were also spotted onto plates with 1% DMSO to test their sensitivity to DMSO and ensure the sensitivity was due to the presence of the chemical and not the carrier (DMSO).

2.4 Molecular biology

2.4.1 Site-directed mutagenesis

Missense mutations in *btn1* in the pREP42GFP-Btn1 plasmid were generated using the QuickChange Site-Directed Mutagenesis kit (Stratagene, UK), and appropriate primers (Table 2.2). Volumes of reagents were the following:

10X reaction buffer	5μl
dNTP mix	1μl
Forward primer (100 ng/μl)	1.25μl
Reverse primer (100 ng/μl)	1.25μl
DNA template	1μl
PfuTurbo DNA polymerase (2.5 U/μl)	1μl
ddH_2O	40.5μl

The reactions were run in a PTC-100 programmable thermal controller machine (MJ Research) on the following program:

1 cycle of	95ºC	30 s
18 cycles of	95ºC	30 s
	55ºC	1 min
	68ºC	15 min

1μl of the *Dpn*I restriction enzyme (10 U/μl) was added to each amplification reaction. The reaction mixtures were spun down for 1 minute and immediately incubated at 37ºC for 1 hour, in order to digest the template DNA. Samples were stored at 4ºC or -20ºC for longer periods.

2.4.2 Polymerase chain reaction (PCR)

To generate the constructs with the *nmt1* promoter, templates were amplified using an Expand Long Template PCR system (Roche Applied Science). All the reagents that were used in these PCR reactions are listed below:

10X Expand Long Template Buffer 2	5μl
dNTP mix (10 mM)	1.75μl
Forward primer (50 μM)	0.3μl
Reverse primer (50 μM)	0.3μl
DNA template (~300ng)	3μl
Expand Long Template enzyme mix (5 U/μl)	0.75μl
ddH_2O	to 50μl

Samples were run in a PTC-100 programmable thermal controller machine on the following program:

1 cycle of	92ºC	2 min
10 cycles of	92ºC	10 sec
	60ºC	30 sec
	68ºC	4 min
20 cycles of	92ºC	15 sec
	60ºC	30 sec
	68ºC	4 min + 20 sec for each successive cycle
1 cycle of	68ºC	7 min

The remaining PCR reactions were done using the GoTaq Flexi enzyme (Promega) and using the appropriate primers (Table 2.2). Reagents and respective volumes for each reaction are listed below:

5X GoTaq Flexi buffer	5μl
25mM $MgCl_2$	5μl
dNTP mix (10 mM)	1μl
Forward primer (5 μM)	1μl (or 2 μl for colony PCR)
Reverse primer (5 μM)	1μl (or 2 μl for colony PCR)
DNA template (~200ng)	1 or 2μl
GoTaq Flexi DNA Polymerase (3 U/μl)	0.5μl
ddH_2O	to 50μl

In colony PCR reactions, a single colony from a plate was resuspended in 20μl of sterile water and 2μl of this suspension used in the PCR reaction.

Samples were run in a PTC-100 programmable thermal controller machine on the following program:

1 cycle of	95ºC	2 min
30 cycles of	95ºC	1 min
	55-65ºC	30 sec
	72ºC	1 min/kb
1 cycle of	72ºC	7 min

For colony PCR reactions the PCR program was:

1 cycle of	95ºC	10 min
30 cycles of	95ºC	1 min

	47-51ºC	1 min
	72ºC	1 min/kb
1 cycle of	72ºC	5 min

All PCR products were purified using the QIAquick PCR Purification Kit (Qiagen), according to the manufacturer's instructions. DNA was eluted in 50 μl of H_2O.

2.4.3 Cloning

Digestion

Purified PCR products (GFP-*btn1* with and without mutations) and plasmid pSL1180 were digested with restriction enzymes *Pst*I and *Apa*I (Promega, UK):

DNA (PCR product/plasmid)	15μl
10X Multicore Buffer (Promega)	5μl
BSA (10 mg/ml)	0.5μl
RNase (5 u/μl)	1μl
Restriction enzymes	1μl
ddH_2O	to 50μl

Reactions were incubated at 37ºC for approximately 2 hours. Cut products were run in a 1% agarose gel to confirm the digestion, and then the DNA was extracted with a QIAquick Gel Extraction kit (Qiagen), according to the manufacturer's instructions.

Ligation

After being digested with restriction enzymes, products were ligated. 4μl of insert and 3μl of vector were mixed with 2μl of 10X T4 DNA ligase buffer

(Promega) and 1μl of T4 DNA ligase (3u/μl; Promega). Reactions were incubated at 23ºC for 3 hours and at 4ºC overnight.

Transformation in *Escherichia coli* competent cells

Ligation products were mixed with 100μl of thawed competent cells (DH5α from Laboratory stock) in chilled eppendorf tubes. Tubes were incubated on ice for 5 minutes, heat shocked at 42ºC for 2 minutes and chilled on ice for 5 minutes. 100μl of SOC medium was added to the cells and they were incubated at 37ºC for 30 minutes with shaking (200 rpm). 200μl were plated onto LB plates with 75 μg/ml ampicillin.

DNA preparation

Single colonies of transformed *Escherichia coli* competent cells were inoculated in 2 to 5 ml of LB and grown at 37ºC overnight with shaking (200 rpm). 1ml of culture was used for plasmid preparation. The preparation was done using a Spin Miniprep kit (Qiagen), according to the manufacturer's instructions. DNA was eluted in water.

Constructs for yeast transformation

All constructs were confirmed prior to transformation by digestion with different enzymes (*Pst*I+*Apa*I and *Mlu*I+*Age*I) and sequencing. Once confirmed, plasmids were digested with the *Mlu*I and *Age*I restriction enzymes, cleaned with a QIAquick Gel Extraction kit and the eluted DNA was directly used for transformation in yeast cells.

2.4.4 Sequencing

To verify constructs, mutations or genes, samples were sent for sequencing to Source Bioscience (Nottingham, UK). Samples were supplied as following: 5μl of 100 ng/μl plasmid DNA and 1 ng/μl per 100bp. Primers were sent at a concentration of 3.2 pmol/μl. Sequence data was analysed using the ApE software (University of Utah).

2.4.5 Electrophoresis in agarose gels

All DNA samples were electrophoresed in 1% agarose gels. The agarose gels were prepared using agarose, 1X TBE buffer (AppliChem, Germany) and 0.001% of 10 mg/ml ethidium bromide. A 1kb DNA ladder was used to check the size of the bands. Gels were electrophoresed at 110 Volts and 400 milliAmperes for 40 minutes to 1 hour, with a PowerPac Basic system (BioRad, UK). Gels were visualized on a Geneflash UV transilluminator (Syngene, UK).

2.4.6 Table of primers

Table 2.2. Table of primers

Name	Direction	Sequence	Description
btn1-P-kan	Forward	CTATTTACAGTTTGTAACAAGTTAA CTCGTCTATGAAGTCATCGATAGAA GGGCTTTAAAGTGTGCTATTTGCGAA ACAACAGCAAATTTGTAGACTAGC – GAATTCGAGCTCGTTTAAAC	Used to create nmt-GFP-btn1 constructs for transformation
GFP_btn1_orf	Reverse	CAGCGGATAAAATTATCACGTAGAG AAGGTTGTTTAACAATCCAAAAATTA GGAAGCAACACCCTACTTTCGCATC TTTTGTTAACCTCAATTTAATCAT - TTTGTATAGTTCATCCATGC	Used to create nmt-GFP-btn1 constructs for transformation
btn1_P_check	Forward	TTTGAACCTGACAACATTACCG	Used to check nmt-GFP-btn1 constructs
kan_check	Reverse	GTGATGTGAGAACTGTATCCTAGC	Used to check nmt-GFP-btn1 constructs
nmt_check	Forward	GCTACTGGATGGTTCAGTCAC	Used to check the homologous recombination of nmt-GFP-btn1 constructs
btn1_ORF_check	Reverse	AGATGCAAGAAAGAGATTTCGC	Used to check the homologous recombination of nmt-GFP-btn1 constructs, and to sequence *btn1*
GFP_PstI	Forward	CCCCTGCAGATGAGTAAAGG	Used to amplify GFP-btn1 from the pREP42GFPbtn1 plasmid
btn1_ApaI	Reverse	GGTTGGGCCCTCAAGTTAAG	Used to amplify GFP-btn1 from the pREP42GFPbtn1 plasmid
btn1_1kbdel_ApaI	Reverse	GGTTGGGCCCCTACACAAAAAAG	Used to amplify GFP-btn1(1kbΔ) from the pREP42GFPbtn1 plasmid, and to sequence *btn1 with* 1kb-deletion
mut_E240K	Forward	CGCAGTTCCTTGTATACTTCTCA AAATATACTATCAATATTGGTGTA	Mutagenesis primer to generate the E240K mutation in *btn1*
mut_E240K	Reverse	TACACCAATATTGATAGTATAT TTTGAGAAGTATACAAGGAACTGCG	Mutagenesis primer to generate the E240K mutation in *btn1*
mut_G136A	Forward	TGCTGGAGTTCCGCAACAGGCT TGGCC	Mutagenesis primer to generate the G136A mutation in *btn1*
mut_G136A	Reverse	GGCCAAGCCTGTTGCGGAAC TCCAGCA	Mutagenesis primer to generate the G136A mutation in *btn1*

btn1	Forward	ATGATTAAATTGAGGTTAAC	Used to sequence *btn1*
btn1_flanks	Forward	GTCTACTATCGTATTGCCGG	Used to check the homologous recombination of GFP-btn1 constructs
btn1_flanks	Reverse	GAAACGTCATAGGTTAACTC	Used to check the homologous recombination of GFP-btn1 constructs

2.5 Work with mammalian models

2.5.1 Mammalian cell culture and assays

The fibroblast lines that were used were HF527N (control) and H480Pa (patient with 1-kb deletion). Fibroblasts were cultured in 1X DMEM with 10% FBS and 1% PenStrep. The cultures were grown at 37ºC with 5% CO_2 in a New Brunswick Galaxy 170R incubator (Eppendorf, USA). Cells were split using trypsin/EDTA and a final concentration of 3 x 10^4 cells/ml was used in each well of 24-well dishes (Nunc). After 1 to 2 days the compounds were added to the fibroblasts (at 5, 10 and 20 μM concentrations) and incubated for 24 hours.

For immunofluorescence, the cells were fixed in 4% PFA in PBS for 20 minutes at room temperature. After PFA was removed, cells were washed thrice with 1X PBS and 0.1% Triton X-100 in 1X PBS was added for 10 minutes. Cells were washed again (as before) and then blocked with 1% BSA (in 0.025% saponin in 1X PBS) for 30 minutes at 4ºC. Cells were incubated with the primary antibody anti *cis*-Golgi marker protein GM130 (mouse) (BD Transduction Laboratories™, UK), at 1:150 in 1%BSA in 0.025% saponin in 1X PBS for 1 hour at room temperature; and washed five times in 1x PBS afterwards. The second antibody was added to the cells: Alexafluor® 488 anti-mouse (Invitrogen, Life Technologies, UK), at 1:700 in 1% BSA in 1X PBS. Cells were washed five times as before. Nuclei were stained with Hoechst (diluted 1:10.000 in 1X PBS) for 2 minutes. After being washed twice, cells were fixed with 2% PFA (in 1X PBS), to prevent dissociation of the secondary antibody. Finally, cells were washed 3 times in 1X PBS and placed onto microscope slides with a drop of mountant (90% glycerol and 3% N-propyl-galate in 1X PBS) in order to be visualized.

The extent of Golgi complex organization in mammalian cells was analysed using the compactness equation: 4π (Σ area)/(Σ perimeter)^2. A value of 1.0 indicates a perfect circle, and as the value approaches 0 it indicates an increasingly elongated and less compact object. The Golgi complex labeling

image threshold was set at ~45, where all the pixels with a value under 45 are excluded from the quantification. Region of interest was defined for each cell and the perimeter and area of the Golgi complex was measured using ImageJ.

2.5.2 Zebrafish generation and assays

All the work done with the juvenile CLN3 disease zebrafish model was done by Dr Claire Russell at the Royal Veterinary College of London.

Zebrafish were housed in a multi-rack aquarium system at 28.5 ± 0.5°C on a 14 hour light and 10 hours dark cycle to mimic the natural zebrafish environment. Following adult breeding, the embryos produced were incubated in the dark at 28°C, in 'fish water', containing aquarium water and methylene blue (0.0002%). To generate *cln3* morphant embryos, 2ng morpholino (MO) anti-sense oligonucleotides against *cln3* messenger RNA were pressure-injected into 1-2 cell stage wild-type *TupLF* strain zebrafish embryos using a glass capillary injection needle. The sequence of MOs (from Gene Tools) were: cln3 ATG MO (CATtgcgactttcacaggagaaatg).

Between 5 and 10 zebrafish embryos per well of a 24 well plate were arrayed and either 1ml of aquarium water, DMSO or test compound added at 12 hours post fertilization (hpf). Compounds were supplied at 100x working strength and diluted into fish water. Test compounds and testing concentrations used were: E-64 50µM, Alloxazine 55µg/ml and Prochlorperazine dimaleate 62.5µM. Embryos were incubated at 31°C and survival analysis and relative activity (at 36hpf) were conducted over the following 4 days.

In the survival assays, animals were scored as dead (no heartbeat) or alive (heartbeat) at daily intervals and dead animals removed.

In the assay measuring the relative activity, a 24 well plate was mounted on a Nikon SMZ1500 stereomicroscope. Videos were made of groups of fish in each well of the 24 well plate for 3 minutes using a DMK21AF04 (Imaging Source) camera at a frame rate of 30 frames/second (fms) and recorded using Media Recorder (Noldus). Each fish was then individually assessed for activity using Ethovision XT software (Noldus). This software detects the number of changes in pixel intensity, which is attributed to movement.

2.6 Microscopy

2.6.1 Fluorescence microscopy

All images were visualized using an Axioimager.A1 microscope (Carl Zeiss, UK) with x63 1.4 oil objective and a fitted Retiga EXi camera (QImaging, Canada). Images were acquired with the Openlab v5.5.2. software (Improvision Ltd).

2.6.2 Confocal microscopy

Images were acquired on the Leica SPE confocal microscope using a Leica x63 1.3 oil objective with the Leica Application Suite Advanced Fluorescence software. Images were posteriorly analysed using ImageJ.

2.7 Drug screen

For the drug screen, wild-type and *btn1*Δ strains were grown overnight in MM to mid-log phase. Afterwards, they were transferred to YES medium with 0.1mg/ml CsA at a final concentration of 5 x 10^4 cells/ml for the wild-type strain and 1 x 10^5 cells/ml for the *btn1*Δ strain. 50µl of cultures were aliquoted into 384-well plates (Nunc) containing the library of pharmacologically active compounds (LoPac) 1280 Navigator collection (Sigma-Aldrich), with each compound replicated four times. The first column (16 wells) of each plate was aliquoted with *btn1*Δ untreated cells (negative control), and the last column (16 wells) aliquoted with wild-type untreated cells (positive control). Plates were incubated for 24 hours at 37°C. 10µl of a solution with 40% calcofluor and 60% propidium iodide diluted in 1X PBS (1:6 dilution) were added to each well, to label the cells. Plates were spun at 2000 rpm for 5 minutes and then imaged in the Opera imaging system. Six images per well were acquired, and all images were analysed in the CellProfiler software. The screen and analysis were performed by Dr Jamie Freeman of the Translational Research Resource Centre in the LMCB.

2.8 Data analysis and statistics

All measurements in yeast and mammalian cells were performed using ImageJ v1.45s software (NIH, USA). Preliminary data was analysed in Microsoft Excel v14.3.2. and subsequent statistical analysis were performed using Graphpad Prism 6.0c software (California, USA). Ordinary one-way ANOVA tests followed by Tukey's multiple comparison post-tests were performed.

All data shown represents the average value with the standard error of the mean (SEM) of at least three independent experiments. For the vacuoles size experiments, over 500 vacuoles were measured for each strain in each experiment; for the septation, cell curving, vacuole pH and viability assays over 300 cells were considered in each independent experiment.

The drug screen analysis was performed by Dr Jamie Freeman in the CellProfiler software and part of the mammalian cell data was analysed by Davide Marotta using the Fiji imaging software.

3 Results 1. Btn1p mutations affect the protein function in different manners

The first aims of this project were:

- to create fission yeast genomic integrants with GFP-tagged Btn1p expressed under the control of *nmt1* promoters with different strengths, and the control of its native promoter to permit uniform endogenous expression;

- to generate fission yeast genomic integrants with GFP-tagged *btn1* containing a deletion equivalent to the human 1-kb deletion and equivalents to the human missense mutations p.Glu295Lys and p.Gly187Ala;

- to assess the relative localisation and expression levels of the different strains;

- to characterise different yeast phenotypes associated with the complete loss of *btn1* and with the newly generated strains: vacuole size, septation index and cell curving.

3.1 Generating *S. pombe* genomic integrants of GFP-tagged Btn1p

In order to study and monitor the endogenous expression of Btn1p in *S. pombe*¸ the N-terminal of the protein was tagged with GFP. Different strains were generated, where GFP was under the control of the *nmt1* promoter and of the *btn1* native promoter.

Three strains with the *nmt1* promoter were generated, with three different types of this promoter: p3, wild-type strongest promoter (*nmt3*); p41, medium-strength promoter (*nmt41*); and p81, the weakest promoter (*nmt81*). The use of these promoters allowed the study of different levels of expression of Btn1p and their effects.

Besides having Btn1p tagged with GFP under the control of different *nmt1* promoters, a strain with GFP-tagged Btn1p under the control of *btn1* native promoter (GFP-*btn1*) was also created in order to study the endogenous level of this protein and look at its cellular location.

Once the four different strains with GFP-tagged Btn1p (GFP-*btn1*, *nmt3*, *nmt41* and *nmt81*) were obtained, they were further analysed, along with a wild-type strain (wt, 972) and a *btn1*Δ strain (*btn1*Δ) (first two rows in Table 2.1).

3.1.1 Making the constructs

For the construction of the *nmt1*-GFP-tagged proteins, a DNA fragment with the GFP cDNA under the control of the *nmt1* promoter (with different strengths) was created to replace the endogenous chromosomal *btn1* promoter by homologous recombination. This DNA fragment originated from a plasmid with the *kan*^{r} gene for selection, the *nmt1* promoter and GFP (Bahler *et al.* 1998). By PCR amplification, 100bp of the 5'UTR (untranslated region) of *btn1* were added upstream the *kan*^{r} gene, and the first 100bp of *btn1* open reading frame (ORF)

added downstream of GFP. The final purified PCR products were transformed into cells of *S. pombe* wild-type strain 972 (Figure 3.1.1 (A)).

In order to tag Btn1p with GFP to allow its expression under the native promoter of *btn1*, a different strategy was used. This consisted of, firstly, amplifying GFP-*btn1* from the plasmid pREP42GFP-Btn1 with primers containing two specific restriction sites (*Pst*I and *Apa*I). This product was then digested and ligated into a plasmid previously digested with the same enzymes and containing *btn1* flanks (pSL1180-Btn1flanks). Afterwards, the new construct was digested with two other specific enzymes (*Mlu*I and *Age*I) in order to obtain a fragment with the *btn1* gene, its flanks (both at 5' and 3'UTR) and the GFP gene upstream. The final fragment that was obtained was transformed in a *btn1::ura4* strain (where the *ura4* gene is replacing *btn1* in the same locus; Table 2.1) and integrants were selected with 5-fluoroorotic acid (FOA) (Figure 3.1.1 (B)). FOA leads to cell death in the presence of a wild-type active *ura3* gene in the yeast strain. FOA is converted to a toxic compound, 5-fluorouracil, and this reaction is mediated by an enzyme encoded by the *ura3* gene. This allows for a negative selection against yeast strains carrying the *ura3* gene.

All constructs, including primer positions and restriction sites, are summarised in Figure 3.1.1.

3.1.2 Protein expression levels and localisation

The different strains showed different levels of GFP expression, since differences were detected in the intensity of fluorescent signal detected by the confocal microscope. The fluorescent signal in the nmt3 *s*train was quite high and clearly visible, showing that *btn1* is overexpressed. The nmt41 strain showed faint but still visible fluorescence. The nmt81-*bnt1* strain did not express GFP at sufficient levels for any fluorescence to be detected. The GFP-*btn1* strain showed a weak fluorescent signal, which was expected since native and endogenous levels of Btn1p are known to be very low (Codlin & Mole 2009).

Therefore, only *nmt3-btn1* and GFP-*btn1* strains were used for localisation experiments.

The GFP tag at the N-terminal of the protein allowed for analysis of the localisation and trafficking of Btn1p. It was expected that, just like the ectopically expressed GFP-Btn1p, all the tagged integrated strains localise in the Golgi and are capable of trafficking to the vacuole (Codlin & Mole 2009). In fact, in both strains (nmt3 and GFP-btn1), Btn1p co-localised mostly with a vacuolar membrane marker, FM4-64. According to the images, Btn1p seems to localise in punctate structures as well, probably in the Golgi (Figure 3.1.2). In order to confirm this, other markers for these cell organelles have to be used in the future.

Figure 3.1.1. Constructing different GFP-tagged Btn1p strains

(A) Construction of *nmt1*-GFP-*btn1* strains. Arrows within the boxes show directions of transcription; White boxes: kanMX6 module containing the promoter and terminator sequences of the *Ashbya gossypii* translation elongation factor 1α gene together with the kan^r gene from *E. coli*; *S. pombe nmt1* promoter, and the GFP tag from the jellyfish *Aequorea victoria*. Grey boxes: sequences from *btn1* gene, including its 5'UTR. The size of the boxes is not proportional to their real size. Forward primer (F primer) has 100bp of 5'UTR of *btn1,* including part of its promoter, and 20bp of the *kan^r* gene and its TEF terminator sequence. Reverse primer (R primer) has the first 100bp of the *btn1* ORF and 20bp of GFP. Construct was integrated into the yeast genome by homologous recombination (HR), after being transformed into the cells.
(B) Construction of GFP-tagged Btn1p under the control of its native promoter. GFP-*btn1* fragment was amplified from the pREP42GFP-Btn1 plasmid using primers containing two restriction sites, *Pst*I and *Apa*I. Both primers and sites are indicated in the diagram. Bold arrows represent ligation between the GFP-*btn1* fragment and the pSL1180 plasmid containing *btn1* flanks separated by multiple restriction sites including *Pst*I and *Apa*I. White arrow represents digestion of pSl1180 plasmid (containing already inserted GFP-*btn1*) with *Mlu*I and *Age*I restriction enzymes, in order to create the final fragment (right side panel) that was transformed into *btn1::ura4* cells. After transformation, the *ura4* gene was replaced with GFP-*btn1* by HR. 5'F and 3'F in the final fragment represent the 5' and 3' *btn1* flanks, respectively.

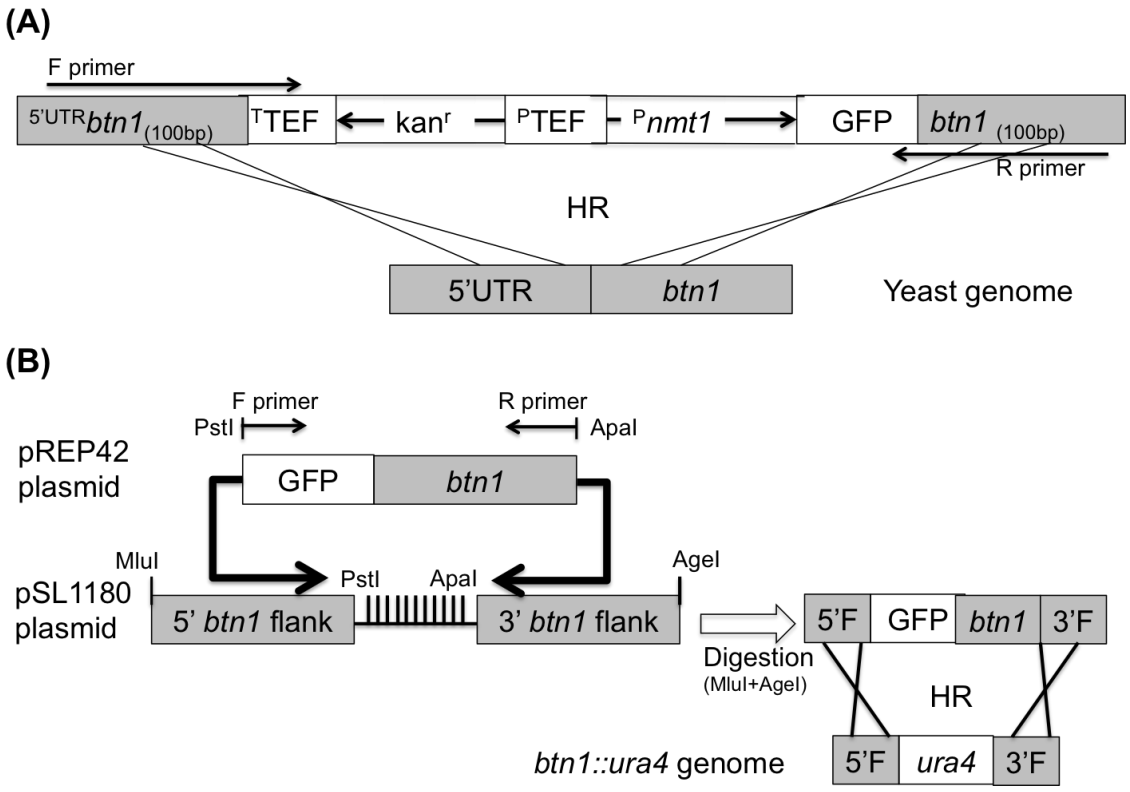

Figure 3.1.2. Localisation of GFP-Btn1p

Strains with GFP-tagged Btn1p. Images obtained by confocal microscopy showing fluorescent signal from Btn1p in green. Strain with GFP-*btn1* under the control of the *nmt1* p3 promoter (nmt3-*btn1*) (upper left side panel) and strain with GFP-tagged Btn1p where Btn1p is expressed at its normal native levels (GFP-*btn1*) (upper right side panel). The image on the right panel was manipulated in order to increase the visible GFP signal that was originally very weak. Btn1p co-localises with vacuolar membrane marker, FM4-64, but not totally (lower panel). Cells labelled with FM4-64 (red), expressing GFP from Btn1p (green) and co-localisation of GFP signal with labelled vacuoles. Scale bars – 4.38µm.

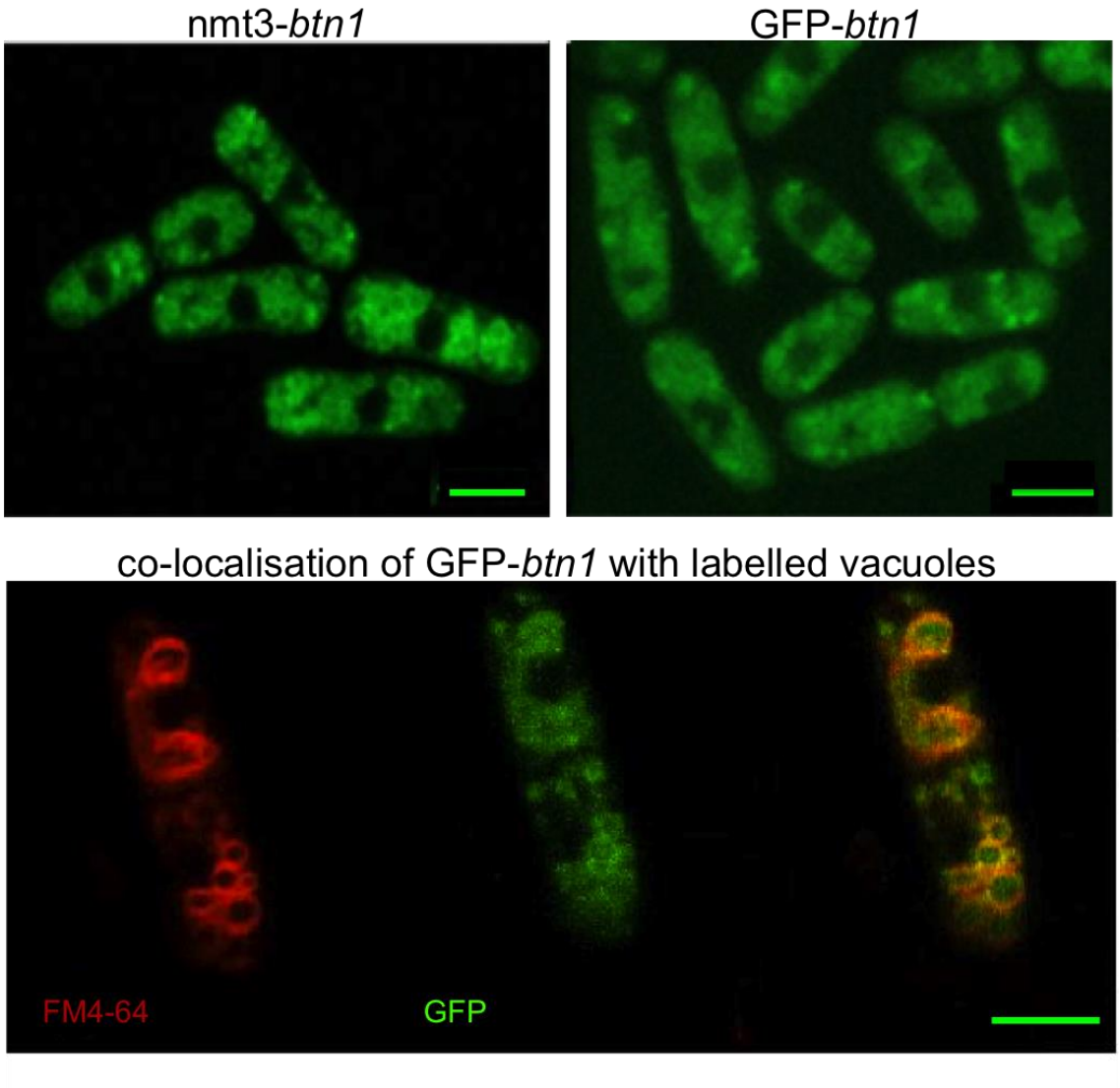

3.2 Generating *S. pombe* genomic *btn1* mutants

Three different strains with integrated GFP-tagged Btn1p containing three different mutations were generated.

The first strain includes the deletion equivalent to the 1-kb deletion in *CLN3* (1kbΔ strain). More specifically, the equivalent to the transcript containing exons 1-6 spliced to exon 9, which, if expressed, would encode the first 153 amino acids of *CLN3* (or 102 amino acids in *S. pombe*) followed by a frame shift, 28 novel amino acids and a stop codon (102fsX5). This strain was designated as 1kbΔ and represents the most common *CLN3* deletion present in juvenile NCL patients.

Moreover, two other strains with genomic *btn1* containing two missense mutations specific to juvenile CLN3 disease were generated: one with the p.E240K mutation (E240K strain), equivalent to the human p.Glu295Lys mutation in CLN3, and the other containing the p.G136A mutation (G136A strain), equivalent to the p.Gly187Ala mutation. The first mutation is associated with the mildest phenotype identified in juvenile NCL, and the second resembles the complete deleted strain *btn1*Δ in terms of phenotype (Haines *et al.* 2009).

3.2.1 Generating the mutants

To construct these three integrated GFP-tagged mutants, a similar approach used to create the GFP-*btn1* strain was used (Figure 3.1.1 (B)).

The initial plasmids used as templates for the first PCR reaction were pREP42GFP-Btn1 plasmids, with *btn1* containing the desired mutations, such as the 1-kb deletion, the p.E240K and the p.G136A mutations. These mutations had been inserted into the *btn1* gene using the QuickChange Site-Directed Mutagenesis approach. The primers used to amplify the mutated *btn1*

contained two specific restriction sites to facilitate the cloning into a plasmid containing *btn1* flanks (pSL1180-Btn1flanks). Afterwards, this plasmid was digested with two other specific enzymes in order to obtain a fragment with the mutated *btn1* gene, its flanks (both 5' and 3'UTR) and GFP upstream. The final fragment that was obtained was transformed in a *btn1::ura4* strain (Table 2.1) and integrants were selected with FOA.

3.2.2 Localisation and expression levels of integrated mutants

One of the goals of tagging Btn1p in these three different mutant strains is to look at the localisation of these mutants in the cell and see how their levels of expression differ from wild-type Btn1p. Although it has been previously reported that the mutant protein with the 1-kb deletion and the p.G136A mutation are localised in the endoplasmic reticulum and/or the Golgi, and the one containing p.E240K in prevacuolar compartments (Haines *et al.* 2009), it was not possible to confirm this with certainty since no co-staining with subcellular markers was done. However, according to the GFP signal present in the cells, it is clear that there are differences between the mutant strains and the wild-type tagged strains mentioned in the sections above, more specifically in their expression levels. The strain with the p.G136A mutation is the one showing the less intense GFP signal, whereas the p.E240K mutation shows similar fluorescence intensity to wild-type Btn1p (Figure 3.2.1). This is expected in regards to the effects that the equivalent human mutations have in the juvenile NCL patients, where p.Glu295Lys underlies the mildest form of the disease. In summary, different mutations cause differences in the levels of GFP expression, based in different intensities of fluorescent signal detected by the confocal microscope. In order to confirm the exact localisation, other markers for cell organelles have to be used in the future. And also to confirm and quantify the differences in expression levels, a Western Blot assay has to be performed, since measurement based on the GFP microscope signal is merely qualitative and relative.

Figure 3.2.1. Localisation of Btn1p integrated mutants

Yeast strains with wild-type GFP-tagged Btn1p (upper left panel) and containing the 1-kb deletion (upper right panel), the G136A mutation (lower left panel) and the E240K mutation (lower right panel). Scale bars – 4.4μm (GFP-*btn1*), 7μm (GFP-1kbΔ) and 10 μm (GFP-E240K and G136A).

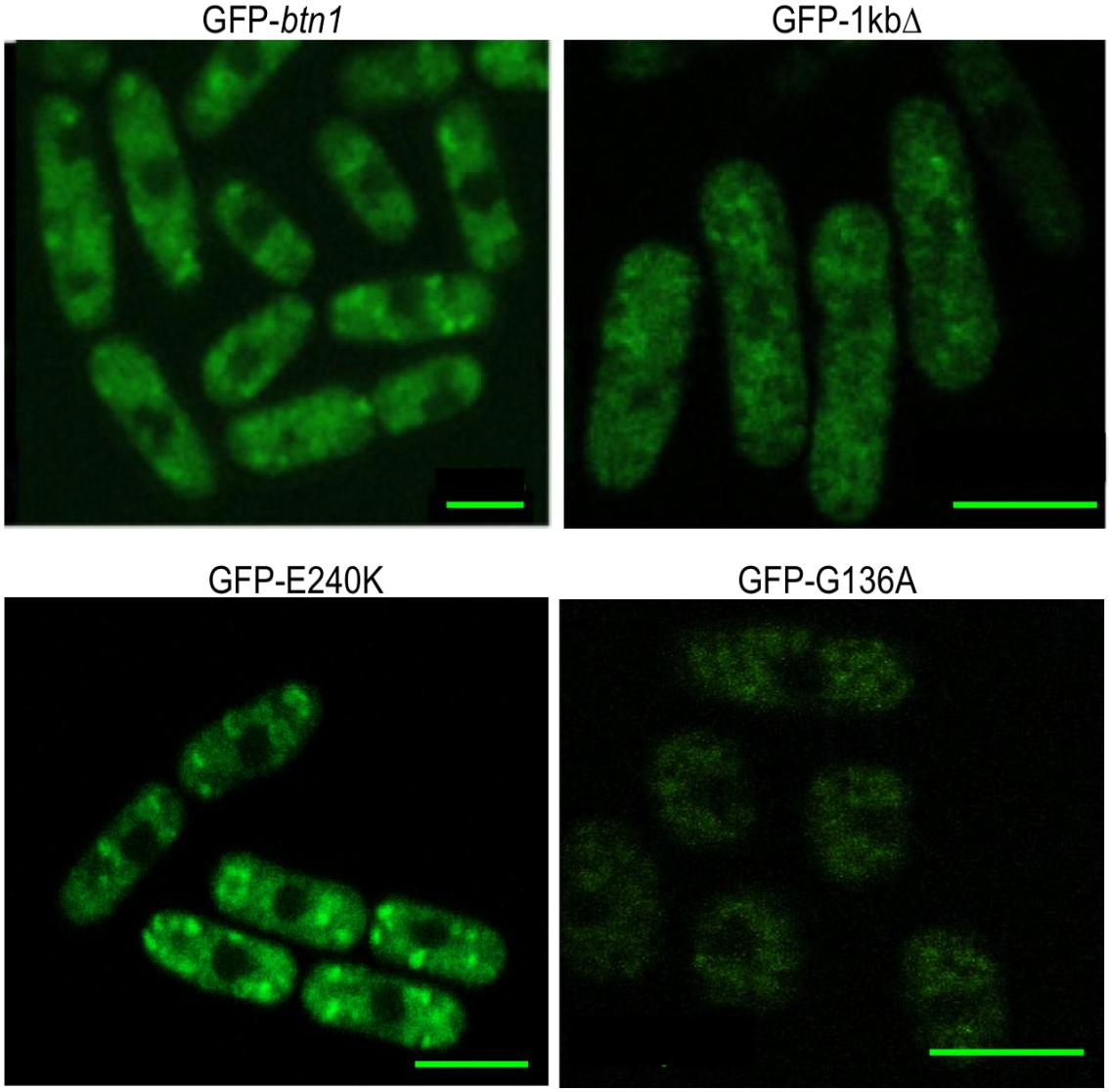

3.3 Characterising phenotypes of integrated Btn1p mutants

It is known that cells deleted for *btn1* exhibit many phenotypes, and that some disease mutant Btn1p proteins exhibit activity that restores one or more of these phenotypes, because the mutation does not completely abolish Btn1p function. Therefore, the newly created integrated mutant strains were investigated and characterised and the effect of the endogenously expressed mutant proteins analysed on the different phenotypes. Three phenotypes were chosen to be analysed first, since these were previously studied in *btn1*Δ cells with ectopically expressed mutant proteins (Haines *et al.* 2009). Two of these phenotypes are present at the permissive growth temperature (30ºC), and the other becomes apparent at a high temperature of 37ºC: an increase in the vacuoles size, a delay in cytokinesis (illustrated by an increase in the number of septated cells) and curving of cells after 4 hours at 37ºC. All three of the phenotypes can be fully rescued by ectopic expression of GFP-Btn1p from the pREP42GFP-Btn1 plasmid (Figures 3.3.1, 3.3.2 and 3.3.3) but not by expression of the empty pREP42 vector (data not shown).

Besides looking at different phenotypes in the mutant strains, the GFP-tagged strains were also analysed, to verify the effect of the tag protein and the Btn1p expression level in the phenotypes. Analysed strains included: the 972 wild-type (wt), the tagged strains where GFP is under the control of the strong *nmt1* promoter p3 (*nmt3*) and the medium promoter *nmt1* p41 (*nmt41*), the tagged strain with GFP under the control of the native promoter of *btn1* (GFP-*btn1*), the GFP-1kbΔ strain (1kbΔ), the mutant tagged strains GFP-E240K (E240K) and GFP-G136A (G136A), and finally the *btn1*-deleted (*btn1*Δ).

3.3.1 Vacuole size

The average vacuole size of different mutant and tagged wild-type strains was measured and compared to wild-type untagged cells and *btn1*Δ cells. Vacuoles

were measured in five independent experiments, where at least 500 vacuoles were measured in each one.

Cells deleted for *btn1* have significantly larger vacuoles than wild-type cells, and ectopic expression of Btn1p significantly reduces the vacuole size to a similar size to those of wild-type cells. In this case, the mean vacuole size of the G136A strain, which models a disease-causing missense mutation that had previously been shown as not being able to rescue vacuole size (Haines *et al.* 2009), was included as an additional negative control, similar to *btn1*Δ. Expression of any of the other mutants (1kbΔ and E240K) was sufficient to significantly rescue the vacuole size defect of *btn1*Δ cells as effectively as Btn1p, with the mean vacuole diameter being around 0.9 μm for these mutants, compared to 1.02 μm for *btn1*Δ cells or 1 μm for G136A (Figure 3.3.1). This suggests that the 1-kb deletion and the p.E240K mutation of *btn1* (and *CLN3*), are not complete null mutations, since expression of protein products modelling these mutations causes vacuole size to decrease in a significant manner, suggesting that they retain significant function in *S. pombe,* as documented before (Haines *et al.* 2009). This result has been confirmed in mammalian cell studies, at least for the 1-kb deletion, using expression of mammalian *CLN3* constructs similar to those described here (Kitzmuller *et al.* 2008).

As expected, wild-type strains (wt, nmt3, nmt41, GFP-btn1) show the smaller vacuoles, with sizes ranging from 0,85 to 0,9 μm. Although slight variations are observed between the four wild-type strains, these differences in the vacuole size are not significant. (Figure 3.3.1).

Figure 3.3.1. Vacuole size of different strains

The *btn1*Δ strain has larger vacuoles than wild-type strain. Images show vacuoles labeled with FM4-64 of wt (left) and *btn1*Δ (right) strains. Scale bars - 10µm. Graph shows the mean (±SEM) of the vacuoles diameter (in µm) in different strains from five independent experiments, where at least 500 vacuoles were measured in each one. Statistical significances between each strain were determined using a one-way ANOVA with a Tukey's multiple comparison post-test. Statistical significances between wild-type and *btn1*Δ and G136A are represented in the graph above the bars (****p= <0.0001). Strains: wt – wild-type; nmt3 – GFP-*btn1* under the control of the *nmt1* p3 promoter; nmt41 - GFP-*btn1* under the control of the *nmt1* p41 promoter; GFPbtn1 – GFP-tagged Btn1p; btn1d – *btn1*Δ strain; 1kbD – *btn1* with 1-kb deletion; E240K – *btn1* with the E240K mutation; G136A – *btn1* with the G136A mutation; btn1D+btn1 – *btn1*Δ strain transformed with the pREP42GFPbtn1 plasmid.

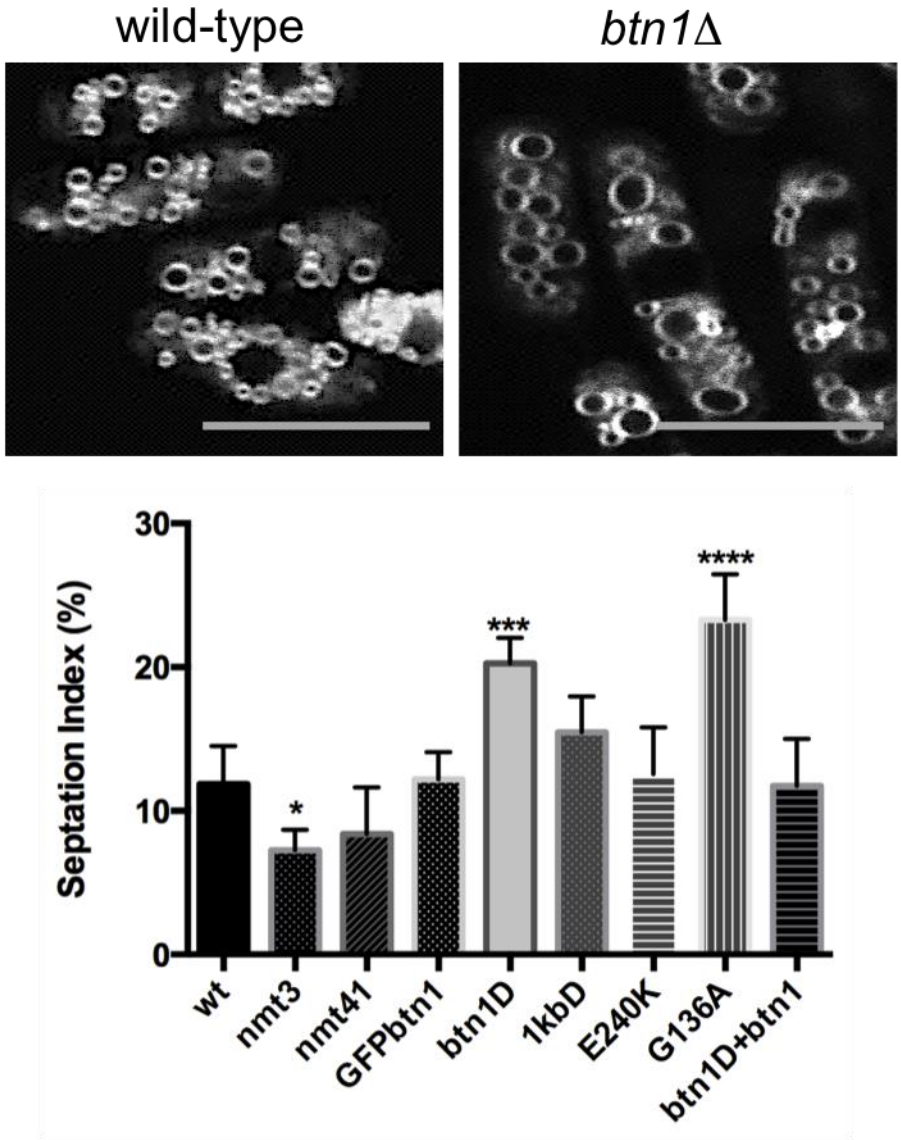

3.3.2 Septation index

Septation index (the percentage of septated cells in the total number of cells) of different strains was calculated and the obtained values from five independent experiments are shown in Figure 3.3.2. At least 300 cells were counted in each experiment. Septation index is an indication of the amount of cells that are halted in the cytokinesis process, and therefore, when this value is higher than normal it suggests a delay in the cell cycle

Wild-type strains, as well as the mutant E240K strain, show significantly less septated cells than the G136A and btn1Δ strains. The wild-type strains show the same pattern as seen in the vacuoles size phenotype, where the nmt3 and the nmt41 strains have a slightly lower septation index (7% and 8.36%) than the wt strain (11.87%) and the GFP-*btn1* (11.19%) is the one with the highest value from the four wild-type strains. In fact, there is a significant difference between the wild-type and the nmt3 strains. Once again this suggests that the level of expression of Btn1p influences the manifestation of the phenotypes associated with its deletion.

The E240K strain has a septation index value that is very similar to the wt strain (11.27%), and the 1kbΔ strain showed a small but significant reduction ($p=<0.1$) in the septation index compared to *btn1*Δ cells (15.3%), suggesting once again that these mutant proteins retain significant function. The other two strains, G136A and *btn1*Δ, showed a value significantly higher than the other six strains (23.28% and 20.26% respectively). Ectopic expression of Btn1p in the *btn1*Δ strain significantly reduces the septation index to a similar value to wild-type strain (11.74%).

Figure 3.3.2. Septation index of different strains

*btn1*Δ strain has a higher septation index than wild-type strain. Images show yeast cells stained with calcofluor, delineating cell walls and septa: wt (left) and *btn1*Δ (right) strains. Scale bars - 10µm. Graph shows the mean (±SEM) septation index (percentage of septated cells in total number of cells) of different strains from five independent experiments, where at least 300 cells were counted in each one. Statistical significances between each strain were determined using a one-way ANOVA with a Tukey's multiple comparison post-test. Statistical significances between wild-type and *btn1*Δ and G136A are represented in the graph above the bars (*p=<0.1***p=<0.001****p=<0.0001). Strains: wt – wild-type; nmt3 – GFP-*btn1* under the control of the *nmt1* p3 promoter; nmt41 - GFP-*btn1* under the control of the *nmt1* p41 promoter; GFPbtn1 – GFP-tagged Btn1p; btn1D – *btn1*Δ strain; 1kbD – *btn1* with 1-kb deletion; E240K – *btn1* with the E240K mutation; G136A – *btn1* with the G136A mutation; btn1D+btn1 – *btn1*Δ strain transformed with the pREP42GFPbtn1 plasmid.

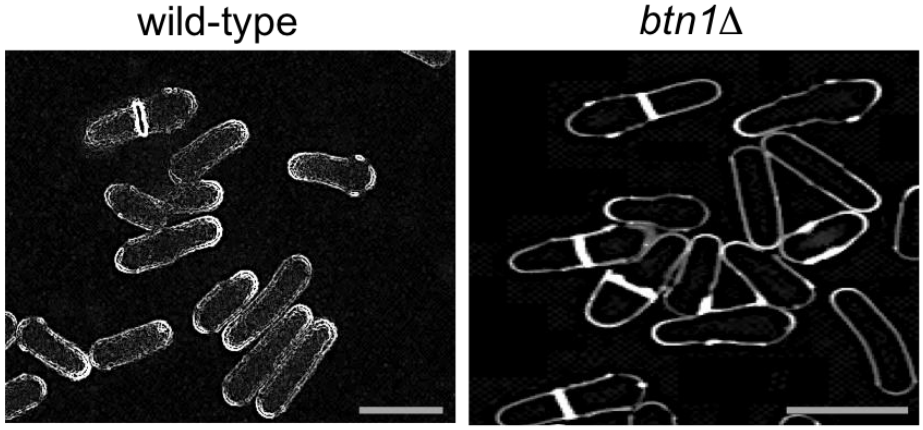

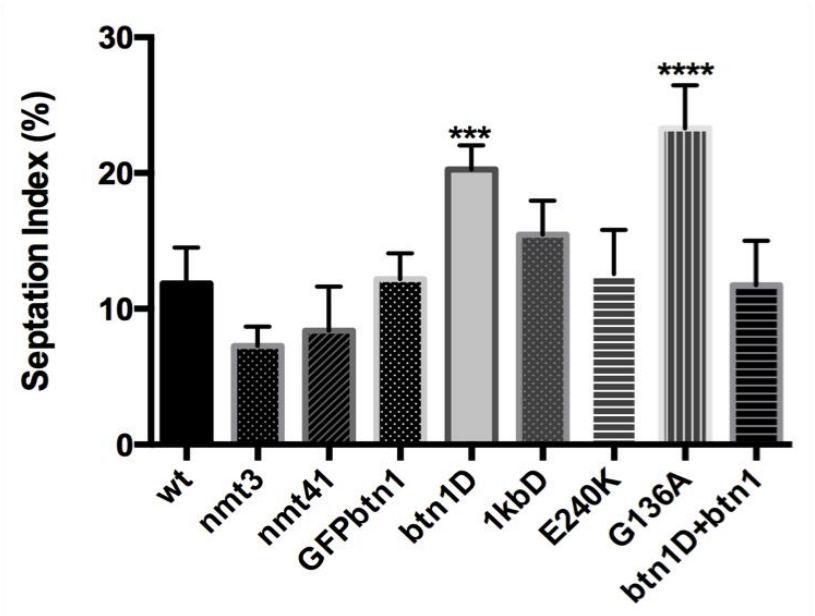

3.3.3 Cell curving

The number of curved cells (cells that lost their normal rod shape and became curved or bent) was calculated for eight different strains, and percentage of curved cells (in total number of cells) obtained from five independent experiments are shown in Figure 3.3.3. At least 300 cells were counted in each experiment. For this phenotype, the nmt41 strain was not included.

1kbΔ, G136A and *btn1*Δ strains show significantly more curved cells than the wild-type strains. The wild-type strains show the same pattern as mentioned above (sections 3.3.1 and 3.3.2), where the nmt3 strain shows slightly less curved cells (9.34%) than the wt strain (10.53%). However, in this case, the GFP-*btn1* strain showed less curved cells than the other two (8.95%). Differences between these wild-type strains are not statistically significant.

The E240K strain has a similar fraction of curved cells to the wt strain (9.02%) and significantly lower than the *btn1*Δ strain, suggesting once again that this mutant protein retains significant function. Other values of strains with higher percentage of curved cells are: 19.84% for the 1kbΔ strain, 23.99% for the G136A strain and 22.45% for the *btn1*Δ strain, the highest value, as expected. These values are significantly different from the three wild-type and the E240K strains. Ectopic expression of Btn1p in the *btn1*Δ strain significantly reduces the number of curved cells to a similar value than wild-type strain (10.58%).

Figure 3.3.3. Cell curving of different strains

The *btn1*Δ strain shows more curved cells than wild-type strain. Images show yeast cells stained with calcofluor, after growth at 37°C for 4 hours: wild-type (left panel), *btn1*Δ (middle panel) and the 1kbΔ (right panel) strains. Arrows indicate curved cells. Scale bars – 10μm. Graph shows the mean (±SEM) cell curving percentage (percentage of curved cells in total number of cells) of different strains from five independent experiments, where at least 300 cells were counted in each one. Statistical significances between each strain were determined using a one-way ANOVA with a Tukey's multiple comparison post-test. Statistical significances between wild-type and *btn1*Δ, 1kbΔ and G136A are represented in the graph above the bars (****p= <0.0001). Strains: wt – wild-type; nmt3 – GFP-*btn1* under the control of the *nmt1* p3 promoter; nmt41 - GFP-*btn1* under the control of the *nmt1* p41 promoter; GFPbtn1 – GFP-tagged Btn1p; btn1D – *btn1*Δ strain; 1kbD – *btn1* with 1-kb deletion; E240K – *btn1* with the E240K mutation; G136A – *btn1* with the G136A mutation; btn1D+btn1 – *btn1*Δ strain transformed with the pREP42GFPbtn1 plasmid.

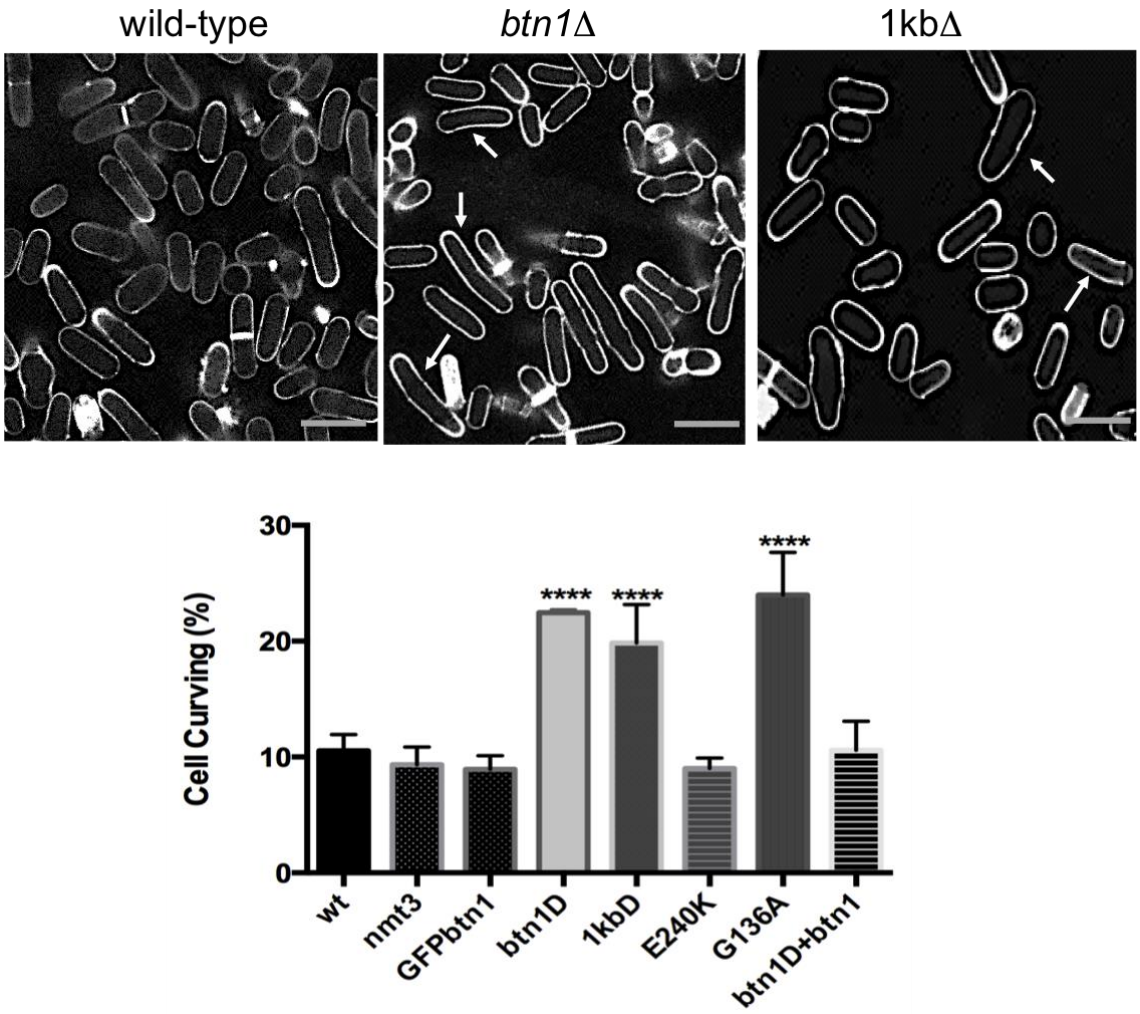

3.4 Summary

Overexpression of *btn1* (when under the control of the *nmt1* p3 promoter) overcompensates phenotypes seen in *btn1*-deleted cells. Values recorded for the nmt3-GFP-*btn1* strain were lower than the wild-type 972 strain values in all the phenotypes that were analysed: vacuole size, septation index and cell curving. This nmt3 strain also has smaller vacuoles and significantly less septated cells than the strain where Btn1p is tagged with GFP under the control of its native promoter.

It had previously been demonstrated that the most common mutation of *CLN3*, a large intragenic deletion of about 1-kb is not a null mutation that completely abolishes CLN3 function, since the mutant protein retains some function (Kitzmuller *et al.* 2008; Haines *et al.* 2009). This observation was corroborated in this study, since the strain containing Btn1p^{102fsX5} (which models a transcript expressed in cells from patients homozygous for the 1-kb deletion) showed significant rescue of two phenotypes (increased vacuole size and septation index) almost as effectively as the full-length protein.

As for the p.E240K mutation, the mutant Btn1 protein is able to rescue all three phenotypes examined in this chapter, showing that this mutation (which is equivalent to the human mutation that underlies a markedly protracted form of juvenile NCL) does not affect the function of Btn1p as much as the 1-kb deletion. Understanding why this is the only mutation capable of rescuing the cell curving phenotype and studying its molecular basis may reveal a novel target for therapies to delay onset of symptoms in juvenile CLN3 disease.

On the other hand, the p.G136A mutation did not rescue any of the phenotypes, indicating that it affects the protein function to a greater extent than the other two mutations. This may be a null mutation that leads to a significant reduction in the protein levels.

All the three mutations are sufficient to change the levels of expression of Btn1p and possibly its localisation, according to the GFP fluorescent signal that was

observed. All showed a different signal pattern when visualized under the microscope. To further clarify the localisation of the different mutant proteins, other organelle markers have to be used.

Taken together these results show that different integrated mutations affect Btn1p function differently leading to diverse phenotypes.

4 Results 2. Drug Screen

The aims of this part of the project were:

- to explore different *btn1*Δ phenotypes in order to identify a robust and specific phenotype suitable for a high-throughput drug screen: sensitivity to chemicals such as ANP, chloroquine and cyclosporine A and to high temperature, and increased vacuole pH;

- to optimise the conditions for the performance of the drug screen;

- to perform the screen based on a library with 1280 FDA-approved small compounds in the Translational Research Resource Centre at the LMCB.

4.1 Exploring different phenotypes as basis of a screen

In order to find a robust and striking phenotype that is easily identified when rescued and significantly different between wild-type and *btn1*-deleted strains, several conditions and characteristics were tested. These included sensitivity to certain chemicals such as ANP, chloroquine and cyclosporine A (CsA); growth at higher temperature (37°C) and differences in vacuole pH. The majority of these phenotypes were not adequate for the desired purposes. However, growth in the presence of cyclosporine A at 37°C was eventually selected as the basis for the drug screen.

4.1.1 Sensitivity to ANP and chloroquine

The first phenotype to be analysed was growth in the presence of ANP, a chemical that was previously reported to differentially affect the *BTN1*Δ strain in *S. cerevisiae* (Pearce & Sherman 1998). In budding yeast, this *BTN1*Δ strain shows resistance to ANP but the average vacuolar pH is more acidic than wild-type cells, contrary to what is seen in fission yeast. Since the resistance to this chemical is pH-dependent, I hypothesized that *btn1*Δ *S. pombe* strain could be more sensitive to ANP than wild-type cells. Therefore, a spot assay was performed in MM plates containing ANP at two different concentrations (0.75 mM and 1 mM) to determine if there was a difference in the growth of wild-type and *btn1*Δ *S. pombe* strains. This experiment was replicated three independent times with three similar plates in each. At both concentrations, there was no striking difference between the patterns of growth of the two strains (Figure 4.1.1). Therefore, the loss of *btn1* does not confer resistance or sensitivity to this chemical, and this phenotype cannot be used for a screen. Cells were also spotted onto MM plates without any added substance as a control (data not shown).

Other chemical, chloroquine, was added to the medium to test if the combination of the two chemicals could reveal a difference between wild-type

and *btn1*Δ. In a study with budding yeast, chloroquine was shown to reverse the resistance of the *BTN1*Δ strain to ANP, by elevating the vacuole pH (Pearce *et al.* 1999a), and therefore this combination (ANP and chloroquine) was chosen to be tested in *S. pombe* to verify if there was sensitivity in the strain lacking *btn1.* The addition of 0.1 mM of chloroquine to the medium didn't change the pattern of growth of the two strains in a significant manner (Figure 4.1.1).

Figure 4.1.1. Spot assays of wild-type and *btn1*Δ strains in plates with ANP and chloroquine

*btn1*Δ strain is not sensitive to ANP and/or chloroquine. Wild-type and *btn1*Δ cells were serially diluted from a log-phase culture ($1x10^6$ cells/ml) and spotted onto Minimal Medium (MM) plates containing either 0,75mM (upper left panel) or 1mM (upper right panel) of ANP; or 1mM ANP+0.1mM chloroquine (lower panel). Plates were then incubated at 30°C for 6-7 days to determine the growth in the presence of these chemicals. This assay was replicated thrice. wt – wild-type strain; *btn1*Δ – *btn1*-deleted strain.

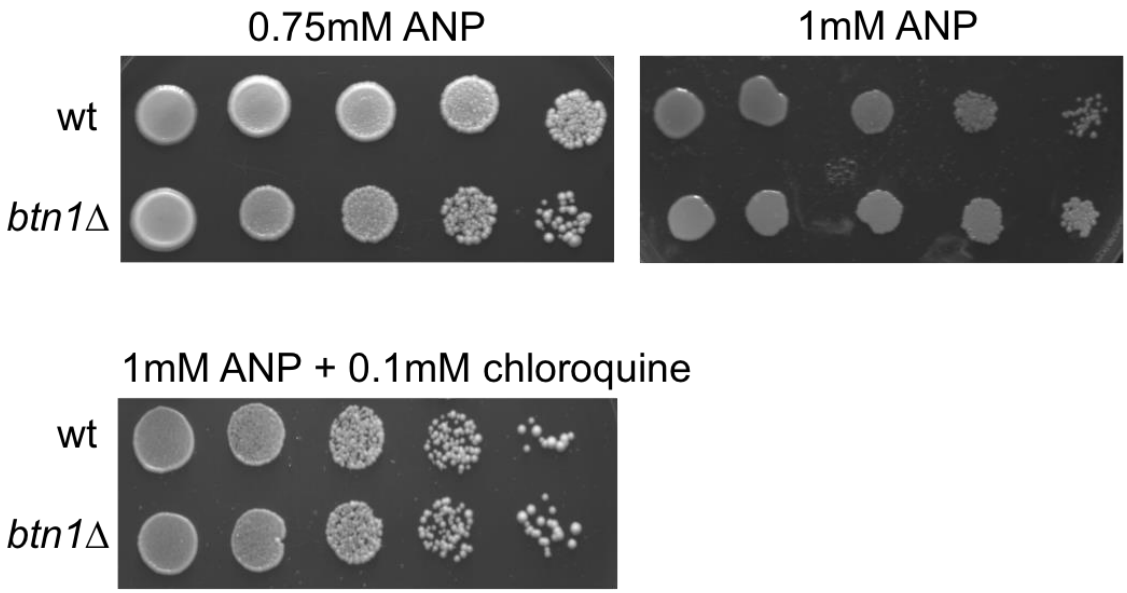

4.1.2 Growth at high temperature (37°C)

Growth in rich medium at a higher temperature than the permissive one, 37°C, was analysed at two different points, after 24 and after 48 hours. Cells were stained with the cell impermeant nucleotide stain propidium iodide to mark dead cells and calcofluor white to mark the total cell population. The viability (percentage of live cells in total number of cells) was measured for four strains: wild-type, *btn1*Δ, E240K and 1kbΔ. At least 300 cells were counted in three independent experiments. Besides this experiment, a spot assay in YES plates incubated at 37°C was done, with the same four strains (not shown).

The high temperature of 37°C affects the growth of mutant and *btn1*-deleted strains but does not cause a strong complete inhibition of growth in these strains, which would be necessary for a rescue screen. For instance, although there was a significant difference between the wild-type and the *btn1*Δ strains, the percentage of dead cells with no *btn1* was not high enough to be able to readily identify a significant rescue by any drug or compound (around 22.1% viability after 48 hours). Moreover, the viability of wild-type cells after 48 hours was not high enough (52.31%). Neither one of the mutant strains (1kbΔ and E240K) showed a significant difference from the wild-type strain (59.22% and 47.83% after 48 hours, respectively) (Figure 4.1.2).

Furthermore, liquid cultures, after growth for 48 hours at 37°C, were plated onto YES plates and incubated at 37°C again, to examine the extent of cell death. However, colonies were able to grow in the plates, and therefore, once again, it was proven that this phenotype is not adequate for developing a drug screen.

Figure 4.1.2. Growth of different strains at 37°C

Cell viability of wt, E240K, 1kbΔ and *btn1*Δ strains upon growth in YES medium at a high temperature of 37°C over two periods of 24 and 48 hours (after the temperature shift). The graph shows the survival curve of different strains at three time points, after cultures were shifted from 30 to 37°C: 0, 24 and 48 hours. Data shown is a mean (±SEM) of 3 independent experiments. Survival is the percentage (%) of live cells in total number of cells. Statistical significances between each strain were determined using a one-way ANOVA with a Tukey's multiple comparison post-test. Statistical significances between wild-type and *btn1*Δ are represented in the graph (***p= <0.001). wt – wild-type; btn1D – *btn1*Δ strain; 1kbD – *btn1* with 1-kb deletion; E240K – *btn1* with the E240K mutation.

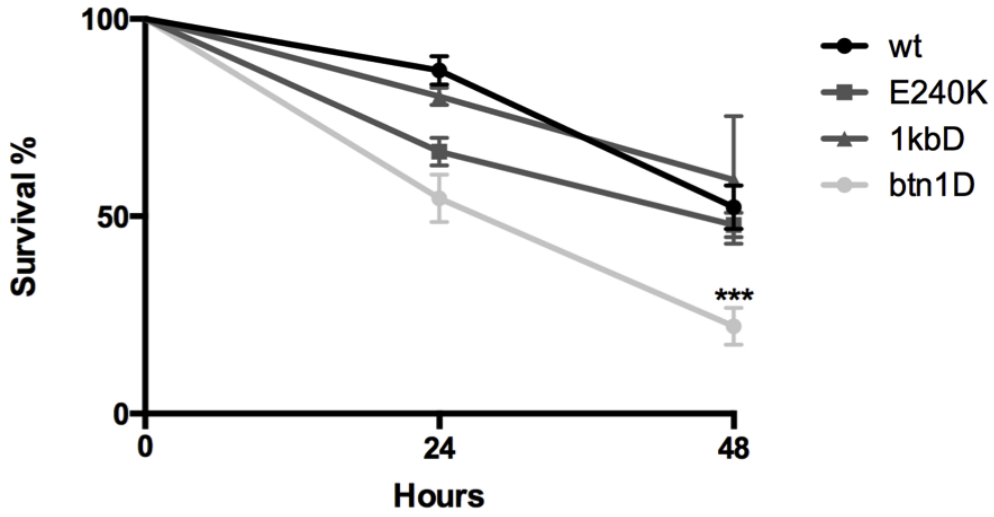

4.1.3 Vacuole pH

It was previously shown that cells deleted for *btn1* have larger and less acidic vacuoles than wild-type cells (Gachet *et al.* 2005). Therefore, these strains, along with 1kbΔ and E240K, were labelled with LysoSensor to compare vacuole pH, where the intensity of fluorescence obtained correlates with vacuole pH – the more intense the fluorescence, the lower the pH. Intensity was measured in units of corrected total cell fluorescence (CTCF). At least 300 cells were counted in three independent experiments. As expected, wild-type cells showed a significantly higher fluorescence than *btn1*Δ cells, corresponding to more acidic vacuoles. 1kbΔ cells showed an intermediate value of fluorescence, with a vacuole pH value between wild-type and *btn1*Δ, but not significantly different from any of them (Figure 4.1.3).

Although this phenotype could be used for a drug screen, since there is a detectable and significant difference between cells with and without *btn1*, after further testing, it was shown that the intensity of fluorescence from the LysoSensor was not high enough to be differentially detected and measured in the Opera Software, and therefore, this phenotype was considered as not suitable for screening with this robot.

Figure 4.1.3. Vacuole pH of different strains

btn1∆ strain have less acidic vacuoles than wild-type strain. The graph shows the mean (±SEM) corrected total cell fluorescence (CTCF) intensity of vacuoles of wild-type (wt), 1kbΔ and *btn1*Δ strains. Vacuoles were labelled with LysoSensor dye: the intensity of fluorescence inversely correlates with vacuole pH - the more intense the fluorescence, the lower the pH. Data shown was collected from 3 independent experiments. Statistical significances between each strain were determined using a one-way ANOVA with a Tukey's multiple comparison post-test. Statistical significances between wild-type and *btn1*Δ are represented in the graph above the btn1D bar (*p= <0.1). wt – wild-type; 1kbD – *btn1* with 1-kb deletion; btn1D - *btn1*Δ strain.

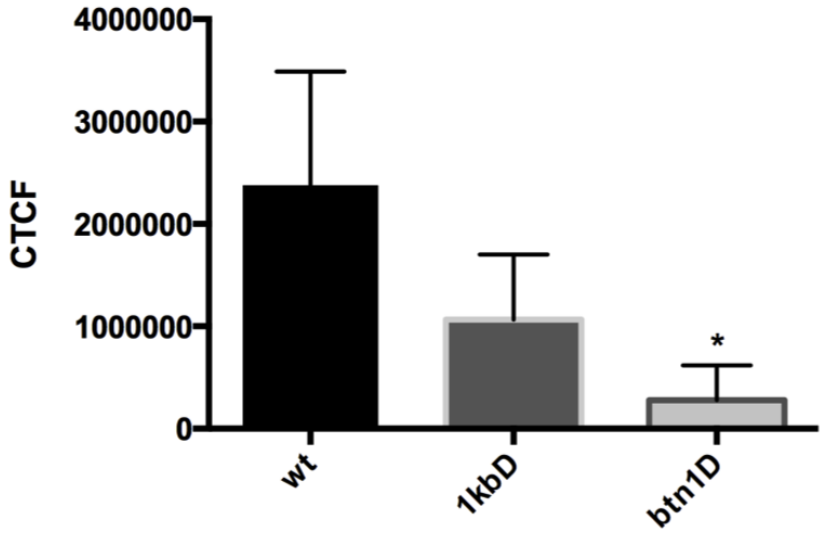

4.1.4 Sensitivity to cyclosporine A at 37°C

It was found that the *btn1*Δ strain is sensitive to cyclosporine A (CsA), an inhibitor of calcineurin. The link between Btn1p and calcineurin and/or CsA will be explored in the Discussion Chapter. Furthermore, in order to exacerbate the phenotype, strains were grown at 37°C. There was a significant difference between viability of wild-type and *btn1*Δ strains when grown in these conditions. In the presence of cyclosporine A (0.1 mg/ml) at a high temperature of 37°C, *btn1*Δ cells were not able to grow; the growth was completely inhibited, both in a spot assay (Figure 4.1.4 A) and when 10^6 cells were plated in plates with CsA (not shown). Since the presence of this chemical was shown to greatly affect the growth of *btn1*Δ strain, growth of all the integrated mutant strains were also analysed in these conditions: 1kbΔ, E240K and G136A. None of these strains showed sensitivity to the chemical, even at a higher concentration of 0.15mg/ml (Figure 4.1.4).

Viability of liquid cultures in the presence of CsA and at 37°C, after 24 hours of growth, was also measured for all the five strains, following the same approach that was used for viability at 37°C with propidium iodide and calcofluor staining (section 4.1.2). At least 300 cells were counted in three independent experiments. A significant difference was seen between the number of wild-type and *btn1*Δ dead cells (viabilities of 94.07% and 5.68%, respectively). Regarding the mutant strains, the G136A strain is the only one showing sensitivity to CsA, in liquid culture (11.79%); E240K and 1kbΔ showed similar viability values to wild-type: 81.71% and 84.86%, respectively (Figure 4.1.4). Thus, once again, partial function of Btn1p was able to be distinguished from complete lack of function.

Therefore, this phenotype was selected to be the basis for a high-throughput screen using the *btn1*Δ strain. However, it was not suitable for mutation-specific screening.

Figure 4.1.4. Sensitivity of different strains to cyclosporine A at 37°C

*btn1*Δ is sensitive to cyclosporine A (CsA). Spot assays of different strains in YES plates with 0.1 mg/ml of CsA were done by serially diluting cells from a log-phase culture ($1x10^6$ cells/ml) and spotted onto YES plates containing 0.1 mg/ml of CsA. Plates were then incubated at 37°C for 3-4 days to determine growth at 37°C in the presence of CsA. Cells were also spotted onto YES plates lacking CsA as a control (data not shown). The graph represents the cell viability of wt, E240K, 1kbΔ, G136A and *btn1*Δ strains upon growth in YES medium with CsA (0.1mg/ml) at a high temperature of 37°C over 24 hours (after the temperature shift). The graph shows the survival curve of different strains at two time points, after cultures were shifted from 30 to 37°C: 0 and 24 hours. Data shown is a mean (±SEM) of 3 independent experiments. Viability is the percentage (%) of live cells in total number of cells. Statistical significances between each strain were determined using a one-way ANOVA with a Tukey's multiple comparison post-test. Statistical significances between wild-type and *btn1*Δ and G136A are represented in the graph (****p= <0.0001). wt – wild-type; *btn1*Δ – *btn1*-deleted strain; 1kbΔ – *btn1* with 1-kb deletion; E240K – *btn1* with the E240K mutation; G136A - *btn1* with the G136A mutation.

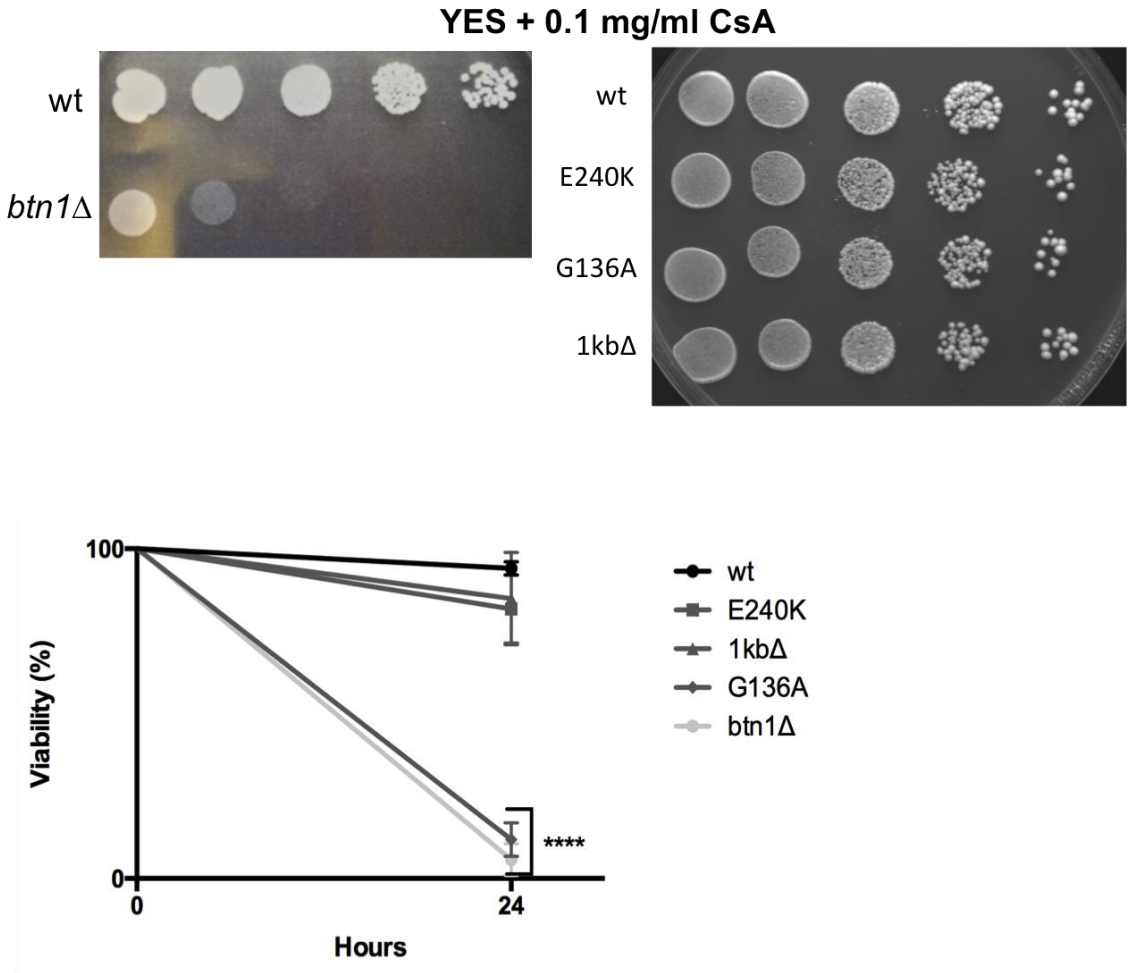

4.2 Drug screen

After choosing the ideal phenotype to be used as basis of the screen, screening conditions were optimized. The developed high-throughput screen used a small compound library (LoPac collection), all at a concentration of 10μM, kindly provided by Dr. Robin Ketteler, and executed by the Opera® system. This screen was optimized and completed in collaboration with Dr Jamie Freeman. All the hits from the screen were validated in further experiments.

4.2.1 Optimisation of the screen

The high-throughput drug screen was executed by the Opera® High Content Screening System, a confocal microplate imaging robot. This system allows for the acquisition of several images in a rapid manner. These images are posteriorly analysed with the CellProfiler software, where the selected phenotype can be quantitatively measured in an automatic way. The analysis was based in the amount of fluorescence seen in the images from wild-type and *btn1*Δ untreated strains, and *btn1*Δ after being treated with the LoPac compounds. The detected fluorescence was from propidium iodide, which labels dead cells. Positive hits were compounds that were able to rescue cell death, characteristic of the *btn1*Δ strain in the presence of CsA at 37°C, and therefore showed less fluorescence than the untreated *btn1*Δ strain.

Several conditions were tested before images with good quality and accurate amount of fluorescence were obtained: initial cell density, different manners of plating and amount of calcofluor and propidium iodide used to stain the cells, amongst others.

All 1280 compounds were tested four times, and two controls, positive and negative, were included in each plate: wild-type and *btn1*Δ cells without any compound.

4.2.2 Results of the screen

For each of the 384 wells in each plate, six images were acquired in order to cover a great part of the area. This means that for each compound that was tested, twenty-four images were acquired, since each compound was replicated in four wells. All images were analysed by Dr. Jamie Freeman using the CellProfiler software. A value corresponding to the amount of fluorescence in the whole area was given to each image, and an average of the different values was calculated for each compound. Values for the negative controls (cells with no *btn1* and no added compound) and positive controls (wild-type cells with no added compound) were also calculated and compared to those of the samples (*btn1*Δ cells with compounds). The average value for the negative controls was 0.723, and therefore only compounds giving numbers less than this value were considered further.

Images corresponding to positive hits were all analysed individually in order to eliminate false positive results where, for instance, no cells were seen in the image.

After the analysis, the six stronger hits were chosen to be validated in further experiments. These were atenolol, alloxazine, L-trans-Epoxysuccinyl-leucylamido(4-guanidino)butane (E-64), prochlorperazine dimaleate, etoposide and daphnetin. Examples of screen images corresponding to controls (wild-type and *btn1*Δ untreated cells) and two positive hits are displayed in Figure 4.2.1.

Figure 4.2.1. Drug screen: negative and positive controls, and two positive hits

Sample images obtained in the drug screen. Cells in log-phase were grown in YES medium with CsA (0.1mg/ml) and a randomly assigned compound of the LoPac collection (10μM) at a high temperature of 37°C over 24 hours. Cells were stained using the cell impermeant nucleotide stain propidium iodide to mark dead cells (red/pink) and calcofluor white to mark the total cell population (blue). Images correspond to: *btn1*Δ untreated cells with no added compound (negative control) (upper left side); wild-type untreated cells with no added compound (positive control) (upper right side); and two positive hits from the screen in the lower panel (*btn1*Δ cells treated with two compounds that were able to rescue the low viability seen in the presence of CsA). In smaller squares zoomed images of the respective larger pictures (positive and negative controls) are shown.

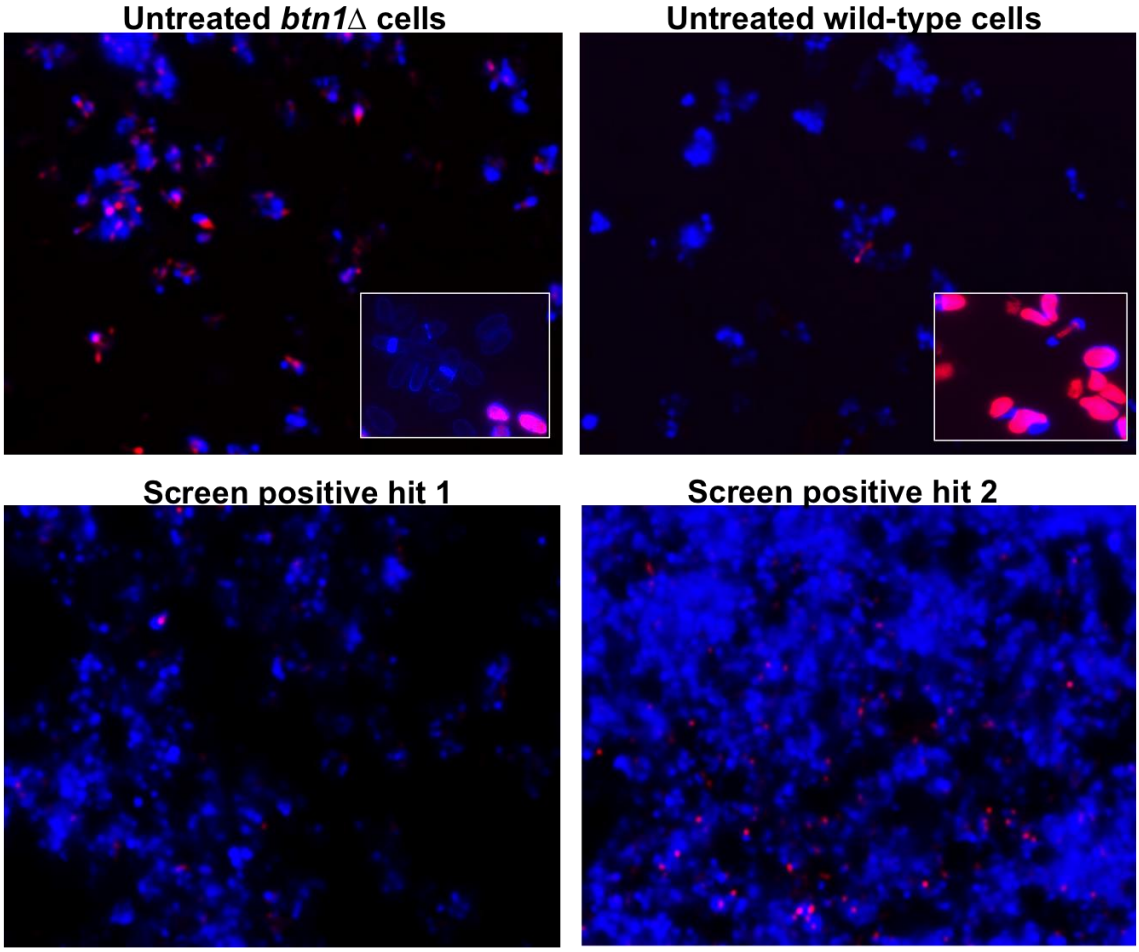

4.3 Summary

The first step towards the development of the drug screen was to find a robust and striking phenotype that is easily identified when rescued and significantly different between strains with and without *btn1*. The ideal is a phenotype based on a type of assay that will assess something as basic as survival/death of the strains, where cells with defective or no Btn1p are unable to grow or survive as well as wild-type cells. These kind of selective screens are not yet possible to be performed in mammalian cells, since no robust adequate phenotype has been reported to date. On the other hand, the fission yeast model is ideal to perform this type of screen, since multiple phenotypes (caused by the loss of *btn1* or associated with the 1-kb deletion mutant) have already been identified.

Four different phenotypes were analysed, and they were chosen for different reasons. Firstly, the growth of *btn1*Δ in the presence of ANP and chloroquine was investigated. It was previously reported that *S. cerevisiae* strains lacking *BTN1* are more resistant to ANP, in a pH-dependent manner (Pearce & Sherman 1998). Since in *S. cerevisiae BTN1*Δ strain the vacuole pH is more acidic, but in *S. pombe* this pH is higher than normal, it was thought that fission yeast strains without *btn1* could be more sensitive to ANP. Moreover, in other study in budding yeast, chloroquine was shown to reverse the resistance to ANP, elevating the vacuole pH (Pearce *et al.* 1999a), and therefore this combination (ANP and chloroquine) was tested in *S. pombe* to verify if there was an exacerbation in the sensitivity of strains without *btn1* to these compounds. However, there was no striking difference between the pattern of growth of wild-type and *btn1Δ* strains, neither in the presence of ANP nor in the presence of ANP and chloroquine.

The next phenotype to be analysed was the growth of strains at a high temperature of 37°C. In a study by Codlin and others (Codlin *et al.* 2008b) it was reported that Btn1p is essential for growth at 37°C, since its absence ultimately results in cell lysis. In fact, in this study, the high temperature was

shown to severely affect the growth of *btn1*Δ strain; however this was not a complete inhibition of growth, which would be desirable for a rescue screen.

It was previously shown that cells deleted for *btn1* have a higher vacuole pH than wild-type cells (Gachet *et al.* 2005), and therefore this was measured in these two types of strains (wild-type and *btn1*Δ). A significant difference was seen between these two strains, and therefore this phenotype was initially selected for the drug screen. However, after further testing by Dr Jamie Freeman, it was shown that the fluorescence intensity from the Lysosensor used to measure vacuole pH was difficult to measure in the Opera Software, and therefore, this phenotype was abandoned.

Finally, work done by Dr Michael Bond (unpublished data) showed that the TOR complex 2 (TORC2) pathway is related to the function of Btn1p, and it was known that the calcineurin phosphatase is consistently active in yeast mutants defective for TORC2 (Mulet *et al.* 2006). Therefore, an inhibitor of calcineurin, cyclosporine A, was tested to verify its effect on the growth of *btn1*Δ strain at a concentration of 0.1mg/ml and at 37°C. *btn1*Δ cells are sensitive to growth in these conditions. Therefore, this phenotype was selected as basis of the drug screen.

The developed high-throughput screen was performed using a library (LoPac collection) with 1280 FDA-approved compounds. The screen was optimized and completed in collaboration with Dr Jamie Freeman. This screen was performed in the Opera system, a high-throughput microscope suitable for this type of screening campaigns.

After acquiring all the images from the screen, these were primarily analysed by Dr. Jamie Freeman using the Cell Profiler software. Afterwards, images from the positive hits were manual and individually analysed in order to eliminate false positive results.

The six stronger hits were selected for further experiments of validation: atenolol, a selective β1 adrenoreceptor antagonist (β-blocker), used mainly in

treatment of cardiovascular diseases; alloxazine, an adenosine A2B receptor antagonist; E-64, an inhibitor of a range of cysteine peptidases; prochlorperazine dimaleate, a D2 dopamine receptor antagonist; etoposide, a topoisomerase inhibitor, used as an anticancer drug; and daphnetin, an inhibitor of several protein kinases, with antioxidant and immunosuppressant properties. Although some of these compounds do not have apparent targets in yeast, these were further explored in this model, since they could be acting in a different pathway than in humans. More details about these hits will be discussed in the following chapters.

5 Results 3. Compounds identified in drug screen are able to rescue other phenotypes arising from loss of *btn1* in fission yeast

The aims of this part of the project were:

- to validate the six strongest positive hits obtained in the drug screen, by manually retesting these in the same conditions as the screen;

- to test three hit compounds on their ability to rescue other phenotypes in *btn1*Δ cells: increased vacuole size, higher septation index and cell curving, and sensitivity to high temperature;

- to test the same compounds for their ability to rescue compactness of the Golgi apparatus in fibroblasts from juvenile CLN3 disease patients;

- to test the same compounds in a zebrafish juvenile NCL model to verify their ability to rescue other phenotypes associated with mutated *cln3*: increased relative activity of the fish and low survival rate.

5.1 Validating hits from the drug screen

In order to validate the results obtained in the drug screen, the six strongest hits, that showed the most significant rescue of sensitivity to cyclosporine A in *btn1*Δ cells, were selected: atenolol, alloxazine, E-64, prochlorperazine dimaleate, etoposide and daphnetin. These compounds were added to both wild-type and *btn1*Δ strains and they were grown in the same exact conditions as the drug screen (Results 2.1.2), but in a larger volume. Strains were grown at 37°C in the presence of CsA (0.1mg/ml) and the respective compound (10μM) for 24 hours. Strains were also treated with the compounds' carrier, DMSO, as a control. Images were taken and analysed manually. At least 300 cells were counted in three independent experiments.

Alloxazine was the first compound to be analysed: its presence significantly rescued the lower viability of the *btn1*Δ strain (49.25% instead of 3.36% in the untreated *btn1*Δ strain) and didn't significantly alter the viability of the wild-type strain (88.93% with alloxazine, compared to 92.22% for untreated wt). Similar results were obtained for E-64 and prochlorperazine dimaleate. Both of these compounds slightly (but not significantly) decreased the viability of the wild-type strain (81.24% for E-64 and 84.32% for prochlorperazine) and significantly increased the viability of the *btn1*Δ strain, especially E-64, validating their ability to rescue the sensitivity to CsA (73.85% and 63.18%, respectively for E-64 and prochlorperazine) (Figure 5.1.1). Therefore, these three compounds (alloxazine, E-64 and prochlorperazine dimaleate) were all selected for further experiments, to verify their ability to rescue other phenotypes associated with the loss of *btn1.*

Only compounds that rescued viability to values above 50% without affecting the wild-type strain were chosen for further studies. Therefore, the other three compounds, atenolol, etoposide and daphnetin were excluded. Atenolol was able to slightly rescue the CsA sensitivity of the *btn1*Δ strain (16.29% instead of 3.36%). However, the rescue was not statistically significant and therefore atenolol was not further tested. On the other hand, the addition of etoposide

significantly rescued the growth of the *btn1*Δ, but also affected the wild-type strain (61.73% instead of 92.22%) and therefore it was not used in further experiments. A similar effect was observed with daphnetin, where the viability of wild-type significantly decreased after treatment (41.24%) (Figure 5.1.1). Due to time restrictions, only the three compounds that led to the strongest rescues were further explored in this project. However, the other three compounds should be considered in the future.

Figure 5.1.1. Validation of six strongest hits from the drug screen in wild-type and *btn1*Δ strains

Alloxazine, E-64 and prochlorperazine dimaleate are able to significantly rescue sensitivity of *btn1*Δ strain to cyclosporine A (CsA). Cell viability of wild-type and *btn1*Δ strains upon growth in YES medium with CsA (0.1mg/ml) and six compounds (10μM) at a high temperature of 37°C after 24 hours. Graphs show the viability (percentage % of live cells in total number of cells) of wild-type (upper graph) and *btn1*Δ strains (lower graph) after treatment with different compounds: alloxazine, atenolol, etoposide, E-64, daphnetin and prochlorperazine dimaleate (proc dimaleate). Strains were also treated with the compounds' carrier, DMSO, as a control. Data shown is a mean (±SEM) of 3 independent experiments. Statistical significances between each treatment were determined using a one-way ANOVA with a Tukey's multiple comparison post-test. Statistical significances between wild-type and *btn1*Δ and all the six compounds are represented in the graph above the compounds' bars (*p= <0.1; **p= <0.01; ****p= <0.0001). In the upper graph significances were calculated against the wild-type strain (wt), and in the lower graph against the *btn1*Δ strain (btn1D), both treated with DMSO.

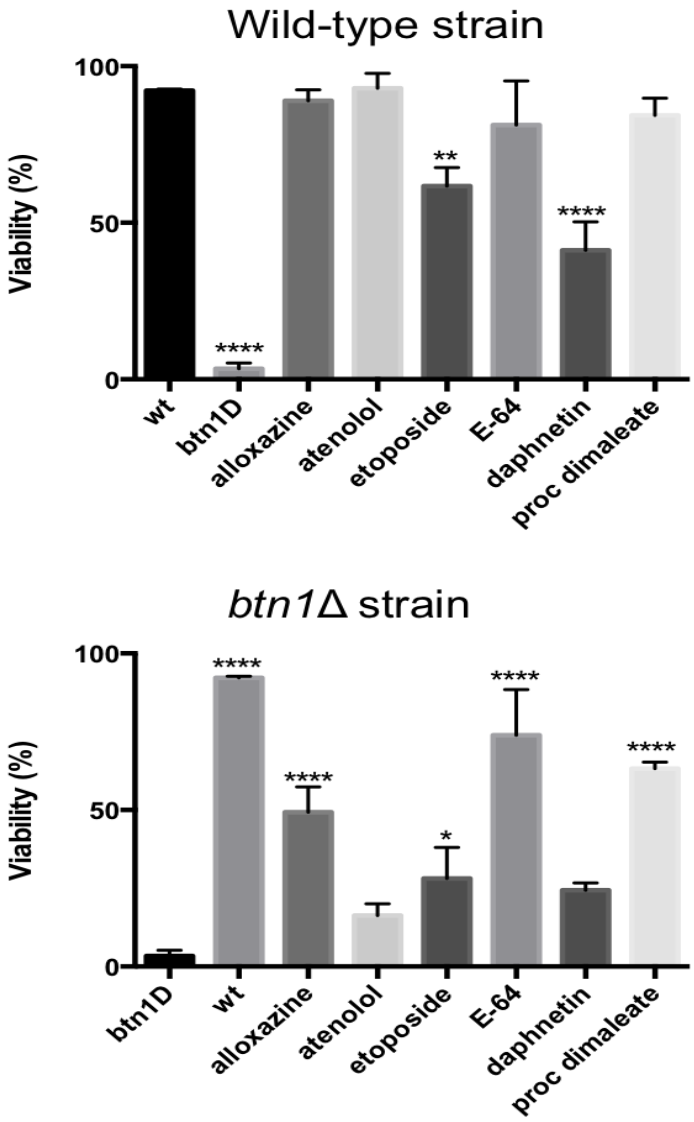

5.2 Testing compounds' ability to rescue other *btn1*Δ phenotypes

The three compounds that were positively selected in the drug screen and subsequently validated (alloxazine, E-64 and prochlorperazine dimaleate) were used in further experiments to verify their ability to rescue other phenotypes associated with the loss of *btn1*: enlarged vacuoles, higher septation index, increased cell curving and sensitivity growth at high temperature.

5.2.1 Vacuole size

The first phenotype to be analysed was vacuole size, which was shown to be significantly larger in *btn1*Δ cells (Results 1.3.1). Wild-type and *btn1*Δ strains were grown in the presence of the three validated compounds prior to labelling the vacuoles: alloxazine, E-64 and prochlorperazine dimaleate. At least 500 vacuoles for each compound were measured in three independent experiments. Strains were also treated with DMSO as a control. After measuring the average vacuole diameter, it was found that all three compounds were able to significantly rescue this phenotype. The average vacuole diameter is smaller in the presence of the compounds than in untreated *btn1*Δ cells, a similar size of vacuoles in wild-type cells: an average size of 0.87 μm for alloxazine, 0.9 μm for E-64 and prochlorperazine dimaleate, when compared to 0.87 μm in the wild-type strain and 1.02 μm in the *btn1*Δ strain (Figure 5.2.1). None of the compounds significantly affected the size of wild-type vacuoles (data not shown).

Figure 5.2.1. Effects of alloxazine, E-64 and prochlorperazine dimaleate on the vacuole size of *btn1*Δ strain

Alloxazine, E-64 and prochlorperazine dimaleate are able to significantly rescue enlarged vacuoles of *btn1*Δ strain. The graph shows the mean (±SEM) of the vacuoles diameter (in μm) in the *btn1*Δ strain treated with DMSO (control) and different compounds (10μM): alloxazine, E-64 and prochlorperazine dimaleate (proc). The average vacuole diameter of the wild-type strain is represented by a grid line in the graph (wt). Data was collected in three independent experiments. Statistical significances between each treatment were determined using a one-way ANOVA with a Tukey's multiple comparison post-test. Statistical significances between *btn1*Δ treated with DMSO and with the three compounds are represented in the graph above the compounds' bars (****p= <0.0001).

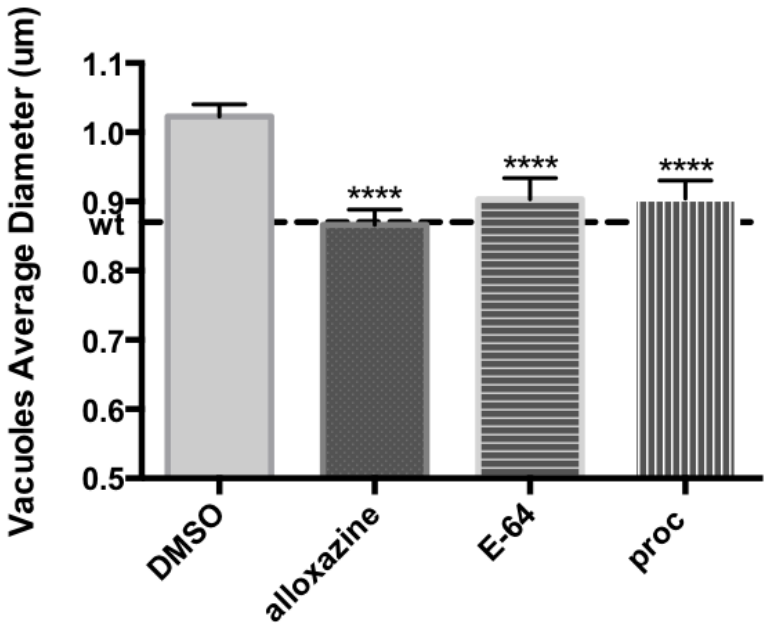

5.2.2 Septation index

Wild-type and *btn1*Δ strains were grown in the presence of alloxazine, E-64 and prochlorperazine dimaleate and then imaged to calculate the respective septation index. Strains were also treated with DMSO as a control. At least 300 cells were counted for each compound in three independent experiments. All three compounds were able to significantly rescue this phenotype, decreasing the number of septated cells to similar values to wild-type, or even slightly lower: 7.135% for alloxazine, 9.09% for E-64 and 12.87% for prochlorperazine dimaleate, when compared to 11.43% for wild-type strain and 20.67% for *btn1*Δ strain (Figure 5.2.2). None of the compounds significantly affected the number of septated cells in the wild-type strain or caused multiseptated cells (data not shown).

Figure 5.2.2. Effects of alloxazine, E-64 and prochlorperazine dimaleate on the septation index of *btn1*Δ strain

Alloxazine, E-64 and prochlorperazine dimaleate are able to significantly rescue the elevated septation index of *btn1*Δ strain. The graph shows the mean (±SEM) of septation index in the *btn1*Δ strain treated with DMSO (control) and different compounds (10μM): alloxazine, E-64 and prochlorperazine dimaleate (proc). The average septation index of the wild-type strain is represented by a grid line in the graph (wt). Septation index is the percentage of septated cells in total number of cells. Data was collected in three independent experiments. Statistical significances between each treatment were determined using a one-way ANOVA with a Tukey's multiple comparison post-test. Statistical significances between *btn1*Δ treated with DMSO and with he three compounds are represented in the graph above the compounds' bars (***p= <0.001; ****p= <0.0001).

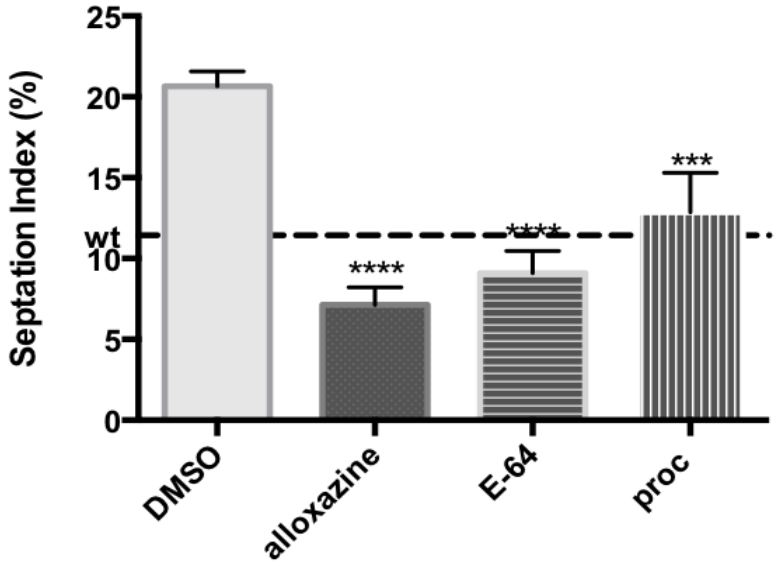

5.2.3 Cell curving

Wild-type and *btn1*Δ strains were treated with the same three compounds as before, in order to determine any effect on the cell curving phenotype. Strains were also treated with DMSO as a control. At least 300 cells were counted for each compound in three independent experiments. All three compounds were able to significantly rescue the curved morphology of cells, decreasing the number of curved cells to similar or lower values than wild-type: 9.82% for alloxazine, 8.55% for E-64 and 9.99% for prochlorperazine dimaleate, when compared to 11.47% for the wild-type strain and 22.4% for the *btn1*Δ strain (Figure 5.2.3). Furthermore, and since the 1kbΔ also showed a significantly higher number of curved cells strain similar to *btn1*Δ strain (19.84%) (Results 1.3.3), this strain was also treated with the same compounds. All three compounds were able to rescue the phenotype in this strain, in a significant manner, to values lower than the wild-type strain: 8.98%, 8.88% and 9.21% for alloxazine, E-64 and prochlorperazine dimaleate, respectively (Figure 5.2.3). None of the compounds significantly affected the number of curved cells in the wild-type strain (data not shown).

Figure 5.2.3. Effects of alloxazine, E-64 and prochlorperazine dimaleate on the cell curving of *btn1*Δ and 1kbΔ strains

Alloxazine, E-64 and prochlorperazine dimaleate are able to significantly rescue the elevated cell curving percentage of *btn1*Δ and 1kbΔ strains. Graphs show the mean (±SEM) of cell curving percentage in the *btn1*Δ (upper graph) and 1kbΔ (lower graph) strains treated with DMSO (controls) and different compounds (10μM): alloxazine, E-64 and prochlorperazine dimaleate (proc). The average cell curving of the wild-type strain is represented by a grid line in both graphs (wt). Cell curving is the percentage of curved cells in total number of cells. Data was collected in three independent experiments. Statistical significances between each treatment were determined using a one-way ANOVA with a Tukey's multiple comparison post-test. Statistical significances between *btn1*Δ and 1kbΔ treated with DMSO and with the three compounds are represented in the graph above the compounds' bars (****p= <0.0001). DMSO – *btn1*Δ strain with DMSO and no compound; 1kbD – 1kbΔ strain with DMSO and no compound.

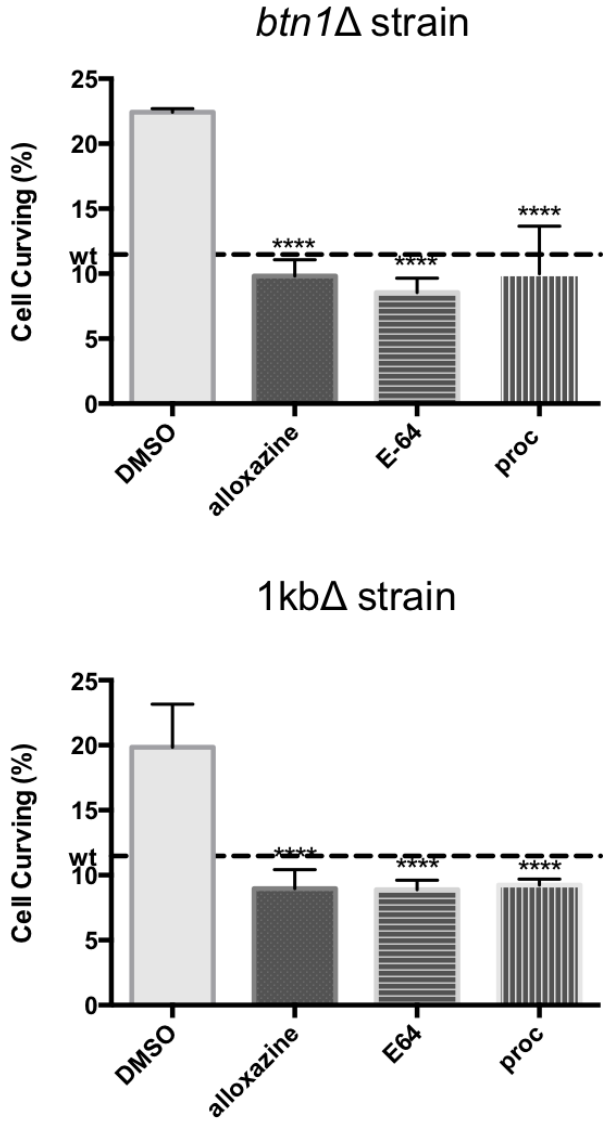

5.2.4 Growth at high temperature

The last phenotype that was analysed was the sensitivity of *btn1*Δ strain to growth at a high temperature of 37°C. Wild-type and *btn1*Δ strains were grown in the presence of alloxazine, E-64 and prochlorperazine dimaleate for 48 hours at 37°C and their viability was measured after 24 and 48 hours. Strains were also treated with DMSO as a control. At least 300 cells were counted for each compound in three independent experiments. None of the compounds significantly affected the viability of wild-type cells. Regarding the *btn1*Δ strain, the effect varied. Only alloxazine was able to significantly rescue the sensitivity of *btn1*Δ strain to high temperature after 24 and 48 hours (91.48% after 24 hours and 58.51% after 48 hours, compared to 54.47% and 22.09% in *btn1*Δ strain). E-64 and prochlorperazine were not able to rescue this phenotype (27.78% and 34.34% after 48 hours, for E-64 and prochlorperazine, respectively) (Figure 5.2.4).

Figure 5.2.4. Effects of alloxazine, E-64 and prochlorperazine dimaleate on the growth of *btn1*Δ strain at 37°C

Alloxazine is able to significantly rescue the sensitivity of *btn1*Δ strain to growth at 37°C. Cell viability of *btn1*Δ strain upon growth in YES medium at a high temperature of 37°C over two periods of 24 and 48 hours (after the temperature shift), and treated with DMSO (control) and three different compounds (10μm): alloxazine, E-64 and prochlorperazine dimaleate (proc). Data from wild-type (wt) strain treated with DMSO is also included in the graph. Graph shows the survival curve of different strains at three time points, after cultures were shifted from 30 to 37°C: 0, 24 and 48 hours. Data shown is a mean (±SEM) of 3 independent experiments. Viability is the percentage (%) of live cells in total number of cells. Statistical significances between each strain were determined using a one-way ANOVA with a Tukey's multiple comparison post-test. Statistical significances between *btn1*Δ treated with DMSO and alloxazine, and wild-type are represented in the graph (***p=<0.001****p= <0.0001). Treatment with the other two compounds was not statistically significant.

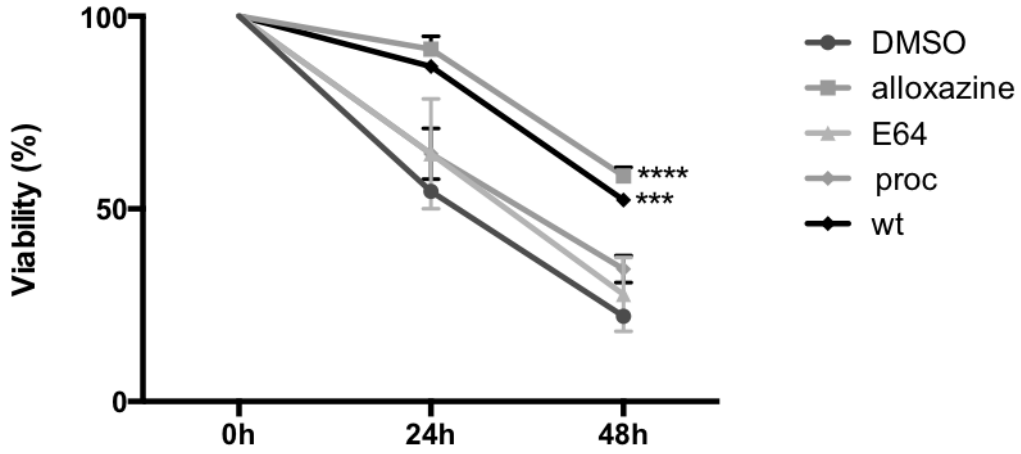

5.2.5 Spot assays

In order to reinforce the previous results that showed the ability of three compounds (alloxazine, E-64 and prochlorperazine dimaleate) to rescue the sensitivity to a temperature of growth of 37°C and the presence of cyclosporine A, wild-type and *btn1*Δ strains were spotted onto YES plates with and without cyclosporine A, and with the respective compound, and incubated at 37°C. The assay was repeated in three independent experiments with three replicas of each plate with the different compounds. Alloxazine was also able to rescue the growth of *btn1*Δ strain in both conditions, but more significantly in plates without CsA. On the other hand, E-64 and prochlorperazine dimaleate were able to completely rescue the growth of *btn1*Δ strain in the presence of CsA (0.1mg/ml), but not in plates without CsA (Figure 5.2.5). Cells were also spotted onto YES plates with DMSO (with or without CsA) without any added compound as a control.

Figure 5.2.5. Effects of alloxazine, E-64 and prochlorperazine dimaleate on the growth of wild-type and *btn1*Δ strains in YES plates with cyclosporine A at 37°C

Alloxazine is able to recover growth of *btn1*Δ cells at 37°C in YES plates with and without cyclosporine A (CsA), whereas E-64 and prochlorperazine dimaleate are only able to recover growth in plates with CsA. Wild-type and *btn1*Δ cells were serially diluted from a log-phase culture ($1x10^6$ cells/ml) and spotted onto YES plates containing or lacking 0.1mg/ml of cyclosporine A (right and left panel, respectively), and containing 10μM of alloxazine, E-64 and prochlorperazine dimaleate (upper, middle and lower panel respectively). Plates were then incubated at 37°C for 3-4 days to determine growth at high temperature in the presence (or absence) of CsA and three compounds.

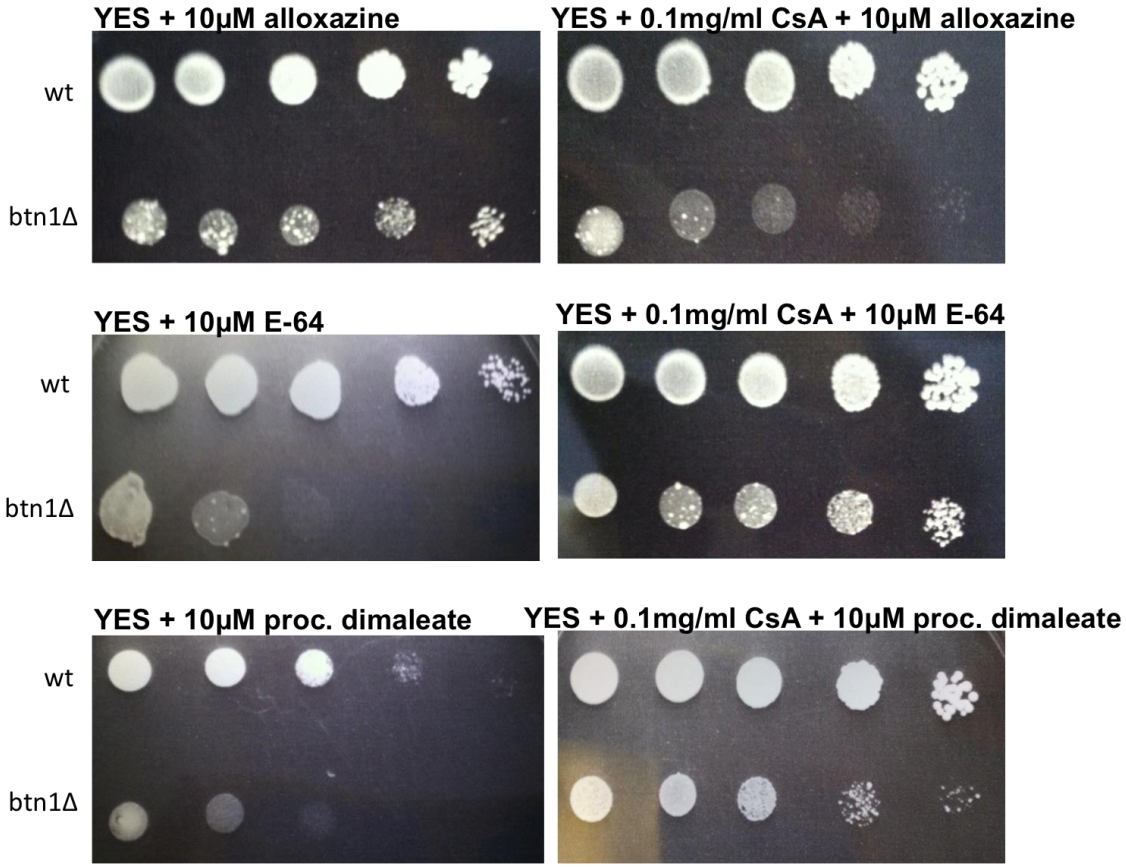

5.3 Testing compounds in other disease models

The three compounds (alloxazine, E-64 and prochlorperazine dimaleate) selected from the drug screen and proved to be able to rescue other phenotypes associated with the loss of *btn1* in fission yeast, were tested in other mammalian models of juvenile CLN3 disease. The ability of these compounds to rescue other phenotypes in patient fibroblasts and in a vertebrate disease model (zebrafish) was tested. In fibroblasts, compactness of the Golgi apparatus was assessed, since this organelle was shown to be less compact in patient cells when compared with healthy control cells (Davide Marotta, unpublished data). In the zebrafish model, relative activity and survival of the fish were assessed. This work was done in collaboration with Davide Marotta (fibroblasts) and with Dr Claire Russell from the Royal Veterinary College (zebrafish).

5.3.1 Compactness of Golgi apparatus in patient fibroblasts

Healthy control and patient fibroblasts (homozygous for the 1-kb deletion in *CLN3*) were incubated with different concentrations of alloxazine, E-64 and prochlorperazine dimaleate (5, 10 and 20μM) for 24 hours. Afterwards, cells were prepared for immunofluorescence and imaged. Compactness of the Golgi apparatus (numerical quantity that shows the degree to which the Golgi is compact when compared to a perfect circle, which has a value of 1.0) was measured for all fibroblasts, with and without compound. These measurements were performed in three independent experiments. Previous work done by Davide Marotta showed that in patient fibroblasts the Golgi apparatus is less compact than in healthy fibroblasts, suggesting that it may be less organised (unpublished data). This difference in Golgi compactness between patient and healthy control untreated fibroblasts was observed again in this study: 0.08 in control and 0.02 in patient cells (figure 5.3.1). After incubation with the three compounds at three different concentrations (5, 10 and 20μM), all except

alloxazine significantly rescue the low compactness of the Golgi apparatus in fibroblasts from patients with the 1-kb deletion. E-64 restores the compactness value to 0.08 at 5 and 10μM and to 0.1 at the higher concentration of 20μM. Prochlorperazine dimaleate also restores the value to 0.09 and 0.08 at 5 and 10μM respectively. At a higher concentration (20μM), it appears to be lethal to the cells, since no fibroblasts were seen in any of the three experiments (Figure 5.3.1). With the exception of prochlorperazine dimaleate at 20μM, none of the compounds affected the Golgi compactness of healthy control fibroblasts, at any concentration.

Figure 5.3.1. Effects of alloxazine, E-64 and prochlorperazine dimaleate on the compactness of the Golgi apparatus in the juvenile CLN3 disease patient fibroblasts

E-64 and prochlorperazine dimaleate are able to significantly rescue compactness of the Golgi apparatus seen in fibroblasts from juvenile NCL patients. Images showing healthy control fibroblasts (left panel) and patient fibroblasts untreated (middle panel) and treated with E-64 (20 μM) (right panel). Nuclei were stained with Hoechst (blue) and the green fluorescence corresponds to GM130 Golgi marker protein. More compact Golgi can be seen in the left and right panels when compared to the middle panel, which shows more distended Golgi staining. Graphs show the mean (±SEM) of Golgi apparatus' compactness in control healthy fibroblasts and juvenile NCL patient fibroblasts: untreated (0μM) or treated with 5, 10 or 20μM of alloxazine, E-64 and prochlorperazine dimaleate. There is no value correspondent to the treatment with 20μM of prochlorperazine dimaleate because at this concentration this compound is lethal to the fibroblasts. Compactness is a numerical quantity that shows the degree to which the Golgi is compact when compared to a perfect circle, which has a value of 1.0. Data was collected in 3 independent experiments. Statistical significances between each treatment were determined using a one-way ANOVA with a Tukey's multiple comparison post-test. Statistical significances between control fibroblasts and patient fibroblasts treated with compounds at different concentrations in relation to untreated patient fibroblasts are represented in the graphs above the bars (****p= <0.0001).

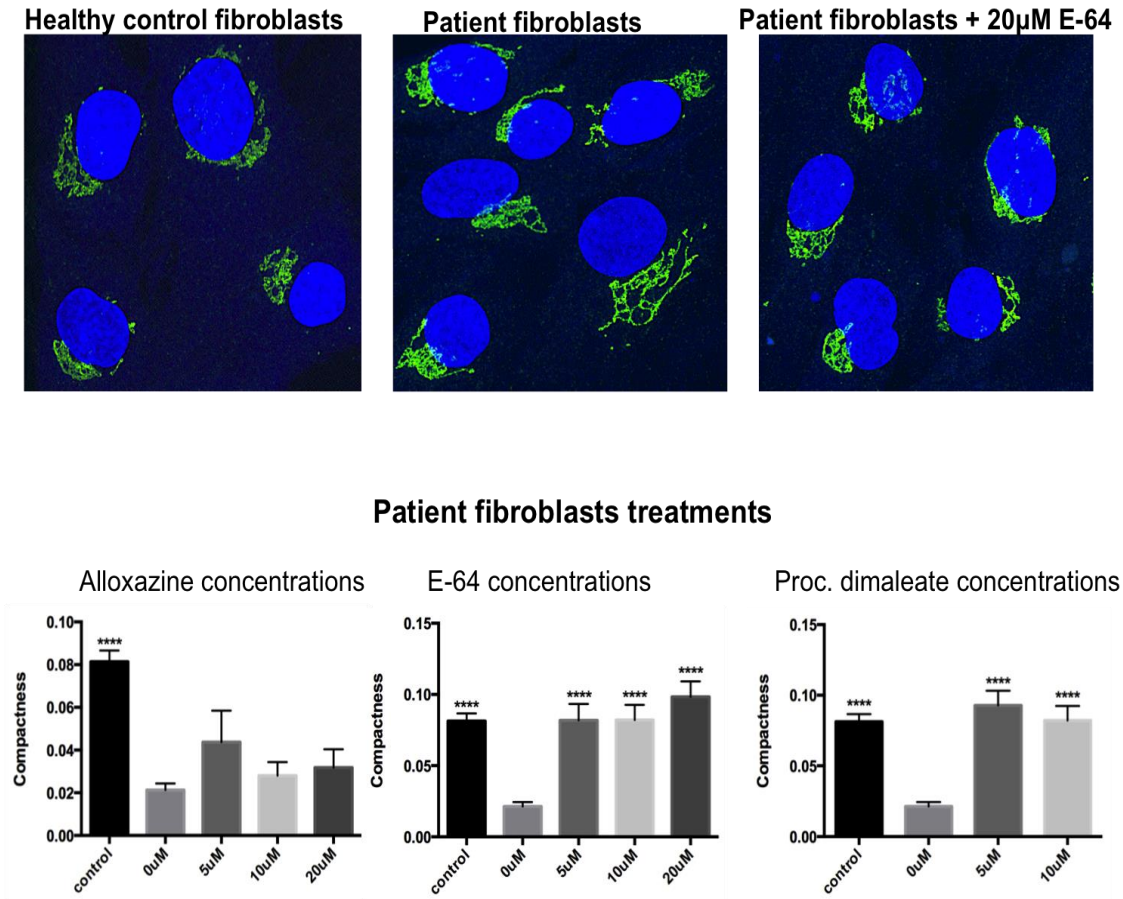

5.3.2 Zebrafish model

Dr Claire Russell at the Royal Veterinary College of London investigated the ability of the three compounds (alloxazine, E-64 and prochlorperazine dimaleate) to rescue two phenotypes in a zebrafish model of the juvenile CLN3 disease. Compounds were added to fish 12 hours post fertilization. Both phenotypes were analysed in three independent experiments.

The first phenotype to be analysed was the relative activity of the fish recorded for 3 minutes. This activity consists of a tail flicking movement, which was previously shown to be more frequently seen in fish with *Cln3* morpholino (*Cln3* MO) (Claire Russell and Kim Wager, personal communication). Relative activity was measured in number of pixels that change in time during the recorded time (3 minutes). All three compounds are able to significantly rescue this phenotype, decreasing the relative activity of the *Cln3* MO fish to values close to wild-type fish treated only with DMSO: 75.27 for E-64, 110 for alloxazine and 200.56 for prochlorperazine dimaleate, compared to 116.13 for wild-type fish and 1281.74 for *Cln3* morpholino fish, both treated with DMSO (Figure 5.3.2). However, prochlorperazine dimaleate also affects the tail flicking of the wild-type zebrafish, increasing the value to 466.47 (data not shown). None of the other compounds have any effect on wild-type fish (data not shown).

The other phenotype that was analysed was the fish survival, which is reduced in the zebrafish model of the juvenile CLN3 disease: *Cln3* morpholino treated with only DMSO normally die after 3 days. E-64 gives a partial rescue of this phenotype, increasing the survival rate to approximately 50% at 125 hpf, compared to almost 0% survival in the *Cln3* morpholino fish treated with only DMSO at this time point. None of the other compounds was able to significantly affect the survival ratio of the morpholino fish.

Figure 5.3.2. Effects of alloxazine, E-64 and prochlorperazine dimaleate on the relative activity and survival of a zebrafish model of the juvenile CLN3 disease

Alloxazine, E-64 and prochlorperazine dimaleate are able to rescue relative activity of a zebrafish model of juvenile CLN3 disease. E-64 is also able to rescue fish survival in this model The upper graph shows the mean (±SEM) of relative activity in zebrafish: control, Cln3 morpholino fish treated with DMSO (DMSO) and treated with alloxazine, E-64 and prochlorperazine dimaleate (proc). The relative activity was measured in number of pixels that change in time during three minutes. The lower graph shows fish survival in zebrafish: control (wild-type treated with DMSO), Cln3 morpholino fish treated with DMSO (DMSO) and treated with alloxazine, E-64 and prochlorperazine dimaleate (proc). Data was collected by Dr. Claire Russell in three independent experiments. Statistical significances between each treatment were determined using a one-way ANOVA with a Tukey's multiple comparison post-test. Statistical significances between morpholino fish and control fish and treatment with compounds are represented in the graphs (*p= <0.1). hpf - hours post fertilization.

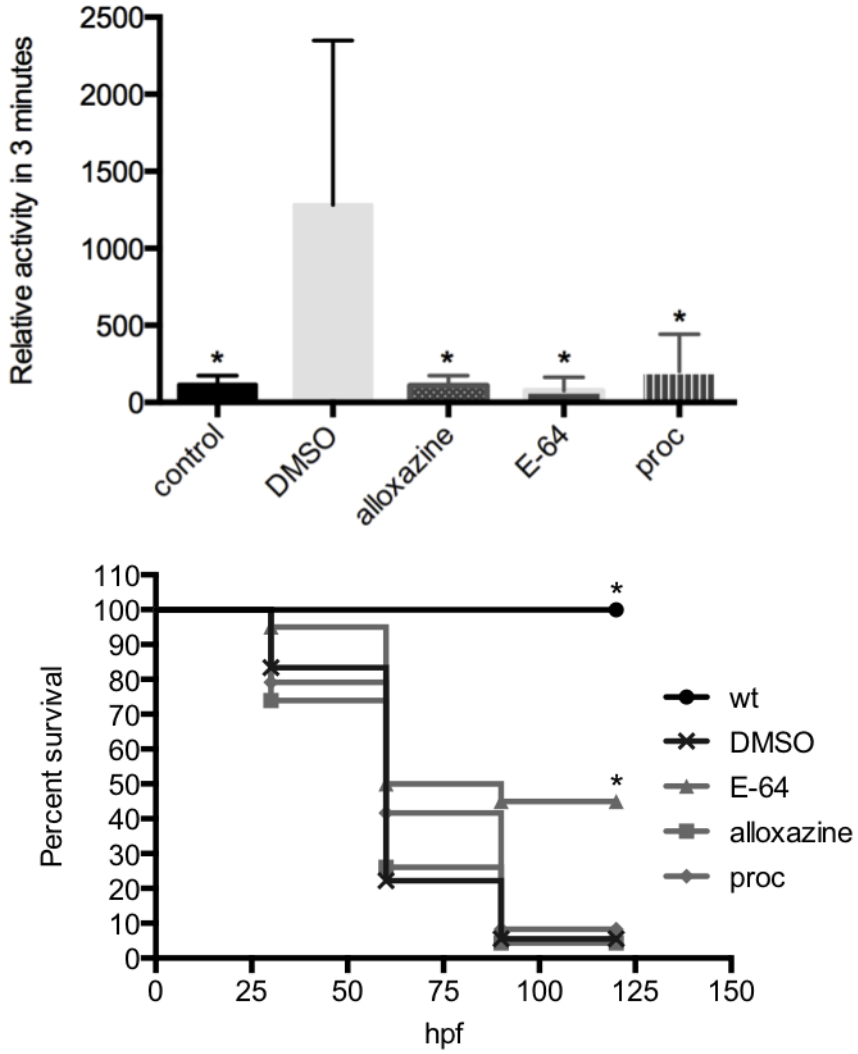

5.4 Summary

After obtaining the results from the drug screen described in the Results Chapter 2 (Chapter 4.2.2), six stronger hits were validated by manually repeating the same assay of the automated screen. Three of the compounds, alloxazine, E-64 and prochlorperazine dimaleate showed again a significant rescue of the cyclosporine A sensitivity, more specifically E-64, which increased the viability of the *btn1*Δ strain to approximately 74%. These compounds were chosen for further validation studies, where they were tested for their ability to rescue four other phenotypes in *btn1*Δ cells.

The first phenotype that was tested was vacuole size, which is larger in the *btn1*Δ strain (Chapter 3.3.1). All compounds (alloxazine, E-64 and prochlorperazine dimaleate) were able to significantly rescue this phenotype to values similar to those seen in wild-type strain, although alloxazine was the drug that led to a better rescue. A similar rescue pattern was seen in other phenotype that was analysed, higher septation index, with all compounds showing ability to rescue the number of septated cells, especially alloxazine, which decreased this number to a value even lower than that seen in the wild-type strain. All three compounds were also able to rescue the cell curving phenotype seen after 4 hours at 37°C, but in this case the compound responsible for the strongest rescue was E-64. All compounds were able to decrease the number of curved cells in the *btn1*Δ strain and in the strain containing the 1-kb deletion, to values lower than those seen in the wild-type strain. On the other hand, sensitivity of *btn1*Δ strain to growth at high temperature, 37°C, after 24 and 48 hours (and in spot assays) was only rescued by alloxazine. Treatments with E-64 and prochlorperazine dimaleate were not sufficient to give a significant rescue of the *btn1*Δ low viability in these conditions. Additionally, all compounds were able to rescue colony growth in spot assays at 37°C in the presence of cyclosporine A.

Finally, compounds were tested in two different mammalian models: patient fibroblasts containing the 1-kb deletion, and a zebrafish model of juvenile CLN3

disease. In the first model, the investigated phenotype was compactness of the Golgi apparatus, which is reduced in patient fibroblasts when compared to healthy control cells. E-64 and prochlorperazine dimaleate were both able to rescue this phenotype at different concentrations, but not alloxazine. At a high concentration of 20µM, prochlorperazine dimaleate induces cell death, which suggests that at higher concentrations this compound is toxic. Work done in the zebrafish model showed that all compounds are able to significantly rescue the fish relative activity, which is normally increased in this model. Furthermore, E-64 was shown to rescue another phenotype, fish survival, which is normally compromised in the CLN3 disease model.

Altogether these preliminary results are very encouraging, with respect to the development of a potential therapy for juvenile CLN3 disease using any of the three compounds that were studied; however, future work is needed to further clarify their mechanism of action in yeast.

6 Results 4. Characterisation of other lysosomal storage disorder yeast strains

The aims of the last part of the project were:

- to characterise phenotypes that were previously associated with *btn1*Δ in three different fission yeast strains that model other lysosomal storage disorders (LSDs): Chédiak Higashi Syndrome (*lvs1*Δ), Niemann-Pick disease type C2 (*npc2*Δ) and CLN10 disease (*sxa1*Δ);

- to test the three hit compounds that were shown to efficiently rescue phenotypes in the *btn1*Δ strain for their ability to rescue the newly described phenotypes in the three LSD yeast models.

6.1 Characterising phenotypes of other lysosomal storage disorders yeast strains

It was shown in the previous chapters (Results Chapters 2 and 3) that the fission yeast model of juvenile CLN3 disease exhibits different phenotypes that can be rescued by three compounds, which were identified in a drug screen. Bearing in mind that the juvenile CLN3 disease is a lysosomal storage disorder, other disorders with the same classification that can be modelled in yeast were chosen for further investigation. All of these diseases have fission yeast models where the orthologue of the responsible human gene is deleted: *lvs1*Δ strain (Chédiak Higashi Syndrome), *npc2*Δ strain (Niemann-Pick disease type C2) and *sxa1*Δ (CLN10 disease). These mutant strains were characterised in terms of phenotypes that are associated with the *btn1*Δ strain. The five chosen phenotypes were: size of the vacuoles, cytokinesis defects (illustrated by the septation index), number of curved cells after 4 hours of growth at 37ºC, viability at 37ºC and sensitivity to cyclosporine A.

6.1.1 Vacuole size

The first phenotype to be analysed was the diameter of vacuoles in the cells. Therefore, *lvs1*Δ, *npc2*Δ and *sxa1*Δ strains were labelled with FM4-64 and vacuoles were measured, in the same manner as for the *btn1* mutant strains (Chapter 3.3.1). All three strains show significantly larger vacuoles when compared to the wild-type strain, specially the *lvs1*Δ strain, whose average vacuole diameter is 1.62 μm. The other two strains, *npc2*Δ and *sxa1*Δ, show a smaller but still large size when compared to wild-type: 1.06 and 1.08 μm, respectively. These values are all significantly higher than the wild-type strain, which shows average size of 0.86 μm (Figure 6.1.1).

Figure 6.1.1. Vacuole size of different lysosomal storage disorders yeast strains

Yeast models of lysosomal storage disorders *lvs1*Δ, *npc2*Δ and *sxa1*Δ show large vacuoles. Images show vacuoles labeled with FM4-64 of wild-type, *lvs1*Δ, *npc2*Δ and *sxa1*Δ strains. Scale bars - 10µm (wild-type and *lvs1*Δ) and 5µm (*npc2*Δ and *sxa1*Δ). Graph shows the mean (±SEM) of the vacuoles diameter (in µm) in different strains from three independent experiments. Statistical significance between each strain was determined using a one-way ANOVA with a Tukey's multiple comparison post-test. Statistical significances between wild-type and *lvs1*Δ, *npc2*Δ and *sxa1*Δ strains are represented in the graph above the bars (*p= <0.1; ****p= <0.0001). wt – wild-type; lvs1D – Chédiak-Higashi syndrome yeast model: *lvs1*Δ strain; npc2D – Niemann-Pick type C2 yeast model: *npc2*Δ strain; sxa1D – congenital CLN10 disease yeast model: *sxa1*Δ strain.

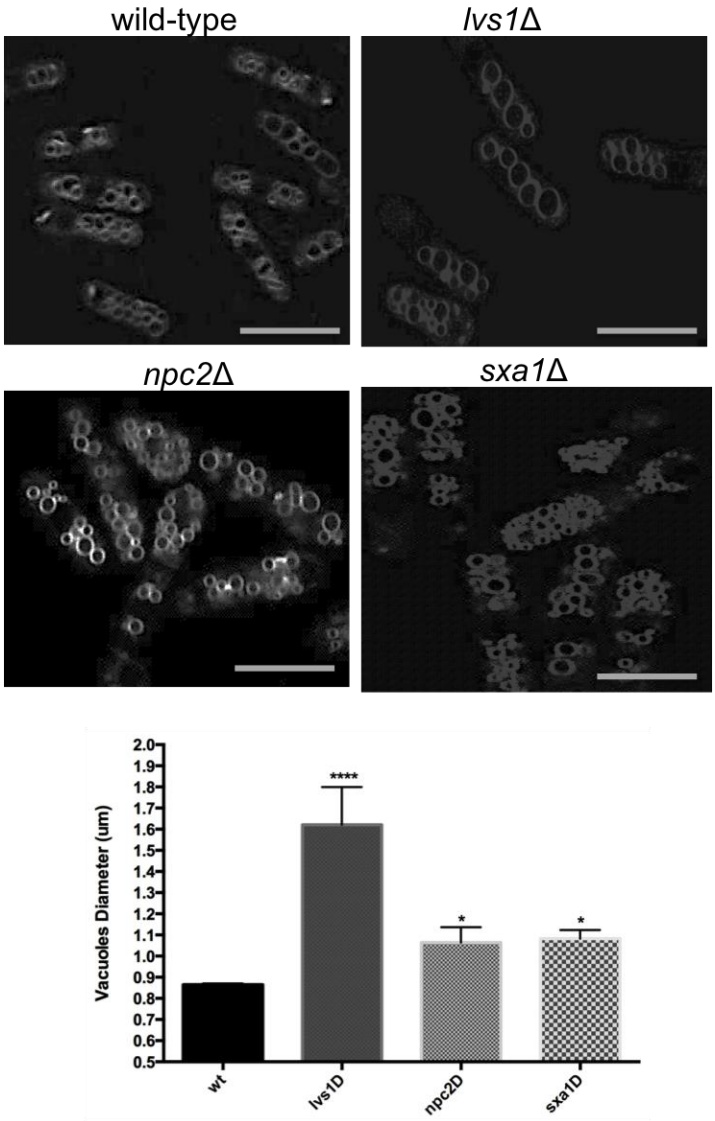

6.1.2 Septation index

Wild-type, *lvs1*Δ, *npc2*Δ and *sxa1*Δ strains were grown in normal conditions and then imaged to calculate the respective septation index. At least 300 cells were counted in three independent experiments. The three LSDs strains (*lvs1*Δ, *npc2*Δ and *sxa1*Δ) show significantly more septated cells than the wild-type strain, similar to what was observed in the *btn1*Δ strain (Chapter 3.3.2): 20.11% for *lvs1*Δ, 24.11% for *npc2*Δ and 18.76% for *sxa1*Δ, when compared to 12.68% for the wild-type strain (Figure 6.1.2).

Figure 6.1.2. Septation index of different lysosomal storage disorders yeast strains

Yeast models of lysosomal storage disorders *lvs1*Δ, *npc2*Δ and *sxa1*Δ have a high septation index. Images show yeast cells stained with calcofluor delineating cell walls and septa: wild-type, *lvs1*Δ, *npc2*Δ and *sxa1*Δ strains. Scale bars - 10µm. Graph shows the mean (±SEM) septation index (percentage of septated cells in total number of cells) of different strains from three independent experiments. Statistical significances between each strain were determined using a one-way ANOVA with a Tukey's multiple comparison post-test. Statistical significances between wild-type and *lvs1*Δ, *npc2*Δ and *sxa1*Δ strains are represented in the graph above the bars (*p= <0.1; **p= <0.01 ***p= <0.001). wt – wild-type; lvs1D – Chédiak-Higashi syndrome yeast model: *lvs1*Δ strain; npc2D – Niemann-Pick type C2 yeast model: *npc2*Δ strain; sxa1D – congenital CLN10 disease yeast model: *sxa1*Δ strain.

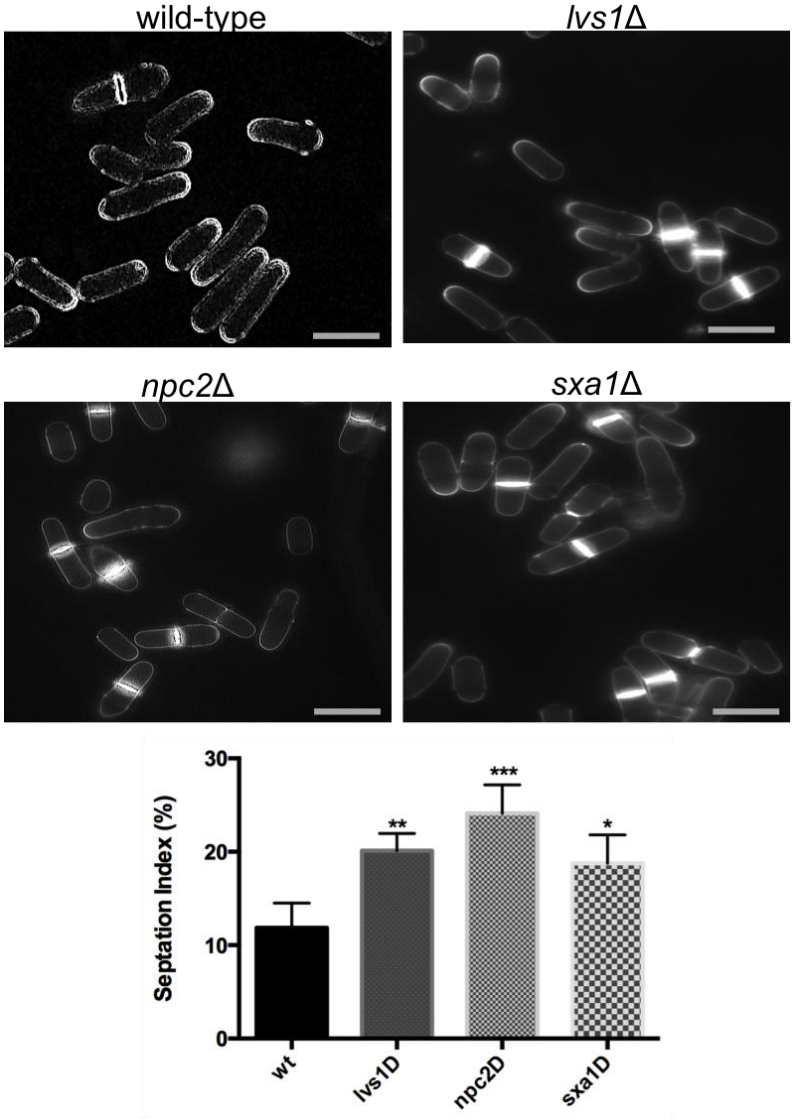

6.1.3 Cell curving

Yeast strains were analysed after growth at a high temperature of 37°C for 4 hours. The high temperature was shown to affect the morphology of the *btn1*Δ strain, represented by an increased number of curved cells when compared to the wild-type strain (Chapter 3.3.3). This phenotype was analysed for the LSD strains *lvs1*Δ, *npc2*Δ and *sxa1*Δ. At least 300 cells were counted in three independent experiments. In contrast to the previously described phenotypes, there is no significant difference between the wild-type and the LSD strains, where the percentage of curved cells with no *lvs1, npc2* and *sxa1* genes is not significantly different from wild-type cells (11.47%): 15.48%, 14.44% and 14.26% respectively (Figure 6.1.3). This suggests that this phenotype might be specific for the *btn1*Δ strain.

Figure 6.1.3. Cell curving of different lysosomal storage disorders yeast strains

Images show yeast cells stained with calcofluor (delineating cell walls and septa), after growth at 37°C for 4 hours: wild-type, *lvs1*Δ, *npc2*Δ and *sxa1*Δ strains. Scale bars – 10µm. Graph shows the mean (±SEM) cell curving percentage (percentage of curved cells in total number of cells) of different strains from three independent experiments. Statistical significances between each strain were determined using a one-way ANOVA with a Tukey's multiple comparison post-test. None of the strains (*lvs1*Δ, *npc2*Δ and *sxa1*Δ) showed a percentage of curved cells significantly different from the wild-type strain. wt – wild-type; lvs1D – Chédiak-Higashi syndrome yeast model: *lvs1*Δ strain; npc2D – Niemann-Pick type C2 yeast model: *npc2*Δ strain; sxa1D – congenital CLN10 disease yeast model: *sxa1*Δ strain.

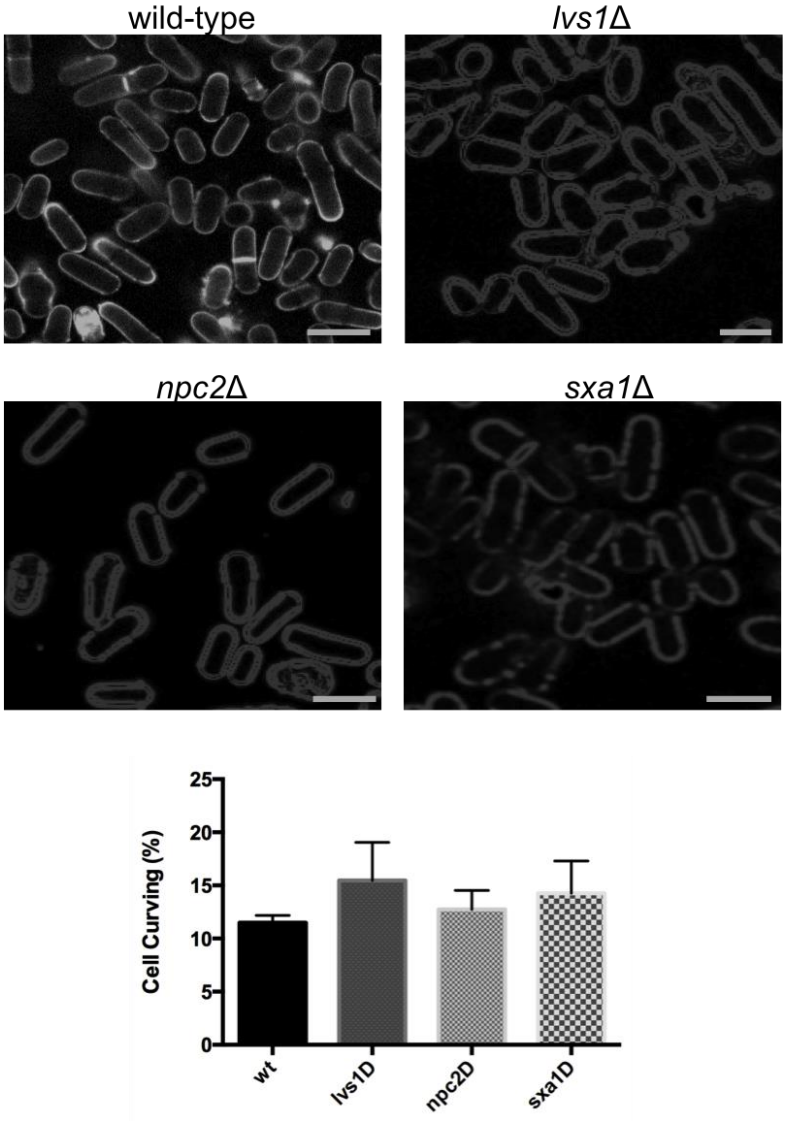

6.1.4 Growth at high temperature

The viability of the three LSD strains after growth at 37°C was calculated (percentage of live cells in the total number of cells), and the mean of three independent experiments was considered. *lvs1*Δ, *npc2*Δ and *sxa1*Δ show similar viability values to the wild-type strain. After 24 hours the viability values were the following: 88.3% for the wild-type strain, 76.74%, 79.11% and 85.43% for *lvs1*Δ, *npc2*Δ and *sxa1*Δ strains respectively. After 48 hours, the values were: 49.74% for the wild-type strain, 53.47% for *lvs1*Δ, 59.94% for *npc2*Δ and 43.04%, for *sxa1*Δ (Figure 6.1.4). None of the LSD strains show sensitivity to growth at high temperature, in contrast to what was seen in the *btn1*Δ strain (Chapter 4.1.2).

Additionally, a spot assay experiment in YES plates incubated at 37°C was performed for the same LSD strains. As expected, and according to the liquid culture viability assay, all colonies were able to grow in the plates, corroborating the fact that these strains are not sensitive to growth at 37°C (Figure 6.1.4).

Figure 6.1.4. Growth at 37°C of different lysosomal storage disorders yeast strains

Spot assays of different strains grown at 37°C in YES plates. Cells were serially diluted from a log-phase culture (1x10^6 cells/ml) and spotted onto YES plates. Plates were then incubated at 37°C for 3-4 days to determine growth at high temperature. The graph represents cell viability of wt, *lvs1*Δ, *npc2*Δ and *sxa1*Δ strains upon growth in YES medium at a high temperature of 37°C over 24 hours. The graph shows the survival curve of different strains at three time points, after cultures were shifted from 30 to 37°C: 0, 24 and 48 hours. Data shown is a mean (±SEM) of three independent experiments. Viability is the percentage (%) of live cells in total number of cells. Statistical significances between each strain were determined using a one-way ANOVA with a Tukey's multiple comparison post-test. None of the strains (*lvs1*Δ, *npc2*Δ and *sxa1*Δ) show sensitivity to growth at 37°C. wt – wild-type; lvs1D – Chédiak-Higashi syndrome yeast model: *lvs1*Δ strain; npc2D – Niemann-Pick type C2 yeast model: *npc2*Δ strain; sxa1D – congenital CLN10 disease yeast model: *sxa1*Δ strain.

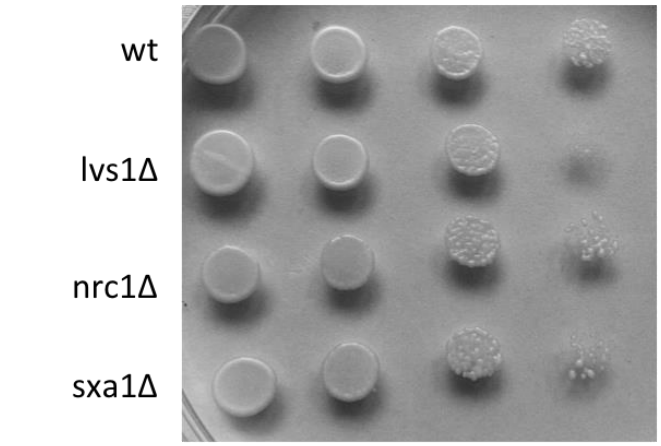

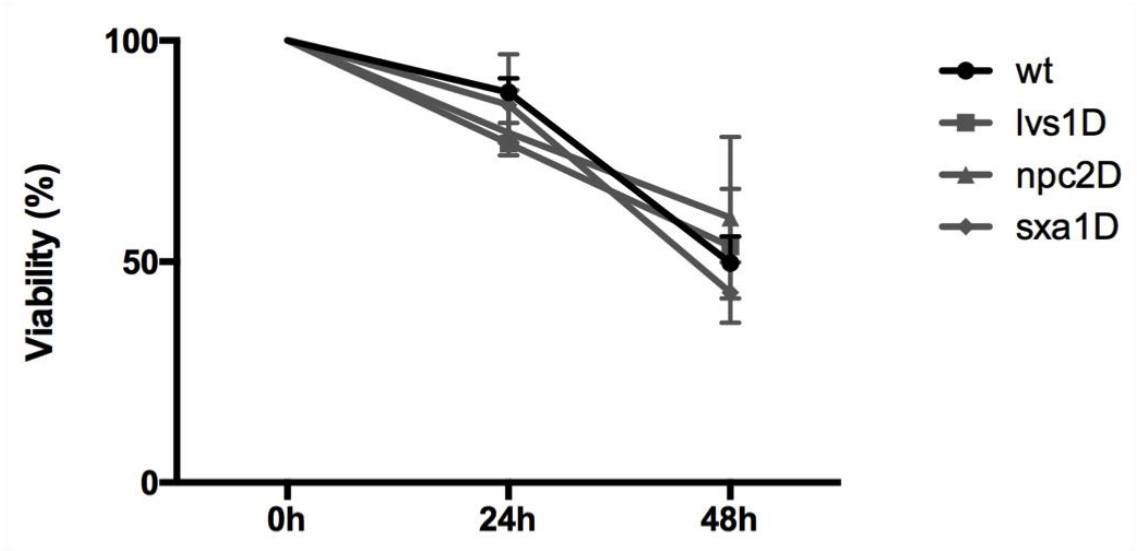

6.1.5 Sensitivity to cyclosporine A

The last phenotype to be analysed was the sensitivity to cyclosporine A (CsA) at 37°C, which was observed in *btn1*Δ cells (Chapter 4.1.4). Wild-type and LSD strains (*lvs1*Δ, *npc2*Δ and *sxa1*Δ) were grown in liquid medium with 0.1mg/ml of cyclosporine A and at 37°C for 24 hours prior to the analysis. At least 300 cells were counted in three independent experiments. After measuring the number of live and total cells in all strains, it was shown that all three LSDs strains are slightly but not significantly sensitive to the presence of CsA. The viability percentages for these strains is slightly less (but not significantly) than wild-type strain, in the presence of the compound: 63.88% for *lvs1*Δ, 69.07% for *npc2*Δ and 74.28% for *sxa1*Δ, when compared to 95.25% for the wild-type (Figure 6.1.5). Concluding, none of the LSD strains show a significant sensitivity to CsA.

A similar result was seen when the LSD strains were spotted onto YES plates with 0.1mg/ml of cyclosporine A: all colonies were able to grow.

Figure 6.1.5. Growth of different lysosomal storage disorders yeast strains in the presence of cyclosporine A

*lvs1*Δ, *npc2*Δ and *sxa1*Δ strains are not sensitive to CsA. Spot assays of different strains in YES plates containing 0.1mg/ml of cyclosporine A (CsA) are shown in the upper panel. Cells were serially diluted from a log-phase culture ($1x10^6$ cells/ml) and spotted onto YES plates containing 0.1 mM of cyclosporine A (CsA). Plates were then incubated at 37°C for 3-4 days to determine growth at high temperature in the presence of CsA. The graph shows the cell viability of wt, *lvs1*Δ, *npc2*Δ and *sxa1*Δ strains upon growth in YES medium with CsA (0.1mg/ml) at a high temperature of 37°C over 24 hours (after the temperature shift), more specifically the survival curve of these different strains at two time points, after cultures were shifted from 30 to 37°C: 0 and 24 hours. Data shown is a mean (±SEM) of three independent experiments. Viability is the percentage of live cells (%) in total number of cells. Statistical significances between each strain were determined using a one-way ANOVA with a Tukey's multiple comparison post-test. None of the strains (*lvs1*Δ, *npc2*Δ and *sxa1*Δ) showed sensitivity to CsA. wt – wild-type; lvs1D – Chédiak-Higashi syndrome yeast model: *lvs1*Δ strain; npc2D – Niemann-Pick type C2 yeast model: *npc2*Δ strain; sxa1D – congenital CLN10 disease yeast model: *sxa1*Δ strain.

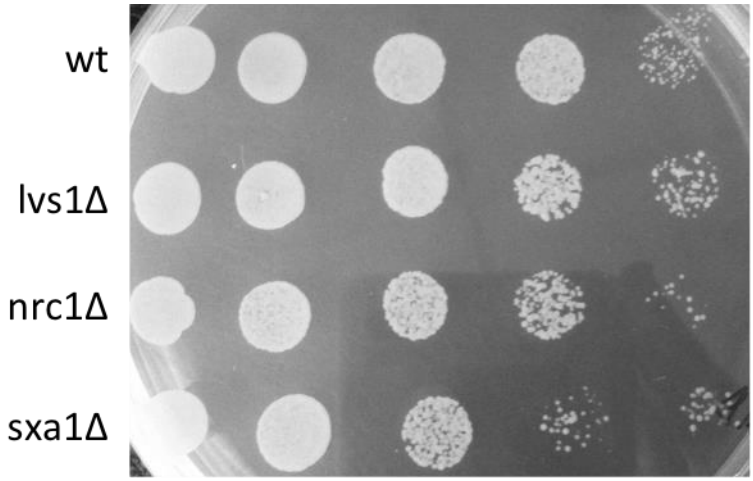

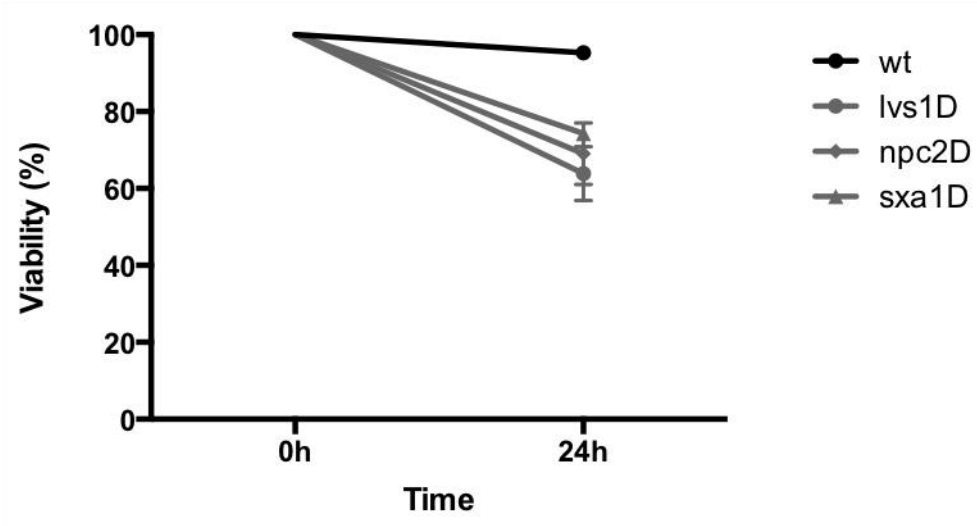

6.2 Testing compounds in other lysosomal storage disorders yeast strains

In the drug screen performed with the *btn1*Δ strain, three compounds were positively selected and subsequently validated in their ability to rescue several phenotypes in *btn1*Δ cells: alloxazine, E-64 and prochlorperazine dimaleate (Results Chapters 2 and 3). Since the yeast strains modelling the lysosomal storage disorders (Chédiak Higashi Syndrome, Niemann-Pick disease type C2 and congenital CLN10 disease) share at least two common phenotypes with the strain modelling juvenile CLN3 disease, the same compounds were tested for their ability to rescue the two phenotypes in these other strains: enlarged vacuoles and high septation index. The three compounds are, in fact, able to rescue the enlarged vacuoles phenotype in all strains. Their effect in the other phenotype was varied.

6.2.1 Vacuole size

The mean vacuole size of all the LSD strains (*lvs1*Δ, *npc2*Δ and *sxa1*Δ) after treatment with three compounds (alloxazine, E-64 and prochlorperazine dimaleate) was measured and compared to the same untreated strains and wild-type treated cells. All strains were also treated with DMSO (the carrier of the compounds) as a control. At least 500 vacuoles were measured for each compound in three independent experiments.

Cells deleted for *lvs1* have the largest vacuoles from all the strains that were analysed; the presence of all the three compounds reduced the vacuole size to a significantly smaller size, but still larger than in the wild-type strain (0.86 μm). After being treated with each compound, the mean vacuole size of the *lvs1*Δ strain, which models the Chédiak Higashi Syndrome, is significantly reduced: approximately 1.2 μm compared to 1.62 μm for *lvs1*Δ untreated cells. After measuring the vacuoles diameter in the *npc2*Δ cells, it was shown that all three

compounds are able to significantly rescue this phenotype. The vacuoles diameter in this strain is significantly reduced in the presence of the compounds: 1.03 µm for alloxazine, 0.97 µm for E-64 and prochlorperazine dimaleate, when compared to 1.06 µm for the *npc2*Δ strain. Finally, the vacuoles size of *sxa1*Δ cells was measured after treatment with all three compounds. Treated cells show significantly smaller vacuoles than the untreated strain (1.08 µm): 1 µm for alloxazine, 0.98 µm for E-64 and prochlorperazine dimaleate (Figure 6.2.1).

Figure 6.2.1. Effect of different compounds on the vacuole size of different lysosomal storage disorders yeast strains

Alloxazine, E-64 and prochlorperazine dimaleate are able to rescue the enlarged vacuoles in yeast models of three lysosomal storage disorders *lvs1*Δ, *npc2*Δ and *sxa1*Δ. Graphs show the mean (±SEM) of the vacuoles diameter (in μm) of the *lvs1*Δ, *npc2*Δ and *sxa1*Δ strains treated with DMSO (control) and different compounds (10μM): alloxazine, E-64 and prochlorperazine dimaleate (proc). The average vacuole diameter of the wild-type strain treated with DMSO is represented by a grid line in all graphs (wt). Data was collected in three independent experiments. Statistical significances between each treatment were determined using a one-way ANOVA with a Tukey's multiple comparison post-test. Statistical significances between *lvs1*Δ, *npc2*Δ and *sxa1*Δ treated with DMSO and with the three compounds are represented in the graph above the compounds bars (****p= <0.0001). lvs1D – Chédiak-Higashi syndrome yeast model: *lvs1*Δ strain; npc2D – Niemann-Pick type C2 yeast model: *npc2*Δ strain; sxa1D – congenital CLN10 disease yeast model: *sxa1*Δ strain. All the strains were treated with DMSO.

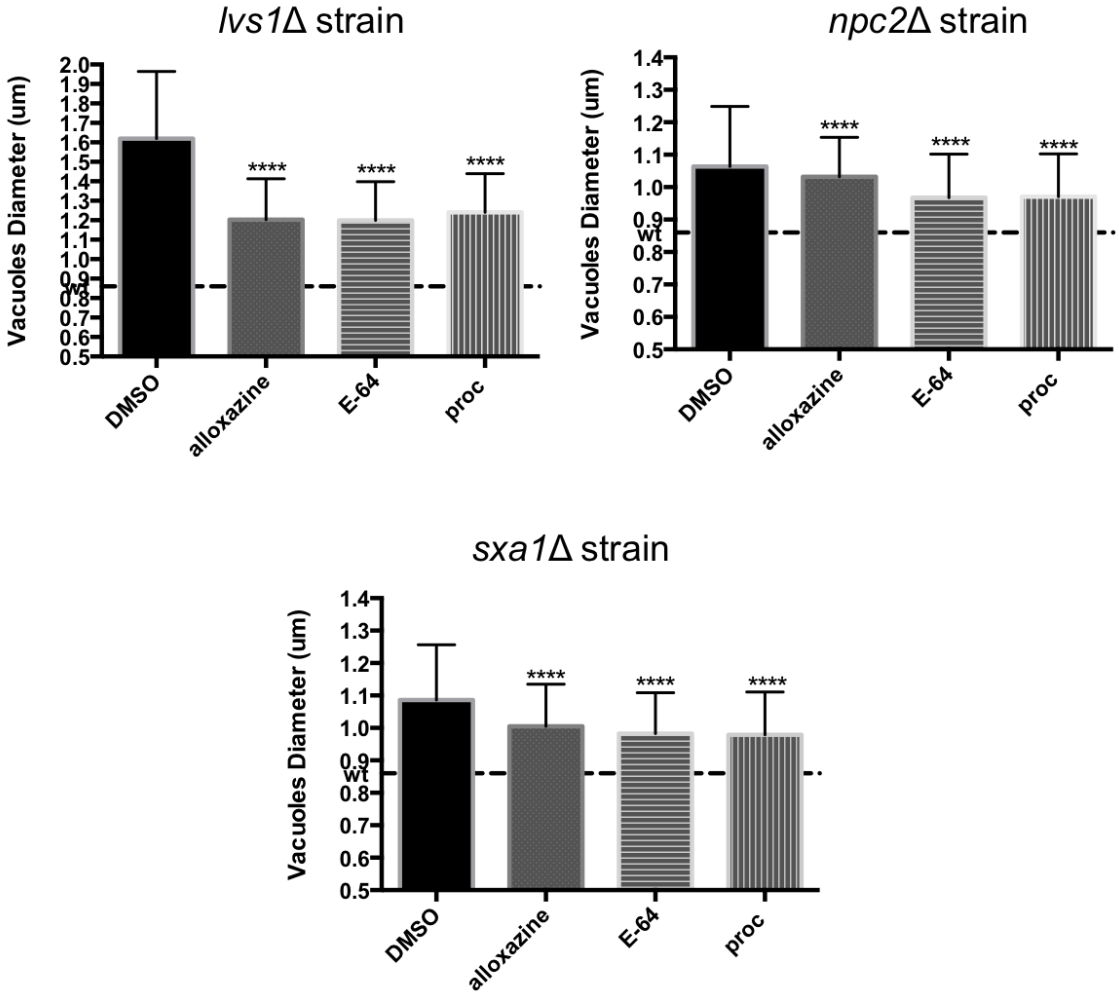

6.2.2 Septation index

It was previously shown that cells deleted for *lvs1*, *npc2* and *sxa1* have a significantly higher septation index than wild-type cells, similar to *btn1*Δ cells (section 6.1.2). Therefore, these strains were treated with the compounds alloxazine, E-64 and prochlorperazine dimaleate and the number of septated cells were counted for each treatment. At least 300 cells were counted for each compound in three independent experiments. All the compounds are able to rescue the high septation index in the *lvs1*Δ strain: 11.07%, 8.42% and 5.3% with alloxazine, E-64 and prochlorperazine dimaleate respectively, compared to 20.12% in untreated cells. For the two remaining strains, only alloxazine and prochlorperazine dimaleate are able to significantly rescue the index in the *npc2*Δ (16.83% and 11.77% respectively, in comparison with 24.11% in untreated cells), and none of the compounds has any effect on the *sxa1*Δ strain (Figure 6.2.2). All strains were also treated with DMSO (the carrier of the compounds) as a control. Some of the compounds were able to rescue this phenotype to values even lower than the wild-type strain (12.68%).

Figure 6.2.2. Effect of different compounds on the septation index of other lysosomal storage disorders yeast strains

Alloxazine, E-64 and prochlorperazine dimaleate are able to rescue the high septation index in the *lvs1*Δ strain. Alloxazine and prochlorperazine dimaleate are able to rescue the high septation index in the *npc2*Δ strain. Graphs shows the mean (±SEM) of septation index in the *lvs1*Δ, *npc2*Δ and *sxa1*Δ strains treated with DMSO (control) and different compounds (10μM): alloxazine, E-64 and prochlorperazine dimaleate (proc). The average septation index of the wild-type strain treated with DMSO is represented by a grid line in all graphs (wt). Septation index is the percentage of septated cells in total number of cells. Data was collected in three independent experiments. Statistical significances between each treatment were determined using a one-way ANOVA with a Tukey's multiple comparison post-test. Statistical significances between *lvs1*Δ, *npc2*Δ and *sxa1*Δ treated with DMSO and with the three compounds are represented in the graph above the compounds' bars (*p= <0.1;***p= <0.001; ****p= <0.0001). lvs1D – Chédiak-Higashi syndrome yeast model: *lvs1*Δ strain; npc2D – Niemann-Pick type C2 yeast model: *npc2*Δ strain; sxa1D – congenital CLN10 disease yeast model: *sxa1*Δ strain. All the strains were treated with DMSO.

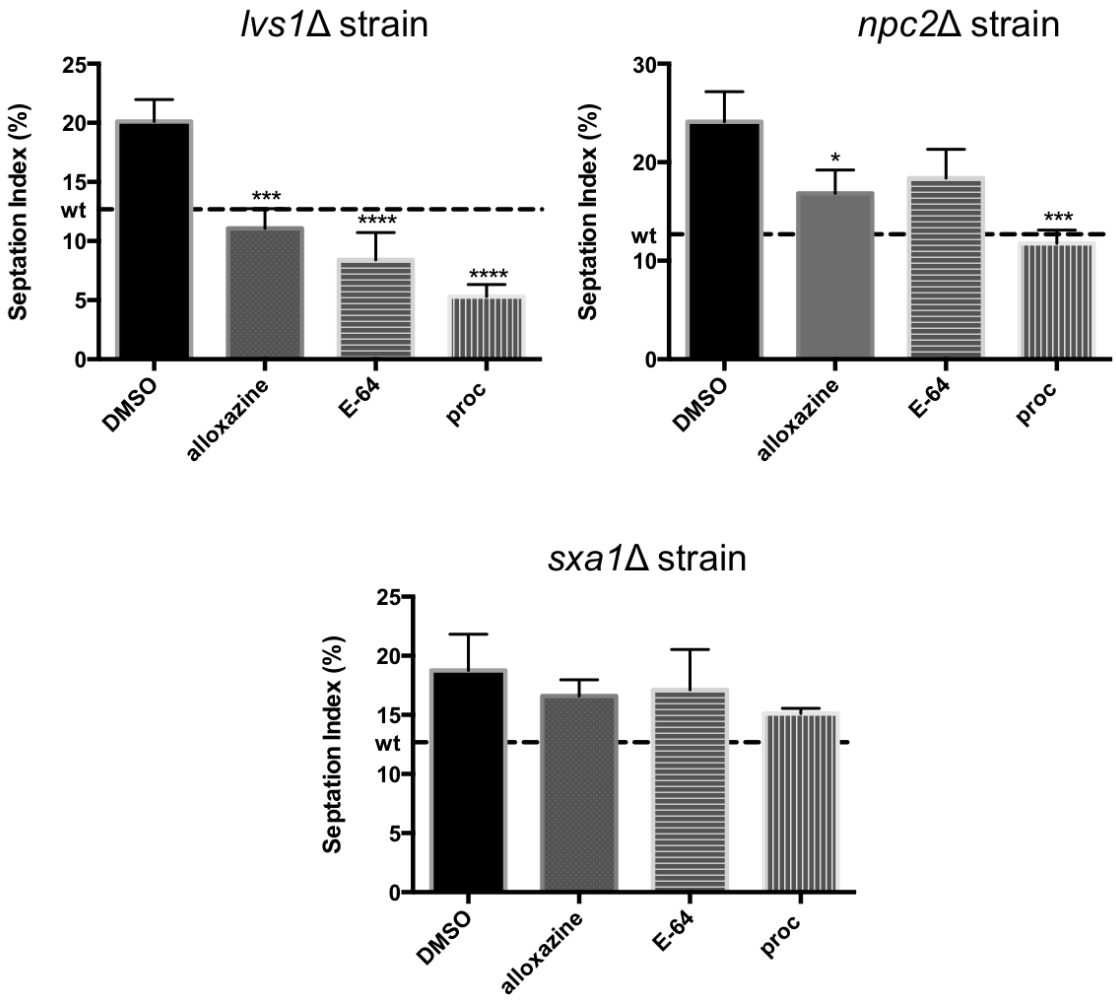

6.3 Summary

The last part of the project consisted in the study and characterisation of fission yeast strains modelling three Lysosomal Storage Disorders: Chédiak Higashi Syndrome, Niemann-Pick disease type C2 and congenital CLN10 disease. The first step was to characterise the strains in terms of the phenotypes that had previously been observed in the yeast model of juvenile CLN3 disease, the *btn1*Δ strain. All three strains presented two of the five phenotypes that were explored. These strains have larger vacuoles and more septated cells than the wild-type strain. The phenotype of increased vacuole size was particularly evidenced in the *lvs1*Δ strain (model of the Chédiak Higashi Syndrome), whose name, given in previous work, reflects this phenotype (unpublished data): *large vacuoles strain*. On the other hand, the septation index phenotype was more apparent in the *npc2*Δ strain (model of the Niemann-Pick disease type C2).

The drug screen that was carried out with the *btn1*Δ strain led to the identification of three compounds that are able to rescue several phenotypes associated with the loss of *btn1* in fission yeast, including the enlarged vacuoles and the high septation index phenotypes. Therefore, the same compounds, alloxazine, E-64 and prochlorperazine dimaleate, were tested in the LSD strains (*lvs1*Δ, *npc2*Δ and *sxa1*Δ) to test whether they were also able to rescue the two phenotypes observed in these strains. All compounds showed significant rescue of the increased vacuoles size in all strains. As for the other phenotype, high septation index, all the compounds were able to rescue the phenotype in the *lvs1*Δ strain. In the *npc2*Δ strain, only alloxazine and prochlorperazine dimaleate were able to rescue the large number of septated cells. Finally, none of the compounds were able to rescue this phenotype in the *sxa1*Δ strain. Taken together these results show that, although some differences in terms of phenotypes were observed between the four LSD strains (*btn1*Δ, *lvs1*Δ, *npc2*Δ and *sxa1*Δ), they might be involved in common pathways, since similar effects were seen in the absence of these proteins.

7 Discussion

The initial findings from this study show that distinct integrated mutations in the *btn1* gene affect Btn1p function differently and, as a consequence, have varying effects on cell phenotypes. Varying levels of Btn1p expression can be related to the different phenotypes, since overexpression of *btn1* leads to an over-compensation of the tested phenotypes, when compared to wild-type cells. Furthermore, mutations in Btn1p seem to affect its expression levels (Chapter 3.2.2). The endogenously expressed *btn1* containing a deletion comparable to that of the common 1-kb intragenic deletion, present in the majority of juvenile NCL patients (Consortium 1995), was shown to retain partial function and prevent the appearance of some *btn1*Δ phenotypes almost as effectively as the full-length protein (Results Chapters 1 and 2). This observation corroborates previous studies where the ectopically expressed mutant Btn1p presented as a partially functional protein (Kitzmuller *et al.* 2008; Haines *et al.* 2009). The endogenous mutant protein expressing the p.E240K mutation prevented the appearance of all phenotypes that were tested in the first part of the project and didn't seem to significantly change the Btn1p expression levels (Results Chapter 1), revealing that it does not affect Btn1p function to the same extent as the 1-kb deletion. These results are consistent with the fact that this mutation underlies the mildest form of juvenile NCL (Aberg *et al.* 2009). Finally, endogenous expression of the mutant protein containing the p.G136A mutation resembled complete deletion of *btn1*, with more phenotypes observed than the 1-kb deletion mutant, and a decrease in the protein expression levels (Results Chapters 1 and 2). This supports the idea that p.G136A is a null mutation as previously suggested (Haines *et al.* 2009).

Current therapeutic strategies for the types of neuronal ceroid lipofuscinosis caused by enzyme defects are not applicable to juvenile CLN3 disease. New tools or therapeutic strategies are urgently required for treatment of this disease. In this project the fission yeast *Schizosaccharomyces pombe* was used in an attempt to identify novel lead compounds suitable for the

development of potential therapeutic strategies for juvenile CLN3 disease. Many genes and cellular pathways are conserved between fission yeast and humans, and therefore compounds that revert JNCL-associated phenotypes in the yeast model may be relevant for patients. At present, readily detectable phenotypes suitable for high-throughput screening approaches have not been identified in mammalian cells. On the other hand, different marker phenotypes have been characterised in fission yeast. *S. pombe* is a genetically tractable model organism, already well established in juvenile NCL research that has less than a fifth of the number of human genes, and is therefore an ideal organism for performing a screen for potential therapeutic drugs for juvenile CLN3 disease, even though some mammalian cellular pathways may not be present in this simpler organism. Moreover, an advantage of phenotypic screening is that the exact function of the protein (in this case CLN3 or Btn1p), or the molecular basis of the phenotype selected for the screen, does not need to be known in order to perform it. In this case, the drug will lead to a cellular effect, which cannot be guaranteed in a target-based screen. Results obtained in this study are complementary but potentially more far-reaching than currently available candidate approaches in mammalian cells or other model systems. Additionally, the compounds identified in the yeast drug screen were also tested in patient fibroblasts and a zebrafish model, and gave good results. This shows that it is possible to translate results obtained in *S. pombe* to human cells, relevant to juvenile CLN3 disease. This strategy could be adopted more widely in research to find new treatments for inherited diseases.

The first step towards the development of the drug screen was to identify a robust and striking phenotype that was easily identified when rescued and significantly different between strains with and without *btn1*. *btn1*Δ cells show a growth sensitivity at 37°C in the presence of cyclosporine A, a calcineurin inhibitor (Results Chapter 2). Therefore, the viability of *btn1*Δ cells (compared to wild-type cells), after growing in these conditions, was selected as the marker phenotype, basis for the screen. This is an ideal phenotype for this purpose since it assesses something as basic as survival/death of the strains, where cells with no *btn1* cannot survive as well as wild-type cells. This phenotype was

not suitable for mutation-specific screening, since strains with *btn1* expressing two mutations (1-kb deletion and p.E240K missense mutation) were not sensitive to cyclosporine A. However, compounds that rescue phenotypes associated with the complete deletion of the gene are likely to be able to correct phenotypes in strains with more mild mutations, as seen with the cell curving phenotype. Nevertheless, it would be desirable to find other mutation-specific phenotypes suitable for a drug screen so that further compounds could be identified.

The developed high-throughput screen was performed using the LoPac collection of 1280 FDA-approved compounds, and the six strongest hits were selected for further validation experiments. These compounds were manually retested in the same conditions as the automated drug screen in at least three independent experiments (Results Chapter 3). Three compounds that were able to consistently rescue the sensitivity of *btn1*Δ cells to cyclosporine A, without significantly affecting the viability of wild-type cells, were selected for further validation experiments: alloxazine, E-64 and prochlorperazine dimaleate.

The final three compounds were then tested for their ability to rescue four other *btn1*Δ specific phenotypes: enlarged vacuoles, increased septation index, elevated number of curved cells and sensitivity to growth at high temperature (Results Chapter 3). All compounds were able to rescue the majority of the tested phenotypes. Finally, they were also tested in juvenile NCL patient fibroblasts and in a zebrafish disease model to verify their ability to rescue other phenotypes associated with mutated *CLN3*. All compounds were able to rescue at least one phenotype in zebrafish, and E-64 and prochlorperazine dimaleate showed a complete rescue of Golgi compactness in fibroblasts. Altogether these preliminary results are very encouraging, with respect to a potential juvenile CLN3 disease therapy. However, much future work is needed. First, to further clarify the mechanism of action of the compounds in fission yeast. Compounds can then be tested in higher organisms (such as mice) in order to determine their efficacy for therapeutic use. Toxicity should not be an issue for

future potential use in patients since all the compounds identified in this study are FDA-approved, and therefore known to be safe.

The last part of this project was the study of three different fission yeast strains that model other lysosomal storage disorders (LSDs): Chédiak Higashi Syndrome, Niemann-Pick disease type C2 and congenital CLN10 disease. These strains were characterised particularly in terms of several phenotypes that are associated with the *btn1*Δ strain (Results Chapter 4). All three strains presented two of the five phenotypes that were explored: enlarged vacuoles and increased septation index, supporting a previously reported impairment of the lysosomal/vacuolar function in these strains (Faigle *et al.* 1998; Wang *et al.* 2010; Kohan *et al.* 2011). After the characterisation, compounds that were efficacious in the *btn1*Δ strain were tested for their ability to rescue the newly described phenotypes associated with the three LSD strains. Notably, all three compounds showed significant rescue of the increased vacuole size in all strains. On the other hand, the effect of the compounds on the septation index phenotype was different among the strains. To summarise, the three tested compounds affected the function of Btn1p, Lvs1p, Npc2p and Sxa1p proteins differently. However, there were some overlapping phenotypes between the four strains, suggesting that some pathological mechanisms are common between them, and this should be further explored in the future in regards to a common therapeutic strategy for these and probably other LSDs.

7.1 *CLN3* mutations affect the protein function in different manners

It has been shown in this study and previous work in the *S. pombe* model of juvenile CLN3 disease (Haines *et al.* 2009) that some mutations in the *btn1* gene have different effects on the protein function. Whilst all the previous work done in *S. pombe* was based on the ectopic expression of mutated and non-mutated Btn1p, this study investigated strains with endogenously expressed mutant protein, where the mutated versions of *btn1* were integrated in the yeast genome under the control of the *btn1* promoter. Three different strains expressing three different *btn1* mutations were created: the 1-kb deletion equivalent to the one present in the majority of juvenile NCL patients (Consortium 1995); the p.E240K missense mutation equivalent to the one that underlies the mildest form of the juvenile CLN3 disease (Aberg *et al.* 2009) and the p.G136A mutation, reported to produce a nonfunctional protein which resembles the complete deletion of Btn1p in terms of phenotypes (Haines *et al.* 2009). The 1-kb deletion and the p.E240K mutation are not complete null mutations, since strains with endogenous expression of these mutant proteins show less severe phenotypes compared to the *btn1*Δ strain, where *btn1* is absent, and are more similar to the wild-type strain, even in terms of protein expression levels. On the other hand, cells expressing *btn1* with the p.G136A mutation display all the phenotypes that are also observed in the *btn1*Δ cells and is sufficient to affect the levels of expression of Btn1p, suggesting that this is truly a null mutation. These observations also suggest that there are regions in the Btn1p protein that are more important for its function when compared to other regions.

7.1.1 Level of expression of Btn1p is relevant to its function

The results obtained in this study showed that the levels of expression of *btn1* influence the protein function the overall cell biology. When overexpressed, under the control of a full strength *nmt1* p3 promoter, some phenotypes associated with the loss of *btn1* are slightly different from the wild-type strain. For instance, the average diameter of vacuoles is smaller, and there is a slight reduction in the number of curved cells at 37°C when compared to the wild-type strain. Furthermore, there is, in fact, a significant difference between the wild-type strain and the one under the control of the *nmt1* p3 promoter in regards to the number of septated cells (Results Chapter 1). Furthermore, when expressed under the control of *nmt1* p41 promoter (weaker than the p3 promoter), the vacuole size and the number of septated and curved cells at 37°C are similar to the wild-type strain. Similar effects were seen in previous studies, where both the overexpression and absence of Btn1p affected the Golgi compartments and trafficking (Codlin & Mole 2009) and increasing levels of Btn1p correlated with decreasing vacuolar size (Gachet *et al.* 2005). The expression of Btn1p appears to be slightly affected when tagged at its N-terminal with GFP, under the control of its native promoter. GFP is a large tag and it is not unexpected for it to slightly affect the function of any tagged protein. The yeast strain with GFP-tagged Btn1p expressed from the *btn1* native promoter showed slight but not significant differences in the phenotypes when compared to the wild-type strain: larger vacuoles, higher septation index but less curved cells. Thus, it is important to be aware of this, and to use both tagged and untagged forms when studying this protein.

The integrated mutant strains explored in this study also seem to affect the Btn1p expression levels. The strain with the p.G136A mutation is the one that has the largest effect, decreasing these levels, whereas the p.E240K mutation shows similar levels to wild-type Btn1p (Chapter 3.2.1). This is expected since in human patients, the p.Glu295Lys mutation in *CLN3* underlies the mildest form of the disease, and the yeast mutant strain has less phenotypes than the complete deletion of *btn1*. Moreover, the p.G136A mutation shows all the same

phenotypes than *btn1*Δ, and is predicted to be a null mutation. In summary, different mutations cause differences in the levels of GFP-tagged protein expression. This conclusion was based on a qualitative observation of the GFP signal produced by these mutant strains. Therefore, to confirm and quantify the differences in expression levels, a Western Blot assay must be performed.

Together, these results support the hypothesis that the level of Btn1p expression is important for protein function, and that it is tightly regulated. This is in accordance with previous results that showed that the wild-type endogenous levels of expression of Btn1p are low (Codlin & Mole 2009).

7.1.2 Mapping functional domains of Btn1p

In order to map functional domains of Btn1p, the position of different mutations in the predicted topology of the protein and the effect of these mutations were analysed.

Two different mutations that share loss of a common amino acid (E240), 1kbΔ (102fsX5) and p.E240K, were both found to rescue the vacuole size, the septation index, the growth at high temperature, and growth in the presence of cyclosporine A defects. Furthermore, the 1kbΔ mutant Btn1p was also shown to be able to marginally improve the vacuole pH, and the p.E240K mutation significantly reduced the cell curving percentage after growth at 37°C. Altogether, these results demonstrate that the first 102 amino acids of Btn1p (equivalent to the first 153 amino acids in human CLN3) are sufficient to be functional in several pathways (maintenance of lysosomal size and pH, control of the cytokinetic process, resistance to cyclosporine A and to high temperature). This region of the protein includes the cytoplasmic N-terminal and two or three predicted transmembrane domains, depending on the topology that is considered (Nugent *et al.* 2008; Ratajczak *et al.* 2014). This N-terminal region is not conserved, contrary to the transmembrane regions, which suggests that the function of Btn1p (and CLN3) is exerted from within the membrane, or from the lumenal loops of the protein. The importance of the lumenal regions in the protein function has previously been reported (Haines *et al.* 2009). Similarly, the G to A point mutation of Btn1p affecting amino acid 136 (equivalent to 187 in CLN3), is also located either in the lumen or in the fourth transmembrane domain (according to the Nugent or Ratajczak topology, respectively), has great effect on the protein function, acting as a loss-of-function mutation. This finding supports the idea that this lumenal and/or transmembrane region of Btn1p (and CLN3) is crucial for its function in the cell. By extrapolation, the C-terminal region of CLN3 is not required at least for the functions mentioned above: lysosomal homeostasis, cytokinesis, resistance to high temperature and to cyclosporine A.

In the case of the curving defect, the region of the protein after the first 102 amino acids (absent in the 1-kb-deleted protein), except when the amino acid E240 in the fifth transmembrane domain is altered, is sufficient to rescue this defect (Figure 1.1.1). This suggests that the region of the protein corresponding to the last four transmembrane domains and the amphipathic helix is important to regulate the function of Btn1p related to cytoskeleton and cell wall morphology.

The 1-kb-deleted protein has been localised to the ER, both in yeast and human fibroblasts (Kitzmuller *et al.* 2008; Haines *et al.* 2009), which suggests that the truncated protein exerts some function from the ER or other early compartment, and not only from the lysosomes/vacuoles. However, any Btn1p/CLN3 functions associated with the cell cytoskeleton and cell wall composition may be exerted from a later compartment, being impaired when the protein is retained in the ER. The effect of mutated Btn1p/CLN3 on the lysosomes, exerted from its location in the ER, is similar to that observed for other NCL proteins, CLN6 and CLN8, which are both located in the ER and affect lysosomes (Mole *et al.* 2004; Vantaggiato *et al.* 2009).

Whilst many functions arise from complete loss of *btn1* function, not all the resultant phenotypes are affected by mutations in *btn1* equivalent to those associated with juvenile CLN3 disease. Thus, therapy need to target only those pathways disrupted by the 1-kb deletion, present in the majority of patients, not all those affected by complete loss of CLN3 function. For instance, and since the 1-kb-deleted Btn1 protein seems to rescue all but the cell curving phenotype, therapeutic approaches that would target any pathway associated with the cell wall morphology or cytoskeleton in yeast, would be ideal. These pathways could then be extrapolated to mammalian cell biology. However, it is worth bearing in mind that 1-kb mutant mammalian cells have lysosomal defects (Sleat *et al.* 1998; Holopainen *et al.* 2001; Kitzmuller *et al.* 2008) and other defects that are less apparent in the yeast model but would need to be rescued in therapy. Focusing on one phenotype is important for the initial steps and

identification of potential therapeutic compounds, but it is crucial to further validate therapeutic strategies in a range of mutant backgrounds.

7.1.3 New insights into CLN3 function

CLN3 has been reported to be localised in different regions in mammalian cells. Btn1p has been localised to the vacuoles and the Golgi complex (Gachet *et al.* 2005; Codlin & Mole 2009). In this study, a similar observation was made: endogenously expressed GFP-Btn1p co-localises with the vacuole marker FM4-64, but there is also some GFP signal elsewhere, which is likely to correspond with the Golgi (Chapter 3.1.2). This was the first study where the localisation of endogenously expressed Btn1p was analysed, since all previous results were performed with ectopically and overexpressed Btn1p.

Furthermore, *btn1* mutations affect the localisation of the protein. As previously reported, the 1-kb deletion changes the localisation of Btn1p to the ER (Haines *et al.* 2009), and mice studies have shown that mutant CLN3 cannot exit the ER due to misfolding or missing localisation signals (Järvelä *et al.* 1999). There are lysosomal targeting signals located at the C-terminal of the protein (Haines *et al.* 2009) that are missing in the truncated Btn1p, which may also contribute to preventing exit of this mutant protein from the ER. A similar observation was made in cells with the mutant Btn1p containing the p.G136A mutation (Gachet *et al.* 2005). The amino acid Gly136 is thought to be localised either in a lumenal or transmembrane region of protein, and is thought to be essential for its function. Therefore when mutated, this amino acid might alter the correct conformation of Btn1p and lead to its retention in the ER, and possibly degradation. Finally, cells expressing Btn1p with the p.E240K mutation were reported to be localised in the vacuoles, but also present in pre-vacuolar compartments (Haines *et al.* 2009). Possibly, the region of the protein affected by this mutation (amino acid 240 in the fifth transmembrane domain) may affect the trafficking of the protein by affecting its conformational state, but not to the same extent as the two other mutations.

It is known that CLN3 and Btn1p have an important role in lysosomal homeostasis. The lysosomal/vacuolar pH is less acidic in patient fibroblasts and *btn1*Δ cells (Holopainen *et al.* 2001; Gachet *et al.* 2005) (Chapter 4.1.3) and

these organelles are larger in *CLN3*-depleted HeLa cells and in *btn1*Δ cells (Gachet *et al.* 2005; Kitzmuller *et al.* 2008). A functional role of CLN3/Btn1p in lysosome/vacuole homeostasis was proposed to be exerted from a prevacuolar compartment in yeast cells, since the vacuole size in the *btn1*Δ/*ypt7*Δ double mutant was even bigger than in *ypt7*Δ mutant alone, where Btn1p is unable to traffic to the vacuoles (Gachet *et al.* 2005). This is in accordance with the observation that CLN3/Btn1p is located in the Golgi and other prevacuolar compartments. Alterations in vacuole pH, and consequently in the activity of the v-ATPase, have been shown to affect the composition of the cell wall in fission yeast, similar to that observed in *btn1*Δ cells (Codlin *et al.* 2008a). This observation, together with the vast array of other phenotypes observed in cells with defective CLN3/Btn1p, suggest that a defective activity of the v-ATPase may have an effect on the trafficking of many other proteins in the endocytic pathway, and possibly other pathways. Furthermore, the v-ATPase plays an important role in the transport of neurotransmitters into vesicles in the brain (Cousin & Nicholls 1997), and therefore when v-ATPAse function is affected there could be a great impact on neuronal transmission potentially leading to neurodegeneration, the hallmark of juvenile CLN3 disease.

Similar to the observations made in this study, as well as in previous works, where *btn1*Δ cells have an abnormally curved morphology suggesting defects in microtubules or their related molecules (Haines *et al.* 2009) (Chapter 3.3.3), the CLN3 protein function has been associated with the organisation and regulation of cytoskeleton (Uusi-Rauva *et al.* 2008). This cytoskeletal disorganisation may affect intracellular transport, once again causing a panoply of cellular defects. For example, it is possible that trafficking of different transporters (like the v-ATPase) through actin is impaired when CLN3 is defective. In yeast, the correct polarization of actin is dependent on the endocytic process (Smythe & Ayscough 2006), suggesting that the actin depolarisation of *btn1*Δ cells (Codlin *et al.* 2008b) is intimately linked with defects in membrane trafficking. It is also known that the activity of v-ATPase is linked to the actin cytoskeleton (Vitavska *et al.* 2003), which can explain the presence of phenotypes affecting both pathways in CLN3/Btn1p-deficient cells. Furthermore, the dynactin complex,

activator of microtubule motor protein dynein, has been reported to be downregulated in a *Cln3* knockout mouse (Luiro *et al.* 2006) validating the hypothesis of a link between CLN3 and microtubule transport.

The defect in cytokinesis of *btn1*Δ cells is independent of the defect in v-ATPase activity, since it is not rescued by the growth of cells in acidic media (Codlin *et al.* 2008a). This defect may be due to a defective exocyst pathway, which is known to regulate the cell separation at the septum during the division process (Wang *et al.* 2002). However, the exact cause of this phenotype remains to be defined. More interestingly, it is known that correct localisation of exocyst proteins in the medial area of dividing cells is actin-dependent. This establishes a link between cytokinesis and the cytoskeleton phenotypes both observed in *btn1*Δ cells. Moreover, the fact that both mutant proteins containing either the 1-kb deletion or the p.E240K mutation are able to rescue the vacuole size defect, the high septation index and the growth at high temperature suggests a possible link between these three phenotypes. In a previous study, all mutants that were able to rescue the enlarged vacuoles in *btn1*Δ cells equally rescued the number of septated cells, reinforcing the idea that these two pathways are linked in some way (Haines *et al.* 2009).

As discussed in the Introduction Chapter, Btn1p (and by inference, CLN3) is thought to be exerting its function in the Golgi apparatus compartments, affecting multiple downstream pathways. Therefore, when this function is disturbed, it eventually leads to defects at the vacuole level, as well as in the processes of cell growth, division, morphology and stress response. It is likely that Btn1p/CLN3 is required for the regulation of membrane trafficking to the lysosomes, the sorting and activity of different transporters and channels and the endocytic process. In fact, the involvement of CLN3/Btn1p in post-Golgi sorting and trafficking of proteins and in endocytosis has previously been reported and is detailed in the Introduction Chapter (Luiro *et al.* 2004; Metcalf *et al.* 2008; Codlin & Mole 2009).

7.1.3.1 CLN3: a potential channel?

The fact that *CLN3* is highly conserved across several species suggests that it plays a pivotal cellular role. It is likely that its complete loss of function may underlie a more severe disease than juvenile CLN3 disease, where partial function of the protein remains (see above in this chapter). The yeast orthologue of *CLN3*, *btn1*, is essential for correct cellular growth and division, especially at high temperature, proposing an essential role in this organism.

As mentioned above, Btn1p is important for vacuole acidification. Although it is possible that this effect is indirect via the correct sorting of v-ATPase, it is also possible that Btn1p is acidifying the vacuoles directly. Btn1p may be a channel or ion transporter, and there are several lines of evidence that support this hypothesis. First, CLN3 and Btn1p are known to be involved in the transport of arginine into the vacuole and in cerebellar cells (Kim *et al.* 2003; Ramirez-Montealegre & Pearce 2005; Chan *et al.* 2009). Second, phenotypes observed in a knockout mouse model of juvenile NCL resemble those seen in a chloride channel CLC-3-deficient mouse (Mitchison *et al.* 1999). Third, the sequence of *CLN3* is distant but significantly similar to the equilibrative nucleoside transporter hENT1 (Baldwin *et al.* 2004), and according to Pfam (a Wellcome Trust Sanger Institute database of protein families, http://pfam.xfam.org/) CLN3 is a member of the major facilitator superfamily (MFS), a membrane transporter superfamily (Pao *et al.* 1998). Finally, it is also known that CLN3 regulates the intracellular levels of cytosolic free calcium (Ca^{2+}) in SH-SY5Y cells (Chang *et al.* 2007) and a calcium channel antagonist, amlodipine, was reported as being able to reverse the elevated intracellular calcium levels seen in rat cortical neurons treated with *CLN3* siRNA (Warnock *et al.* 2013). CLN3 may be a lysosomal calcium channel. These type of channels are responsible for maintaining the lysosomal calcium content at a specific concentration (Lemons & Thoene 1991) and therefore, when defective, lead to alterations of calcium levels in these organelles and consequently in the cytosol. Furthermore, dysregulated calcium levels in lysosomes greatly affects the endocytic transport

(Kiselyov *et al.* 2010), which could explain the fact that several cellular proteins are affected in the absence of CLN3/Btn1p.

Changes in intracellular levels of calcium and dysfunction of lysosomal calcium channels have a great effect on crucial processes in nerve cells, and calcium overload eventually leads to cell death, neurodegeneration (Siesjo *et al.* 1986; Heizmann & Braun 1992; Kiselyov *et al.* 2010), a common feature of lysosomal storage disorders (Jeyakumar *et al.* 2005; Kiselyov *et al.* 2010; Lloyd-Evans & Platt 2011). Calcium homeostasis is also linked to mitochondrial function (Duchen *et al.* 2008) and mitochondrial defects have been reported in CLN3 disease (Fossale *et al.* 2004; Luiro *et al.* 2006; Lojewski *et al.* 2014), suggesting that these defects may be leading to dysregulation of calcium levels in these diseases.

Yeast vacuoles are the major site of intracellular calcium storage (Denis & Cyert 2002). The regulation of intracellular calcium levels in yeast is crucial for several cellular functions to be carried out appropriately: cytokinesis, cytoskeletal organization and cell wall integrity. All of these pathways are regulated by calcium signalling pathways, which in turn are mediated by calcium channels, pumps and transporters (Cortes *et al.* 2004). These channels and transporters are responsible for the uptake and release of calcium into or out of the cell/organelles via the respective membranes. Btn1p may be acting as a vacuolar channel in yeast regulating calcium levels in these organelles and cells.

7.1.3.2 Btn1p and TOR signalling pathway

Btn1p is also linked to the target of rapamycin (TOR) signalling pathway and other connected pathways in yeast. In response to glucose limitation, fission yeast appropriately represses TORC1, and activates TORC2 to maintain viability until glucose becomes available (Ikai *et al.* 2011). The TORC2 pathway is also involved in a correct response to exogenous stress, whereas TORC1

represses this stress response (Ikeda *et al.* 2008). Work performed by Dr Michael Bond (unpublished data) showed that *btn1*Δ cells are unable to correctly respond to limited nutrient conditions and high temperature (due to a reduced signalling in the TORC2 pathway) which could be rescued by reducing TORC1 or increasing TORC2 function. This inability to respond to stress is consistent with the phenotypes seen at 37°C, such as reduced viability, cell curving and sensitivity to cyclosporine A. Furthermore, a role for the mammalian TOR (mTOR) pathway in regulating microtubule-dependent protein transport was identified in rat fibroblasts (Jiang & Yeung 2006) suggesting that there is a link between this signalling pathway, the cytoskeleton organization (known to be disrupted in *CLN3*- and *btn1*-depleted cells) and the defective transport of certain proteins.

There are a lot of similarities between the processes regulated by Btn1p and a small GTPase Ypt3p, the yeast orthologue of the mammalian Rab11, proposing that they might share a similar function. Ypt3p is localised in the Golgi and endosomes, similarly to Btn1p (He *et al.* 2006); and cells with mutated *ypt3* show similar phenotypes to *btn1*Δ: defects in the cell wall composition, cytokinesis and vacuolar fusion processes, and aberrant Golgi compartments (Cheng *et al.* 2002). Furthermore, Gad8p, a kinase lying downstream of TORC2 in the TORC2 signalling cascade, is affected in both Ypt3p and Btn1p mutant cells (Tatebe *et al.* 2010) (Mike Bond, unpublished data). Ypt3p has been reported to interact with calcineurin, a Ca^{2+}-dependent phosphatase that negatively regulates and is regulated by TORC2 (Cheng *et al.* 2002). Ypt3p mutants require calcineurin activity for vegetative growth and double mutants (Ypt3p and calcineurin) are synthetically lethal, suggesting that these proteins have overlapping functions. Since *btn1*Δ cells are sensitive to growth in the presence of cyclosporine A, an inhibitor of calcineurin, it is likely that Btn1p function is linked to the calcineurin pathway. For instance, Btn1p may have an overlapping function with calcineurin, similarly to Ypt3p. Furthermore, Ypt3p was reported to be involved in the transport of proteins from the Golgi compartments and in the exocytic pathway, and calcineurin was proposed to regulate these events (Cheng *et al.* 2002). If this is the case, the role in protein

transport may be the overlapping function between Btn1p and calcineurin. Future work has to be done in order to further elucidate the interplay between Btn1p and calcineurin, and also to better understand the reported similarities between Btn1p and Ypt3p.

7.2 Using a drug screen approach in a yeast model to develop therapy for juvenile CLN3 disease

The choice of using a *S. pombe* model of juvenile CLN3 disease to perform a drug screen is due to the fact that fission yeast is easy to genetically manipulate, grows rapidly, and has a high degree of conservation of genes and molecular pathways with mammalian cells. *S. pombe* is a good model for the study of lysosomal storage disorders since it contains numerous vacuoles, the yeast equivalent to lysosomes (Bone *et al.* 1998). Furthermore, yeast has been established as a good model for the study of neurodegeneration (Khurana & Lindquist 2010), and for drug discovery (Howitz *et al.* 2003; Hoon *et al.* 2008; Su *et al.* 2010). These drugs act on targets that are highly conserved and are able to rescue disease pathology not only in yeast but also in neurons (Su *et al.* 2010), demonstrating that drugs identified in yeast can act on highly conserved biological processes and be translated into higher organisms. In fact, there are reports that show a translation from concept to drugs in the clinic in less than 3 years (Howitz *et al.* 2003). There are disadvantages in using *S. pombe* as a model for high-throughput drug screening that could be used for human disease therapies: the possibility of a drug not being permeable to the yeast cell wall or not being soluble in the yeast growing medium giving rise to false negative results, and the obvious fact that several cellular pathways existent in human are not conserved in fission yeast, and therefore drugs acting in these pathways cannot be detected in this organism. However, *S. pombe* has been previously used in high-throughput screening in a successful manner (Yashiroda *et al.* 2010; Demirbas *et al.* 2013). Fission yeast can, in fact, be powerful tools for fast drug discovery in neurodegenerative diseases, such as juvenile CLN3 disease. The efficacy of screen hit compounds can be quickly verified in other model organisms, such as zebrafish or mammalian cells (as it was done in this study), a crucial step before the preclinical trials are carried out in mouse models, for example.

Currently, there are no readily detectable phenotypes suitable for high-throughput screening for NCL diseases in mammalian cells. On the other hand,

multiple marker phenotypes have been characterised in fission yeast, which also indicates that Btn1p (just like CLN3) has a complex function that affects different pathways in the cell. It is important to gain more information about the pathways where Btn1p/CLN3 is involved, to further understand the molecular mechanisms of juvenile CLN3 disease. This type of information can be inferred from the results obtained in the drug screen, if one considers the typical targets of the compounds that were identified.

The phenotype chosen as the basis for the drug screen was the growth at 37°C in the presence of cyclosporine A, since there is a very significant difference in the viabilities of wild-type and *btn1*Δ cells when grown in these conditions. The viability can be easily measured by the presence of propidium iodide inside the dead cells. 1280 FDA-approved compounds were tested for their ability to rescue the percentage of dead *btn1*Δ cells to levels similar to wild-type cells. Three compounds that strongly rescued the viability of the *btn1*Δ strain were first validated and then selected for further experiments to assess their ability of rescuing other phenotypes associated with the loss of *btn1* or *CLN3*. All three compounds were able to rescue other phenotypes in *btn1*Δ cells, and some of them in juvenile NCL patient fibroblasts and in a zebrafish disease model. Each compound will be discussed in the sections below, as well as the possible role of calcineurin and the TOR pathway in juvenile CLN3 disease.

7.2.1 Calcineurin and TOR signalling pathway

Calcineurin is a serine/threonine phosphatase that is regulated by the Ca^{2+}/calmodulin-dependent signalling pathway (Klee *et al.* 1979). In yeast, calcineurin stimulates cell survival upon exogenous stress (Cyert 2003). In response to stress, calcineurin dephosphorylates transcription factors (such as Crz1p) that then activates target genes involved in pathways such as vesicular transport, ion homeostasis and cell wall maintenance. Calcineurin is also responsible for the actin cytoskeleton depolarization and delay in the cell cycle upon stress (Mizunuma *et al.* 1998; Shitamukai *et al.* 2004). Calcineurin-null yeast cells show a delay in cytokinesis (Yoshida *et al.* 1994).

In *S. cerevisiae*, calcineurin negatively regulates TORC2 signalling and TORC2 negatively regulates calcineurin via the Slm proteins (Mulet *et al.* 2006). There are some differences in *S. pombe*: the growth of cells lacking tor1, the Tor kinase in TORC2 is strongly inhibited by cyclosporine A, the inhibitor of calcineurin (Kawai *et al.* 2001). Furthermore, in budding yeast calcineurin-null cells are resistant to the presence of calcium and grow better in these conditions, whereas fission yeast cells null for calcineurin are highly sensitive to calcium (Hirayama *et al.* 2003). Therefore, the function of calcineurin is likely to be different in the two types of yeast, and probably the function in fission yeast is more equivalent to mammalian cells. Evidence from this study supports this idea, since *btn1*Δ calcineurin-null cells are not able to survive, and as mentioned above, it is known that in *btn1*Δ cells TORC2 activity is affected and that CLN3-deficient cells have increased levels of intracellular calcium.

According to results presented in this work and elsewhere, it is proposed that Btn1p/CLN3 and calcineurin have an overlapping function. Several lines of evidence support this hypothesis: 1) as mentioned above (1.1.3.2) vegetative growth of Ypt3p mutant cells is calcineurin-dependent, Ypt3p was proposed as having overlapping function with calcineurin and Ypt3p mutant cells show several common phenotypes to *btn1*Δ cells; 2) both calcineurin and CLN3 have been reported to regulate intracellular calcium levels (Klee *et al.* 1979; Chang *et al.* 2007) and calcineurin-null cells are sensitive to high calcium levels

(Hirayama *et al.* 2003), which are known to be present in SH-SY5Y cells treated with *CLN3* siRNA (An Haack *et al.* 2011); 3) Cni1p, a calcineurin-binding protein, promotes growth of fission yeast cells at high pH (Cyert 2003), and defects in *btn1*Δ cells are known to be rescued by growth in acidic media, suggesting that when both Btn1p and calcineurin are defective, yeast cells are unable to survive; 4) a yeast orthologue of a mammalian subunit of the clathrin-associated adaptor protein complex, Apm1p, and calcineurin double mutant cells are synthetically lethal, and *apm1*Δ cells show similar phenotypes to *btn1*Δ cells: temperature sensitivity, tacrolimus (a calcineurin inhibitor) sensitivity, cytokinesis and vacuole fusion defects and larger Golgi stacks, all of these accentuated by a temperature up-shift (Kita *et al.* 2004). Apm1p is also localised to the Golgi and endosomes, and its role was proposed to be associated with a function in these organelles that will affect several cellular processes, analogously to what is suggested for Btn1p; 5) calcineurin may be associated with the release and action of neurotransmitters due to the fact that it regulates the levels of calcium in the nervous system and this are known to play a crucial role in neuronal transmitters at the synaptic terminals (Klee *et al.* 1979). Similarly, v-ATPase, known to be defective in CLN3-deficient cells, was reported to play a role in neurotransmitters transport in the brain (Cousin & Nicholls 1997). Therefore, when *btn1* and calcineurin are defective, this could affect neuronal transmission and potentially lead to neurodegeneration.

After the realization that Btn1p function was related to the TORC2 pathway, and in order to identify a robust phenotype for the screen, *btn1*Δ cells were tested for their ability to withstand a pharmacological treatment that other TORC2 mutants have been shown to be sensitive to: the presence of cyclosporine A. The CsA sensitivity of *btn1*Δ cells was only present when cells were grown at the non-permissive temperature of 37°C which may suggest CsA acts by exacerbating the underlying temperature sensitivity of these strains (or *vice versa*).

7.2.2 Alloxazine

Alloxazines are degradation products of flavocoenzymes, proteins containing riboflavin, a crucial constituent of all living cells and organisms (Ferreira *et al.* 2014). Alloxazine is an antagonist of the adenosine A_{2b} receptor (Brackett & Daly 1994) and was also reported as being able to inhibit the splicing process (Kim & Park 2000).

The adenosine A_{2b} receptor has been implicated in several biological functions, from regulation of neuroglia function to calcium homeostasis (Fiebich *et al.* 1996; Pilitsis & Kimelberg 1998). Although the biological roles of adenosine and adenosine A_{2b} receptor, target of alloxazine, are well known, the target of alloxazine in yeast is still unclear, since these receptors are not present in this organism. It is not possible to effectively speculate on what alloxazine action is in yeast based on the evidence from this study. However, there are examples of drugs with a known target in humans that were shown to have a different target in yeast. For example, Guanabenz, an antihypertensive drug and an agonist of α2-adrenergic receptors, has an antiprion activity in yeast cells (Tribouillard-Tanvier *et al.* 2008).

Despite encouraging results obtained in fission yeast, the use of alloxazine as a template for a therapeutic drug for juvenile CLN3 disease might be unrealistic. First, because the results obtained with alloxazine treatment in patient fibroblasts were not encouraging: the compound was not able to rescue the Golgi phenotype (Chapter 5.3.1). Moreover, work done by Yamagata *et al* (2007) reported that adenosine when bound to the adenosine A_{2b} receptor induce the expression of glial cell line-derived neurotrophic factor (GDNF) and this is repressed by alloxazine (Yamagata *et al.* 2007). The fact that GDNF promotes the survival of neurons, and neurodegeneration is a hallmark of juvenile NCL, discredits the possibility of using alloxazine towards a therapeutic goal.

7.2.3 E-64

L-trans-Epoxysuccinyl-leucylamido(4-guanidino)butane, commonly known as E-64, is an irreversible and potent inhibitor of several cysteine peptidases, such as papain, actinidin, cathepsins B, H and L, among others (Hashida *et al.* 1980; Barrett *et al.* 1982; Varughese *et al.* 1989; Matsumoto *et al.* 1999). E-64 is also able to strongly inhibit trypsin-catalysed hydrolysis, and trypsin is the only serine protease that E-64 has an effect on (Sreedharan *et al.* 1996). E-64 is widely used *in vivo* and as a potential template for drugs used in disease treatment mainly due to its specificity, cell permeability, ease of synthesis, stability and low toxicity (Katunuma & Kominami 1995).

Since it is able to inhibit several cysteine peptidases involved in different biochemical processes in the cell, E-64 action directly influences multiple cellular pathways. It has been shown to inhibit neutrophil chemotaxis (Barna & Kew 1995) and invasion of human bladder carcinoma cells through basement membranes via cathepsin B inhibition (Redwood *et al.* 1992); it has antiparasitic properties (Carvalho *et al.* 2014; Wadhawan *et al.* 2014); and it has been reported to delay muscular dystrophy progression in mice (Komatsu *et al.* 1986). Furthermore, E-64 also inhibits the chicken calcium-activated neutral protease (Sugita *et al.* 1980), establishing an indirect link with calcium homeostasis. The inhibition of the calcium-dependent cysteine protease calpain by E-64 has varying effects on several cellular pathways. For example, the development of Th17 cells is impaired (Iguchi-Hashimoto *et al.* 2011), together with apoptosis triggered by the T-cell receptor complex (Sarin *et al.* 1993), and the IL-6 and IL-1β cytokines production is inhibited, which leads to an amelioration of rheumatoid arthritis (Yoshifuji *et al.* 2005). Calpain is also involved in the processing of amyloid precursor protein (APP) (Tanabe *et al.* 2013). APP when cleaved by β- or γ-secretases originates amyloid-β, the protein that accumulates in Alzheimer's disease. On the other hand, when cleaved by α-secretases, APP produces a soluble form (sAPPα) that has neuroprotective properties. When there is an increased production of amyloid-β, there is no secretion of sAPPα, a phenotype observed in Alzheimer's patients.

Calpain inhibition by E-64 is able to revert the reduced secretion of sAPPα, suggesting a neuroprotective role for E-64 and a potential for treatment of Alzheimer's disease based on this compound. As Alzheimer's is a neurodegenerative disease like juvenile CLN3 disease, and that amyloid-β processing is also altered in juvenile NCL (Kitaguchi *et al.* 1990), the same treatment may work for both.

The fact that E-64 is able to reduce apoptosis in a mouse hybridoma (Sarin *et al.* 1993) makes this compound a good candidate for the development of therapy for juvenile CLN3 disease. The analgesic flupirtine, which has been reported to slow disease progression and clinically benefit juvenile NCL patients, is also able to reduce apoptosis in patient lymphoblasts and neurons (Dhar *et al.* 2002). Apoptosis has been reported as one of the mechanisms of neurodegeneration in juvenile NCL (Lane *et al.* 1996), and CLN3 also exerts an anti-apoptotic role (Puranam *et al.* 1999; Narayan *et al.* 2006a).

E-64 has at least one identified target in *S. cerevisiae*, Ycp1p, a cysteine protease (Pei *et al.* 1995), suggesting that it may have at least one target in *S. pombe*. In fact, there are several cysteine peptidases in fission yeast, and although none of these were identified as E-64 targets to date, it is possible that E-64 exerts its action through one or all of them. Potential targets of E-64 in fission yeast, all of them cysteine proteases are listed below:

1) Pca1p, a caspase-like protein involved in lipid-induced apoptosis (Low & Yang 2008). As discussed above, apoptosis is the main cause of neurodegeneration in juvenile CLN3 disease.

2) Cut1p, a separase that is involved in several cellular roles. For example, it is involved in the cytokinetic process, more specifically in the separation of sister chromatids (Funabiki *et al.* 1996). Cytokinesis is known to be affected in *btn1*Δ cells (as previously discussed throughout this work), suggesting a link between Btn1p function and Cut1p, and possibly E-64 inhibitory action on the latter. Cut1p also represses the TORC2 pathway (Yuasa *et al.* 2004). Since the signalling in this pathway

is already affected in *btn1*Δ cells, E-64 may be targeting Cut1p and releasing TORC2 pathway from inhibition. In fact, it was reported that unbalanced high levels of Cut1p seem to be harmful for TORC2, when its activity is diminished (Ikai *et al.* 2011). This is also consistent with the sensitivity that *btn1*Δ cells show to CsA, an inhibitor of calcineurin, a component of the TORC2 pathway.

3) Some deubiquitinating enzymes (like Ubp9p) involved in signalling pathways that regulate cell polarity and endocytosis (Kouranti *et al.* 2010). These mechanisms are known to be deregulated in juvenile CLN3 disease (Chapter 1.1.2).

7.2.4 Prochlorperazine dimaleate

Prochlorperazine dimaleate or 2-Chloro-10-[3[(4-methyl-1-piperazinyl)propyl]-10*H*-phenothiazine dimaleate is a salt composed of prochlorperazine and two molecules of maleate. Prochlorperazine is a phenothiazine (Lummis & Baker 1997) and a D2 dopamine receptor antagonist (Creese *et al.* 1976) that also interacts directly with 5-hydroxytryptamine$_3$ (5-HT$_3$) receptors (Lummis & Baker 1997), which are responsible for several roles mainly in the central nervous system (Kilpatrick *et al.* 1990). Prochlorperazine is also able to promote the release of the neurotransmitter acetylcholine (ACh) in the cerebral cortex (Ghelardini *et al.* 2004).

Prochlorperazine has antipsychotic, antiemetic and antinociceptive activity *in vivo*. The first to be discovered was the antiemetic ability of prochlorperazine (Moertel *et al.* 1963); this drug is able to stop nausea and vomiting. Prochlorperazine was also reported to increase the pain threshold in mice, exerting an antinociceptive effect, mediated by release of ACh (Ghelardini *et al.* 2004). Furthermore, prochlorperazine is effective in the treatment of acute migraines, namely by alleviating pain and nausea (Tanen *et al.* 2003).

Action of prochlorperazine affects several proteins in different manners. It was reported to increase the activity of integral membrane enzymes uridine 5'-diphospho-glucuronosyltransferase and glucose-6-phosphatase in microsomes, via disruption of organized lipid-protein interactions (Dannenberg & Zakim 1988). Prochlorperazine was also proposed to affect clathrin distribution, which led to an antiviral effect against the dengue virus (Simanjuntak *et al.* 2014). Furthermore, prochlorperazine modulates the human P2X7 receptor, an ATP cation channel involved in immune cell activation and neurological disorders such as Alzheimer's disease and schizophrenia (Skaper *et al.* 2009). In this case, prochlorperazine acts as an open pore blocker and inhibits calcium entry into the cell (Hempel *et al.* 2013). This establishes a link between this compound's action, neurodegeneration and calcium homeostasis. Other example of its link to calcium is the fact that prochlorperazine is able to inhibit growth of *Acanthamoeba castellanii*, the causative agent of blinding keratitis, by

an inhibitory action on amoeba calcium-regulatory proteins or by disruption of the amoeba plasma membrane (Baig *et al.* 2013). Moreover, prochlorperazine inhibits release of pro-inflammatory mediators from human mast cells, probably by decreasing the levels of intracellular calcium (Clemons *et al.* 2011). From all these roles and processes, only some are relevant to yeast and could be the underlying mechanism of drug action in this organism: disruption of lipid-protein interactions or pore blocking activity. Although the other processes are not relevant to yeast work, it is important to bear them in mind in order to avoid potential side effects or potential synergistic effects when translated to other organisms.

Although prochlorperazine (dimaleate) and its action have not been associated with fission yeast, and there is no identified targeted yeast protein, it is possible that this compound has a target in these cells that is different from its original one. It is possible that this compound is in some way involved in a calcium homeostasis pathway in yeast, since it has been associated with it in several studies conducted in human cells, as mentioned above, and that this pathway is known to be disrupted in juvenile CLN3 disease and supposedly in *btn1*Δ cells. Further work needs to be done in order to identify and clarify the action of prochlorperazine in *S. pombe.*

7.2.5 Summary of all compounds

The three compounds that were identified in the drug screen and that were subsequently validated (alloxazine, E-64 and prochlorperazine dimaleate) do not have any reported targets in fission yeast. For instance, adenosine and dopamine receptors, the principal human targets of alloxazine and prochlorperazine respectively, do not exist in this unicellular organism. This suggests that these two compounds are probably acting in a different manner, targeting another yeast pathway(s). Regarding the other compound, E-64, its targets are cysteine protease and there are several in *S. pombe*. Therefore, it is plausible that E-64 is exerting its inhibitory effect on one or more of them.

Alloxazine is the only one among the three compounds able to rescue the temperature sensitivity phenotype of *btn1*Δ cells, both in liquid media and in spot assays (Chapter 5.2.4). This temperature sensitivity is related to the inability that *btn1*Δ cells have of adequately responding to different types of stress, which in turn, is linked to disruption in the TORC2 pathway (see above, section 7.2.1). This suggests that alloxazine may be involved in stress response pathways. On the other hand, alloxazine does not rescue the Golgi compactness phenotype in juvenile NCL patient fibroblasts, which may mean that it cannot be used with a therapeutic purpose for juvenile CLN3 disease.

As mentioned above (section 7.2.3), E-64 may be inhibiting any cysteine protease activities in *S. pombe*. Different cysteine peptidases have been described in these cells, involved in different cellular processes, some of which that have been associated with Btn1p: autophagy, cytokinesis, endocytosis, cell polarity, vacuolar function (Funabiki *et al.* 1996; Low & Yang 2008; Kouranti *et al.* 2010; Mikawa *et al.* 2010; Sun *et al.* 2013) and most importantly the TORC2 pathway (Yuasa *et al.* 2004). Consistent with its Cut1p protease inhibitory action, and its involvement in the TORC2 pathway, is the observation that E-64 was the compound that most efficiently rescued the CsA sensitivity phenotype in *btn1*Δ cells out of the three compounds (Chapter 5.1). It was also the one that elicited the strongest rescue of the *btn1*Δ cell curving phenotype, the juvenile NCL fibroblasts' less compact Golgi, and the activity and survival of the

Cln3 MO zebrafish. E-64 was also able to rescue all the other tested phenotypes in *btn1*Δ cells, except the defective growth at 37°C (Results Chapter 3). All of these results indicate that E-64 may be very useful for the development of new therapeutic tools towards juvenile CLN3 disease. Furthermore, E-64 has previously been reported as having a neuroprotective role in Alzheimer's disease (Tanabe *et al.* 2013), and decreasing apoptosis (Sarin *et al.* 1993), one of the mechanisms of neurodegeneration in juvenile NCL (Lane *et al.* 1996).

Prochlorperazine (dimaleate) action has not been previously associated with fission yeast; its known targets are not present in these cells (D2 dopamine receptor, 5-HT3 receptors and ACh); and its well-known use as an antipsychotic, antiemetic and antinociceptive drug is not relevant for yeast work. However, juvenile NCL patients do suffer from severe psychotic episodes as the disease advances (Mole *et al.* 2011), so a drug that addresses the underlying cause may be a very helpful component of juvenile NCL therapy. It is possible that this drug is acting in a different manner in yeast, maybe in a calcium-related pathway, due to its reported link to calcium, more specifically by potentially decreasing its intracellular levels (Clemons *et al.* 2011). Prochlorperazine dimaleate rescues all tested phenotypes in *btn1*Δ cells, except defective growth at 37°C, similarly to E-64 (Results Chapter 3). It is also able to rescue the tested phenotypes in juvenile NCL patient fibroblasts and in Cln3 MO zebrafish (tail flicking activity), which strongly supports its ability to revert or complement the lack of Btn1p in fission yeast cells, and probably dysfunctional CLN3 in human cells and fish.

To conclude, all three compounds seem to be acting differently in the *btn1*Δ strain. However, two of them share some common features, for example their link to calcium: prochlorperazine decrease intracellular calcium levels (Pilitsis & Kimelberg 1998; Clemons *et al.* 2011) and E-64 inhibits calcium-dependent proteins (Sugita *et al.* 1980; Iguchi-Hashimoto *et al.* 2011). This could be a plausible explanation for their ability to rescue disease-related phenotypes, since CLN3 is known to regulate the intracellular levels of free calcium in SH-

SY5Y cells (Chang *et al.* 2007). Furthermore, a study reported the ability of amlodipine, a calcium channel antagonist, to decrease the calcium levels in CLN3 siRNA–treated neurons (Warnock *et al.* 2013). As mentioned above (section 7.1.3.1), CLN3 may be working as a calcium channel, maintaining intracellular calcium levels, an important condition for several proteins to carry out their functions correctly. It is important to elucidate the role of Btn1p as a potential calcium channel.

E-64 appears to be the most promising compound for the development of therapeutic tools for juvenile CLN3 disease, since it was able to rescue all the tested phenotypes (except one) in different models, and its action spectrum is broad. However, future work must be conducted regarding all three compounds in order to further clarify their mechanisms of action in fission yeast, and consequently in human cells.

7.3 Insights into therapy of other lysosomal storage disorders

Fission yeast models of three lysosomal storage disorders, Chédiak Higashi syndrome, Niemann-Pick disease type C2 and congenital CLN10 disease, were characterised and further explored in the last part of this work. Considerations about their mechanism of action and potential therapy will be discussed below.

The *S. pombe* strain modelling CHS is the *lvs1*Δ strain. This strain is characterised by the presence of exceptionally large vacuoles, and according to this work, a higher septation index when compared to a wild-type strain (Chapter 6.1.2). Alloxazine, E-64 and prochlorperazine dimaleate were able to rescue both these phenotypes in these cells, suggesting that these compounds should be considered for further studies concerning therapeutic alternatives for CHS. Similar to juvenile CLN3 disease, calcium homeostasis is also disrupted in CHS, where the levels of lysosomal calcium are elevated in neutrophils, due to an hyperactivation of the calcium uptake process (Styrt *et al.* 1988). This observation establishes a possible link between this disorder, calcium homeostasis and action of E-64 and prochlorperazine dimaleate compounds (see the section above).

E-64 has been shown to rescue several phenotypes in the mouse model of CHS, the *beige* mouse, and in patient cell lines: decreased activity of natural killer cells, increased concanavalin A-induced cap formation, formation of giant granules, reduced cathepsin G and lysosomal elastase activities, susceptibility to bacterial infection; all due to its effect on reversing the decline of protein kinase C activity, by preventing its calpain-mediated proteolysis (Ito *et al.* 1989; Sato *et al.* 1990; Tanabe *et al.* 2000; Cui *et al.* 2001; Morimoto *et al.* 2007; Tanabe *et al.* 2009). These observations suggest that E-64 is a good candidate for the development of a CHS therapeutic drug.

Niemann-Pick type C2 protein is conserved in fission yeast. The *npc2*Δ strain was characterised in this work (Results Chapter 4). This strain contains large vacuoles and an increased number of septated cells. The first phenotype was rescued by alloxazine, E-64 and prochlorperazine dimaleate, whereas the

septation index was only decreased after treatment with alloxazine and prochlorperazine. However, and in contrast with these results, E-64 seems to be the most promising compound regarding therapy of NPC. Levels and activity of cathepsin B are increased in the brains of NPC mutant mice (Liao *et al.* 2007). Cathepsin B is a target of E-64, and therefore this compound may be able to revert some phenotypes associated with the increased levels of this lysosomal enzyme in NPC. In fact, this increase has been associated with neurodegeneration in NPC (Amritraj *et al.* 2009), and therefore the action of E-64 may be relevant for therapy attenuating NPC pathology. Further supporting this hypothesis is the observation that cathepsins B and L are involved in secretion of NPC2, and treatment with E-64 (inhibitor of these cathepsins) increases the intracellular levels of NPC2, by blocking its secretion (Hannaford *et al.* 2013). Similarly to juvenile CLN3 disease, mitochondrial defects have been reported in NPC (Vilaca *et al.* 2014), and mitochondrial function is linked to calcium homeostasis (Duchen *et al.* 2008), suggesting that there is a link between dysregulation of calcium levels in these diseases and the mechanisms of action of E-64 and prochlorperazine dimaleate.

The *sxa1*Δ *S. pombe* strain models congenital CLN10 disease. This strain, similar to the other two LSD strains, is characterised by enlarged vacuoles and a high septation index. Treatment with alloxazine, E-64 and prochlorperazine dimaleate rescued the vacuoles size but not the number of septated cells in this strain. Total activity of cathepsin D (deficient in CLN10) is increased in E-64-treated fibroblasts (Samarel *et al.* 1989); however, this compound is known to affect the proteolytic maturation of procathepsin D (Ishidoh *et al.* 1999), leading to accumulation of the processing intermediates (Laurent-Matha *et al.* 2006). This effect of E-64 on cathepsin D is not relevant to treatment as cathepsin D is essentially null in congenital CLN10 disease. As long as E-64 is known to have a positive effect on parallel pathways (as the vacuoles size rescue data mentioned above suggests, Results Chapter 4), it could still be useful for the development of CLN10 disease therapeutic tools.

Results obtained in this work with the LSD yeast strains are preliminary, since these strains were characterised in terms of the phenotypes that were previously associated with the loss of *btn1* in the yeast strain modelling juvenile CLN3 disease. Work to confirm a direct link between the phenotypes and the deleted LSD gene (for example, expression of the respective genes in the deletion strains in order to verify if they were able to rescue the phenotypes) still needs to be done. Furthermore, the compounds tested in these strains were the ones identified in the drug screen performed with *btn1*Δ cells, and not specific to the other three LSD strains. Therefore, the results obtained here must be regarded as preliminary; additional work must be done in order to further elucidate the disease pathways involved in these *S. pombe* disease strains as well as the action of compounds in these pathways. Nevertheless, it may be that these diseases share common downstream disease phenotypes, such as vacuole homeostasis, in which case a compound addressing these could be efficacious for more than one disease.

7.4 Conclusions and Future Work

The principal aims of this project were to study the impact of different mutations on the function of fission yeast Btn1p and to identify novel lead compounds that can be developed to treat juvenile CLN3 disease as a first stage to new therapeutic development. In the first part of this work, it was confirmed that different mutations in the *btn1* gene have different effects on the protein function, affecting its expression and cell phenotypes. According to the results obtained with strain expressing different mutant Btn1p, it is proposed that its lumenal and/or transmembrane regions are particularly important for its function. Furthermore, the levels of *btn1* expression influence its function, suggesting that this is important and tightly regulated. New insights regarding the function of Btn1p (and CLN3) were gained. These orthologue proteins are known to affect the function of several proteins involved in different cellular pathways. Their effect may be exerted from the Golgi compartments, by affecting the sorting and activity of several proteins and downstream pathways. On the other hand, it is also possible that Btn1p (and CLN3) is acting as a channel or ion transporter, and that its dysfunction affects the endocytic transport, which would affect many cellular proteins. Furthermore, Btn1p function is related to the TORC2 signalling pathway, most likely via its link to calcineurin. It is possible that Btn1 has an overlapping function with calcineurin. Conclusions obtained regarding the potential therapeutic compounds identified in this study, are discussed in detail below (section 7.4.2). Beforehand, suggestions on future work that need to be done are presented.

7.4.1 Future work

Further work is needed to conclude the work started of this study. Below is a list of some experiments that will be useful to fully comprehend and complement the findings made in this study.

1) Further clarify the action mechanism of calcineurin in wild-type and *btn1Δ* cells – for example, the creation of a calcineurin and Btn1p double mutant to verify its viability or synthetic lethality (if these proteins have, in fact, an overlapping function);

2) Determine if *btn1*Δ cells are sensitive to growth in the presence of another calcineurin inhibitor, FK506, to ensure that the sensitivity of these cells is related to the absence of calcineurin;

3) Investigate the relationship between Btn1p and Ypt3p, to verify if they have common functions, as suggested by the results from several studies;

4) Further clarify the role of calcium homeostasis in disease pathology and in the fission yeast model, by measuring calcium cytosolic and vacuolar levels in wild-type and *btn1*Δ cells; and testing whether any calcium channel antagonists are able to reverse phenotypes in *btn1*Δ (and mammalian cells).

5) Perform a drug screen with the same library using one or more *btn1*-mutated *S. pombe* strains, after identification of a mutation-specific phenotype in these cells;

6) Test the ability of alloxazine, E-64 and prochlorperazine dimaleate to rescue more phenotypes of CLN3-depleted/deficient mammalian cells;

7) Perform a dose response assay for alloxazine, E-64 and prochlorperazine dimaleate;

8) Test other positive hits from the drug screen already performed, that showed a less significant rescue than the six that were followed up;

9) Test the three initial hit compounds (atenolol, etoposide and daphnetin) that were excluded from the yeast work due to their toxicity in wild-type yeast cells, in mammalian cells/models where their action could be beneficial;

9) Test the effect of other compounds structurally similar to the ones studied here in *btn1Δ* cells;

10) A great amount of work for the CHS, NPC and CLN10 yeast strains: characterising them in terms of phenotypes, performing a drug screen with the same library (or a different one) using each strain, further analysing the effect that alloxazine, E-64 and prochlorperazine dimaleate (and potential newly identified compounds) have in their phenotypes;

7.4.2 Potential therapeutic compounds for juvenile CLN3 disease

Three compounds were identified in a drug screen with *btn1*Δ cells: alloxazine, E-64 and prochlorperazine dimaleate. All three compounds seem to be acting differently in the *btn1*Δ strain, and none of their targets have been identified in fission yeast. The exact mechanism of action of alloxazine in yeast cannot be inferred from the results that were obtained. The same statement is valid for prochlorperazine dimaleate, although this compound may be affecting calcium-related pathways, along with regulating calcium intracellular levels. In fact, this compound shares a common link with CLN3/Btn1p and E-64 to calcium-related pathways and proteins.

Many yeast pathways are conserved in human and other eukaryotic organisms, therefore pathways targeted by these compounds in yeast are probably present in human cells, even though it is already known that these compounds work on different targets in humans. Actions of the three compounds are unlikely to be yeast-specific as they were able to successfully rescue phenotypes in a zebrafish disease model.

E-64 seems to be the compound with the most potential for development of therapeutic tools for juvenile CLN3 disease, since it was able to rescue all (except one) phenotypes in fission yeast, zebrafish disease models and patient fibroblasts. Furthermore, this compound has been previously reported to rescue several phenotypes in the CHS mouse model and in CHS patient cell lines, suggesting that it could be used as a template for a CHS therapeutic drug. A similar conclusion can be drawn regarding NPC, since E-64 is able to decrease high levels of cathepsin B in brains of NPC mice models. These observations may be linked to the fact that E-64 is the compound with the largest pattern of action from the three that were tested. This makes it a good candidate as a template for the development of drugs that will target specific proteins in different diseases. However, it is very important to achieve an acceptable safety profile, in order to avoid side effects.

Reference list

Aberg L., Lauronen L., Hamalainen J., Mole S.E. & Autti T. (2009) A 30-year follow-up of a neuronal ceroid lipofuscinosis patient with mutations in CLN3 and protracted disease course. *Pediatr Neurol* **40**, 134-7.

Aerts J.M., Kallemeijn W.W., Wegdam W., Joao Ferraz M., van Breemen M.J., Dekker N., Kramer G., Poorthuis B.J., Groener J.E., Cox-Brinkman J., Rombach S.M., Hollak C.E., Linthorst G.E., Witte M.D., Gold H., van der Marel G.A., Overkleeft H.S. & Boot R.G. (2011) Biomarkers in the diagnosis of lysosomal storage disorders: proteins, lipids, and inhibodies. *J Inherit Metab Dis* **34**, 605-19.

Ahtiainen L., Kolikova J., Mutka A.L., Luiro K., Gentile M., Ikonen E., Khiroug L., Jalanko A. & Kopra O. (2007) Palmitoyl protein thioesterase 1 (Ppt1)-deficient mouse neurons show alterations in cholesterol metabolism and calcium homeostasis prior to synaptic dysfunction. *Neurobiol Dis* **28**, 52-64.

Ahtiainen L., Luiro K., Kauppi M., Tyynela J., Kopra O. & Jalanko A. (2006) Palmitoyl protein thioesterase 1 (PPT1) deficiency causes endocytic defects connected to abnormal saposin processing. *Exp Cell Res* **312**, 1540-53.

Aiello C., Terracciano A., Simonati A., Discepoli G., Cannelli N., Claps D., Crow Y.J., Bianchi M., Kitzmuller C., Longo D., Tavoni A., Franzoni E., Tessa A., Veneselli E., Boldrini R., Filocamo M., Williams R.E., Bertini E.S., Biancheri R., Carrozzo R., Mole S.E. & Santorelli F.M. (2009) Mutations in MFSD8/CLN7 are a frequent cause of variant-late infantile neuronal ceroid lipofuscinosis. *Hum Mutat* **30**, E530-40.

Allen N.M., O'HIci B., Anderson G., Nestor T., Lynch S.A. & King M.D. (2012) Variant late-infantile neuronal ceroid lipofuscinosis due to a novel heterozygous CLN8 mutation and de novo 8p23.3 deletion. *Clin Genet* **81**, 602-4.

Amritraj A., Peake K., Kodam A., Salio C., Merighi A., Vance J.E. & Kar S. (2009) Increased activity and altered subcellular distribution of lysosomal enzymes determine neuronal vulnerability in Niemann-Pick type C1-deficient mice. *Am J Pathol* **175**, 2540-56.

An Haack K., Narayan S.B., Li H., Warnock A., Tan L. & Bennett M.J. (2011) Screening for calcium channel modulators in CLN3 siRNA knock down SH-SY5Y neuroblastoma cells reveals a significant decrease of intracellular calcium levels by selected L-type calcium channel blockers. *Biochim Biophys Acta* **1810**, 186-91.

Anderson G.W., Goebel H.H. & Simonati A. (2013) Human pathology in NCL. *Biochim Biophys Acta* **1832**, 1807-26.

Arsov T., Smith K.R., Damiano J., Franceschetti S., Canafoglia L., Bromhead C.J., Andermann E., Vears D.F., Cossette P., Rajagopalan S., McDougall A., Sofia V., Farrell M., Aguglia U., Zini A., Meletti S., Morbin M., Mullen S., Andermann F., Mole S.E., Bahlo M. & Berkovic S.F. (2011) Kufs disease, the major adult

form of neuronal ceroid lipofuscinosis, caused by mutations in CLN6. *Am J Hum Genet* **88**, 566-73.

Bahler J., Wu J.Q., Longtine M.S., Shah N.G., McKenzie A., 3rd, Steever A.B., Wach A., Philippsen P. & Pringle J.R. (1998) Heterologous modules for efficient and versatile PCR-based gene targeting in Schizosaccharomyces pombe. *Yeast* **14**, 943-51.

Baig A.M., Iqbal J. & Khan N.A. (2013) In vitro efficacies of clinically available drugs against growth and viability of an Acanthamoeba castellanii keratitis isolate belonging to the T4 genotype. *Antimicrob Agents Chemother* **57**, 3561-7.

Baldwin S.A., Beal P.R., Yao S.Y., King A.E., Cass C.E. & Young J.D. (2004) The equilibrative nucleoside transporter family, SLC29. *Pflugers Arch* **447**, 735-43.

Barbosa M.D., Nguyen Q.A., Tchernev V.T., Ashley J.A., Detter J.C., Blaydes S.M., Brandt S.J., Chotai D., Hodgman C., Solari R.C., Lovett M. & Kingsmore S.F. (1996) Identification of the homologous beige and Chediak-Higashi syndrome genes. *Nature* **382**, 262-5.

Barna J.B. & Kew R.R. (1995) Inhibition of neutrophil chemotaxis by protease inhibitors. Differential effect of inhibitors of serine and thiol proteases. *Inflammation* **19**, 561-74.

Barrat F.J., Auloge L., Pastural E., Lagelouse R.D., Vilmer E., Cant A.J., Weissenbach J., Le Paslier D., Fischer A. & de Saint Basile G. (1996) Genetic and physical mapping of the Chediak-Higashi syndrome on chromosome 1q42-43. *Am J Hum Genet* **59**, 625-32.

Barrett A.J., Kembhavi A.A., Brown M.A., Kirschke H., Knight C.G., Tamai M. & Hanada K. (1982) L-trans-Epoxysuccinyl-leucylamido(4-guanidino)butane (E-64) and its analogues as inhibitors of cysteine proteinases including cathepsins B, H and L. *Biochem J* **201**, 189-98.

Bateman A. & Bennett H.P. (2009) The granulin gene family: from cancer to dementia. *Bioessays* **31**, 1245-54.

Berkovic S.F., Carpenter S., Andermann F., Andermann E. & Wolfe L.S. (1988) Kufs' disease: a critical reappraisal. *Brain* **111 (Pt 1)**, 27-62.

Bessa C., Teixeira C.A., Dias A., Alves M., Rocha S., Lacerda L., Loureiro L., Guimaraes A. & Ribeiro M.G. (2008) CLN2/TPP1 deficiency: the novel mutation IVS7-10A>G causes intron retention and is associated with a mild disease phenotype. *Mol Genet Metab* **93**, 66-73.

Bond M., Holthaus S.M., Tammen I., Tear G. & Russell C. (2013) Use of model organisms for the study of neuronal ceroid lipofuscinosis. *Biochim Biophys Acta* **1832**, 1842-65.

Bone N., Millar J.B., Toda T. & Armstrong J. (1998) Regulated vacuole fusion and fission in Schizosaccharomyces pombe: an osmotic response dependent on MAP kinases. *Curr Biol* **8**, 135-44.

Brackett L.E. & Daly J.W. (1994) Functional characterization of the A2b adenosine receptor in NIH 3T3 fibroblasts. *Biochem Pharmacol* **47**, 801-14.

Broom M.F. & Zhou C. (2001) Fine mapping of ovine ceroid lipofuscinosis confirms orthology with CLN6. *Eur J Paediatr Neurol* **5 Suppl A**, 33-5.

Burkhardt J.K., Wiebel F.A., Hester S. & Argon Y. (1993) The giant organelles in beige and Chediak-Higashi fibroblasts are derived from late endosomes and mature lysosomes. *J Exp Med* **178**, 1845-56.

Burneo J.G., Arnold T., Palmer C.A., Kuzniecky R.I., Oh S.J. & Faught E. (2003) Adult-onset neuronal ceroid lipofuscinosis (Kufs disease) with autosomal dominant inheritance in Alabama. *Epilepsia* **44**, 841-6.

Cadieux-Dion M., Andermann E., Lachance-Touchette P., Ansorge O., Meloche C., Barnabe A., Kuzniecky R.I., Andermann F., Faught E., Leonberg S., Damiano J.A., Berkovic S.F., Rouleau G.A. & Cossette P. (2013) Recurrent mutations in DNAJC5 cause autosomal dominant Kufs disease. *Clin Genet* **83**, 571-5.

Cao Y., Espinola J.A., Fossale E., Massey A.C., Cuervo A.M., MacDonald M.E. & Cotman S.L. (2006) Autophagy is disrupted in a knock-in mouse model of juvenile neuronal ceroid lipofuscinosis. *J Biol Chem* **281**, 20483-93.

Carstea E.D., Morris J.A., Coleman K.G., Loftus S.K., Zhang D., Cummings C., Gu J., Rosenfeld M.A., Pavan W.J., Krizman D.B., Nagle J., Polymeropoulos M.H., Sturley S.L., Ioannou Y.A., Higgins M.E., Comly M., Cooney A., Brown A., Kaneski C.R., Blanchette-Mackie E.J., Dwyer N.K., Neufeld E.B., Chang T.Y., Liscum L., Strauss J.F., 3rd, Ohno K., Zeigler M., Carmi R., Sokol J., Markie D., O'Neill R.R., van Diggelen O.P., Elleder M., Patterson M.C., Brady R.O., Vanier M.T., Pentchev P.G. & Tagle D.A. (1997) Niemann-Pick C1 disease gene: homology to mediators of cholesterol homeostasis. *Science* **277**, 228-31.

Carvalho T.B., Oliveira-Sequeira T.C. & Guimaraes S. (2014) In vitro antigiardial activity of the cysteine protease inhibitor E-64. *Rev Inst Med Trop Sao Paulo* **56**, 43-7.

Chan C.H., Ramirez-Montealegre D. & Pearce D.A. (2009) Altered arginine metabolism in the central nervous system (CNS) of the Cln3-/- mouse model of juvenile Batten disease. *Neuropathol Appl Neurobiol* **35**, 189-207.

Chang J.W., Choi H., Kim H.J., Jo D.G., Jeon Y.J., Noh J.Y., Park W.J. & Jung Y.K. (2007) Neuronal vulnerability of CLN3 deletion to calcium-induced cytotoxicity is mediated by calsenilin. *Hum Mol Genet* **16**, 317-26.

Chattopadhyay S., Muzaffar N.E., Sherman F. & Pearce D.A. (2000) The yeast model for batten disease: mutations in BTN1, BTN2, and HSP30 alter pH homeostasis. *J Bacteriol* **182**, 6418-23.

Cheng H., Sugiura R., Wu W., Fujita M., Lu Y., Sio S.O., Kawai R., Takegawa K., Shuntoh H. & Kuno T. (2002) Role of the Rab GTP-binding protein Ypt3 in the fission yeast exocytic pathway and its connection to calcineurin function. *Mol Biol Cell* **13**, 2963-76.

Cho S. & Dawson G. (2000) Palmitoyl protein thioesterase 1 protects against apoptosis mediated by Ras-Akt-caspase pathway in neuroblastoma cells. *J Neurochem* **74**, 1478-88.

Cho S.K. & Hofmann S.L. (2004) pdf1, a palmitoyl protein thioesterase 1 Ortholog in Schizosaccharomyces pombe: a yeast model of infantile Batten disease. *Eukaryot Cell* **3**, 302-10.

Clemons A., Vasiadi M., Kempuraj D., Kourelis T., Vandoros G. & Theoharides T.C. (2011) Amitriptyline and prochlorperazine inhibit proinflammatory mediator release from human mast cells: possible relevance to chronic fatigue syndrome. *J Clin Psychopharmacol* **31**, 385-7.

Codlin S., Haines R.L., Burden J.J. & Mole S.E. (2008a) Btn1 affects cytokinesis and cell-wall deposition by independent mechanisms, one of which is linked to dysregulation of vacuole pH. *J Cell Sci* **121**, 2860-70.

Codlin S., Haines R.L. & Mole S.E. (2008b) btn1 affects endocytosis, polarization of sterol-rich membrane domains and polarized growth in Schizosaccharomyces pombe. *Traffic* **9**, 936-50.

Codlin S. & Mole S.E. (2009) S. pombe btn1, the orthologue of the Batten disease gene CLN3, is required for vacuole protein sorting of Cpy1p and Golgi exit of Vps10p. *J Cell Sci* **122**, 1163-73.

Consortium T.I.B.D. (1995) Isolation of a novel gene underlying Batten disease, CLN3. *Cell* **82**, 949-57.

Coppieters F., Van Schil K., Bauwens M., Verdin H., De Jaegher A., Syx D., Sante T., Lefever S., Abdelmoula N.B., Depasse F., Casteels I., de Ravel T., Meire F., Leroy B.P. & De Baere E. (2014) Identity-by-descent-guided mutation analysis and exome sequencing in consanguineous families reveals unusual clinical and molecular findings in retinal dystrophy. *Genet Med* **16**, 671-80.

Cortes J.C., Katoh-Fukui R., Moto K., Ribas J.C. & Ishiguro J. (2004) Schizosaccharomyces pombe Pmr1p is essential for cell wall integrity and is required for polarized cell growth and cytokinesis. *Eukaryot Cell* **3**, 1124-35.

Cotman S.L., Vrbanac V., Lebel L.A., Lee R.L., Johnson K.A., Donahue L.R., Teed A.M., Antonellis K., Bronson R.T., Lerner T.J. & MacDonald M.E. (2002) Cln3(Deltaex7/8) knock-in mice with the common JNCL mutation exhibit progressive neurologic disease that begins before birth. *Hum Mol Genet* **11**, 2709-21.

Cousin M.A. & Nicholls D.G. (1997) Synaptic vesicle recycling in cultured cerebellar granule cells: role of vesicular acidification and refilling. *J Neurochem* **69**, 1927-35.

Creese I., Burt D.R. & Snyder S.H. (1976) Dopamine receptor binding predicts clinical and pharmacological potencies of antischizophrenic drugs. *Science* **192**, 481-3.

Croopnick J.B., Choi H.C. & Mueller D.M. (1998) The subcellular location of the yeast Saccharomyces cerevisiae homologue of the protein defective in the juvenile form of Batten disease. *Biochem Biophys Res Commun* **250**, 335-41.

Cui S.H., Tanabe F., Terunuma H., Iwatani Y., Nunoi H., Agematsu K., Komiyama A., Nomura A., Hara T., Onodera T., Iwata T. & Ito M. (2001) A thiol proteinase inhibitor, E-64-d, corrects the abnormalities in concanavalin A cap formation and the lysosomal enzyme activity in leucocytes from patients with Chediak-Higashi syndrome by reversing the down-regulated protein kinase C activity. *Clin Exp Immunol* **125**, 283-90.

Cyert M.S. (2003) Calcineurin signaling in Saccharomyces cerevisiae: how yeast go crazy in response to stress. *Biochemical and Biophysical Research Communications* **311**, 1143-50.

Dannenberg A. & Zakim D. (1988) Effects of prochlorperazine on the function of integral membrane proteins. *Biochem Pharmacol* **37**, 1259-62.

Das A.K., Becerra C.H., Yi W., Lu J.Y., Siakotos A.N., Wisniewski K.E. & Hofmann S.L. (1998) Molecular genetics of palmitoyl-protein thioesterase deficiency in the U.S. *J Clin Invest* **102**, 361-70.

de Voer G., Jansen G., van Ommen G.-J.B., Peters D.J.M. & Taschner P.E.M. (2001) *Caenorhabditis elegans* homologues of the *CLN3* gene, mutated in juvenile neuronal ceroid lipofuscinosis. *European Journal of Paediatric Neurology* **5 SupplA**, 115-20.

Demirbas D., Wyman A.R., Shimizu-Albergine M., Cakici O., Beavo J.A. & Hoffman C.S. (2013) A yeast-based chemical screen identifies a PDE inhibitor that elevates steroidogenesis in mouse Leydig cells via PDE8 and PDE4 inhibition. *PLoS One* **8**, e71279.

Denis V. & Cyert M.S. (2002) Internal Ca(2+) release in yeast is triggered by hypertonic shock and mediated by a TRP channel homologue. *J Cell Biol* **156**, 29-34.

Dhar S., Bitting R.L., Rylova S.N., Jansen P.J., Lockhart E., Koeberl D.D., Amalfitano A. & Boustany R.M. (2002) Flupirtine blocks apoptosis in batten patient lymphoblasts and in human postmitotic CLN3- and CLN2-deficient neurons. *Ann Neurol* **51**, 448-66.

Duchen M.R., Verkhratsky A. & Muallem S. (2008) Mitochondria and calcium in health and disease. *Cell Calcium* **44**, 1-5.

Eliason S.L., Stein C.S., Mao Q., Tecedor L., Ding S.L., Gaines D.M. & Davidson B.L. (2007) A knock-in reporter model of Batten disease. *J Neurosci* **27**, 9826-34.

Ezaki J., Takeda-Ezaki M., Koike M., Ohsawa Y., Taka H., Mineki R., Murayama K., Uchiyama Y., Ueno T. & Kominami E. (2003) Characterization of Cln3p, the gene product responsible for juvenile neuronal ceroid lipofuscinosis, as a lysosomal integral membrane glycoprotein. *J Neurochem* **87**, 1296-308.

Ezaki J., Takeda-Ezaki M., Oda K. & Kominami E. (2000) Characterization of endopeptidase activity of tripeptidyl peptidase-I/CLN2 protein which is deficient

in classical late infantile neuronal ceroid lipofuscinosis. *Biochem Biophys Res Commun* **268**, 904-8.

Faigle W., Raposo G., Tenza D., Pinet V., Vogt A.B., Kropshofer H., Fischer A., de Saint-Basile G. & Amigorena S. (1998) Deficient peptide loading and MHC class II endosomal sorting in a human genetic immunodeficiency disease: the Chediak-Higashi syndrome. *J Cell Biol* **141**, 1121-34.

Ferreira P., Martinez-Julvez M. & Medina M. (2014) Electron transferases. *Methods Mol Biol* **1146**, 79-94.

Fiebich B.L., Biber K., Gyufko K., Berger M., Bauer J. & van Calker D. (1996) Adenosine A2b receptors mediate an increase in interleukin (IL)-6 mRNA and IL-6 protein synthesis in human astroglioma cells. *J Neurochem* **66**, 1426-31.

Forsburg S.L. & Rhind N. (2006) Basic methods for fission yeast. *Yeast* **23**, 173-83.

Fossale E., Wolf P., Espinola J.A., Lubicz-Nawrocka T., Teed A.M., Gao H., Rigamonti D., Cattaneo E., MacDonald M.E. & Cotman S.L. (2004) Membrane trafficking and mitochondrial abnormalities precede subunit c deposition in a cerebellar cell model of juvenile neuronal ceroid lipofuscinosis. *BMC Neurosci* **5**, 57.

Funabiki H., Kumada K. & Yanagida M. (1996) Fission yeast Cut1 and Cut2 are essential for sister chromatid separation, concentrate along the metaphase spindle and form large complexes. *EMBO J* **15**, 6617-28.

Gachet Y., Codlin S., Hyams J.S. & Mole S.E. (2005) btn1, the Schizosaccharomyces pombe homologue of the human Batten disease gene CLN3, regulates vacuole homeostasis. *J Cell Sci* **118**, 5525-36.

Gao H., Boustany R.M., Espinola J.A., Cotman S.L., Srinidhi L., Antonellis K.A., Gillis T., Qin X., Liu S., Donahue L.R., Bronson R.T., Faust J.R., Stout D., Haines J.L., Lerner T.J. & MacDonald M.E. (2002) Mutations in a novel CLN6-encoded transmembrane protein cause variant neuronal ceroid lipofuscinosis in man and mouse. *Am J Hum Genet* **70**, 324-35.

Getty A., Kovacs A.D., Lengyel-Nelson T., Cardillo A., Hof C., Chan C.H. & Pearce D.A. (2013) Osmotic stress changes the expression and subcellular localization of the Batten disease protein CLN3. *PLoS One* **8**, e66203.

Getty A.L., Benedict J.W. & Pearce D.A. (2011) A novel interaction of CLN3 with nonmuscle myosin-IIB and defects in cell motility of Cln3(-/-) cells. *Exp Cell Res* **317**, 51-69.

Ghelardini C., Galeotti N., Uslenghi C., Grazioli I. & Bartolini A. (2004) Prochlorperazine induces central antinociception mediated by the muscarinic system. *Pharmacol Res* **50**, 351-8.

Gieselmann V. (2006) Cellular pathophysiology of lysosomal storage diseases. In: *Fabry Disease: Perspectives from 5 Years of FOS* (eds. by Mehta A, Beck M & Sunder-Plassmann G). Oxford PharmaGenesis, Oxford.

Goebel H.H. & Lake B.D. (1998) Lysosomal and peroxisomal disorders. Recent advances: introduction. *Brain Pathol* **8**, 73-8.

Golabek A.A., Kida E., Walus M., Kaczmarski W., Michalewski M. & Wisniewski K.E. (2000) CLN3 protein regulates lysosomal pH and alters intracellular processing of Alzheimer's amyloid-beta protein precursor and cathepsin D in human cells. *Mol Genet Metab* **70**, 203-13.

Gottlob I., Leipert K.P., Kohlschutter A. & Goebel H.H. (1988) Electrophysiological findings of neuronal ceroid lipofuscinosis in heterozygotes. *Graefes Arch Clin Exp Ophthalmol* **226**, 516-21.

Haines R.L., Codlin S. & Mole S.E. (2009) The fission yeast model for the lysosomal storage disorder Batten disease predicts disease severity caused by mutations in CLN3. *Dis Model Mech* **2**, 84-92.

Haltia M. (2006) The neuronal ceroid-lipofuscinoses: from past to present. *Biochim Biophys Acta* **1762**, 850-6.

Haltia M., Rapola J., Santavuori P. & Keranen A. (1973) Infantile type of so-called neuronal ceroid-lipofuscinosis. 2. Morphological and biochemical studies. *J Neurol Sci* **18**, 269-85.

Hannaford J., Guo H. & Chen X. (2013) Involvement of cathepsins B and L in inflammation and cholesterol trafficking protein NPC2 secretion in macrophages. *Obesity (Silver Spring)* **21**, 1586-95.

Hashida S., Towatari T., Kominami E. & Katunuma N. (1980) Inhibitions by E-64 derivatives of rat liver cathepsin B and cathepsin L in vitro and in vivo. *J Biochem* **88**, 1805-11.

Haskell R.E., Carr C.J., Pearce D.A., Bennett M.J. & Davidson B.L. (2000) Batten disease: evaluation of CLN3 mutations on protein localization and function. *Hum Mol Genet* **9**, 735-44.

He Y., Sugiura R., Ma Y., Kita A., Deng L., Takegawa K., Matsuoka K., Shuntoh H. & Kuno T. (2006) Genetic and functional interaction between Ryh1 and Ypt3: two Rab GTPases that function in S. pombe secretory pathway. *Genes Cells* **11**, 207-21.

Hedges S.B. (2002) The origin and evolution of model organisms. *Nat Rev Genet* **3**, 838-49.

Heizmann C.W. & Braun K. (1992) Changes in Ca(2+)-binding proteins in human neurodegenerative disorders. *Trends Neurosci* **15**, 259-64.

Hempel C., Norenberg W., Sobottka H., Urban N., Nicke A., Fischer W. & Schaefer M. (2013) The phenothiazine-class antipsychotic drugs prochlorperazine and trifluoperazine are potent allosteric modulators of the human P2X7 receptor. *Neuropharmacology* **75**, 365-79.

Herva R., Tyynela J., Hirvasniemi A., Syrjakallio-Ylitalo M. & Haltia M. (2000) Northern epilepsy: a novel form of neuronal ceroid-lipofuscinosis. *Brain Pathol* **10**, 215-22.

Higashi O. (1954) Congenital gigantism of peroxidase granules; the first case ever reported of qualitative abnormity of peroxidase. *Tohoku J Exp Med* **59**, 315-32.

Higgins M.E., Davies J.P., Chen F.W. & Ioannou Y.A. (1999) Niemann-Pick C1 is a late endosome-resident protein that transiently associates with lysosomes and the trans-Golgi network. *Mol Genet Metab* **68**, 1-13.

Hirayama S., Sugiura R., Lu Y., Maeda T., Kawagishi K., Yokoyama M., Tohda H., Giga-Hama Y., Shuntoh H. & Kuno T. (2003) Zinc finger protein Prz1 regulates Ca2+ but not Cl- homeostasis in fission yeast. Identification of distinct branches of calcineurin signaling pathway in fission yeast. *J Biol Chem* **278**, 18078-84.

Hobert J.A. & Dawson G. (2007) A novel role of the Batten disease gene CLN3: association with BMP synthesis. *Biochem Biophys Res Commun* **358**, 111-6.

Holland P., Torgersen M.L., Sandvig K. & Simonsen A. (2014) LYST Affects Lysosome Size and Quantity, but not Trafficking or Degradation Through Autophagy or Endocytosis. *Traffic*.

Holopainen J.M., Saarikoski J., Kinnunen P.K. & Jarvela I. (2001) Elevated lysosomal pH in neuronal ceroid lipofuscinoses (NCLs). *Eur J Biochem* **268**, 5851-6.

Hoon S., St Onge R.P., Giaever G. & Nislow C. (2008) Yeast chemical genomics and drug discovery: an update. *Trends Pharmacol Sci* **29**, 499-504.

Howitz K.T., Bitterman K.J., Cohen H.Y., Lamming D.W., Lavu S., Wood J.G., Zipkin R.E., Chung P., Kisielewski A., Zhang L.L., Scherer B. & Sinclair D.A. (2003) Small molecule activators of sirtuins extend Saccharomyces cerevisiae lifespan. *Nature* **425**, 191-6.

Hu J., Lu J.Y., Wong A.M., Hynan L.S., Birnbaum S.G., Yilmaz D.S., Streit B.M., Lenartowicz E.M., Thompson T.C., Cooper J.D. & Hofmann S.L. (2012) Intravenous high-dose enzyme replacement therapy with recombinant palmitoyl-protein thioesterase reduces visceral lysosomal storage and modestly prolongs survival in a preclinical mouse model of infantile neuronal ceroid lipofuscinosis. *Mol Genet Metab* **107**, 213-21.

Iguchi-Hashimoto M., Usui T., Yoshifuji H., Shimizu M., Kobayashi S., Ito Y., Murakami K., Shiomi A., Yukawa N., Kawabata D., Nojima T., Ohmura K., Fujii T. & Mimori T. (2011) Overexpression of a minimal domain of calpastatin suppresses IL-6 production and Th17 development via reduced NF-kappaB and increased STAT5 signals. *PLoS One* **6**, e27020.

Ikai N., Nakazawa N., Hayashi T. & Yanagida M. (2011) The reverse, but coordinated, roles of Tor2 (TORC1) and Tor1 (TORC2) kinases for growth, cell cycle and separase-mediated mitosis in Schizosaccharomyces pombe. *Open Biol* **1**, 110007.

Ikeda K., Morigasaki S., Tatebe H., Tamanoi F. & Shiozaki K. (2008) Fission yeast TOR complex 2 activates the AGC-family Gad8 kinase essential for stress resistance and cell cycle control. *Cell Cycle* **7**, 358-64.

Imai Y. & Yamamoto M. (1992) Schizosaccharomyces pombe sxa1+ and sxa2+ encode putative proteases involved in the mating response. *Mol Cell Biol* **12**, 1827-34.

Ioannou Y.A. (2000) The structure and function of the Niemann-Pick C1 protein. *Mol Genet Metab* **71**, 175-81.

Ishidoh K., Takeda-Ezaki M., Watanabe S., Sato N., Aihara M., Imagawa K., Kikuchi M. & Kominami E. (1999) Analysis of where and which types of proteinases participate in lysosomal proteinase processing using bafilomycin A1 and Helicobacter pylori Vac A toxin. *J Biochem* **125**, 770-9.

Isosomppi J., Vesa J., Jalanko A. & Peltonen L. (2002) Lysosomal localization of the neuronal ceroid lipofuscinosis CLN5 protein. *Hum Mol Genet* **11**, 885-91.

Ito M., Sato A., Tanabe F., Ishida E., Takami Y. & Shigeta S. (1989) The thiol proteinase inhibitors improve the abnormal rapid down-regulation of protein kinase C and the impaired natural killer cell activity in (Chediak-Higashi syndrome) beige mouse. *Biochem Biophys Res Commun* **160**, 433-40.

Iwaki T., Goa T., Tanaka N. & Takegawa K. (2004) Characterization of Schizosaccharomyces pombe mutants defective in vacuolar acidification and protein sorting. *Mol Genet Genomics* **271**, 197-207.

Järvelä I., Lehtovirta M., Tikkanen R., Kyttala A. & Jalanko A. (1999) Defective intracellular transport of CLN3 is the molecular basis of Batten disease (JNCL). *Hum Mol Genet* **8**, 1091-8.

Järvelä I., Sainio M., Rantamaki T., Olkkonen V.M., Carpen O., Peltonen L. & Jalanko A. (1998) Biosynthesis and intracellular targeting of the CLN3 protein defective in Batten disease. *Hum Mol Genet* **7**, 85-90.

Jeyakumar M., Dwek R.A., Butters T.D. & Platt F.M. (2005) Storage solutions: treating lysosomal disorders of the brain. *Nat Rev Neurosci* **6**, 713-25.

Jiang X. & Yeung R.S. (2006) Regulation of microtubule-dependent protein transport by the TSC2/mammalian target of rapamycin pathway. *Cancer Res* **66**, 5258-69.

Josephson S.A., Schmidt R.E., Millsap P., McManus D.Q. & Morris J.C. (2001) Autosomal dominant Kufs' disease: a cause of early onset dementia. *J Neurol Sci* **188**, 51-60.

Ju W., Zhong R., Moore S., Moroziewicz D., Currie J.R., Parfrey P., Brown W.T. & Zhong N. (2002) Identification of novel CLN2 mutations shows Canadian specific NCL2 alleles. *J Med Genet* **39**, 822-5.

Kalviainen R., Eriksson K., Losekoot M., Sorri I., Harvima I., Santavuori P., Jarvela I., Autti T., Vanninen R., Salmenpera T. & van Diggelen O.P. (2007) Juvenile-

onset neuronal ceroid lipofuscinosis with infantile CLN1 mutation and palmitoyl-protein thioesterase deficiency. *Eur J Neurol* **14**, 369-72.

Kama R., Kanneganti V., Ungermann C. & Gerst J.E. (2011) The yeast Batten disease orthologue Btn1 controls endosome-Golgi retrograde transport via SNARE assembly. *J Cell Biol* **195**, 203-15.

Kama R., Robinson M. & Gerst J.E. (2007) Btn2, a Hook1 ortholog and potential Batten disease-related protein, mediates late endosome-Golgi protein sorting in yeast. *Mol Cell Biol* **27**, 605-21.

Kaplan J., De Domenico I. & Ward D.M. (2008) Chediak-Higashi syndrome. *Curr Opin Hematol* **15**, 22-9.

Karim M.A., Nagle D.L., Kandil H.H., Burger J., Moore K.J. & Spritz R.A. (1997) Mutations in the Chediak-Higashi syndrome gene (CHS1) indicate requirement for the complete 3801 amino acid CHS protein. *Hum Mol Genet* **6**, 1087-9.

Karim M.A., Suzuki K., Fukai K., Oh J., Nagle D.L., Moore K.J., Barbosa E., Falik-Borenstein T., Filipovich A., Ishida Y., Kivrikko S., Klein C., Kreuz F., Levin A., Miyajima H., Regueiro J., Russo C., Uyama E., Vierimaa O. & Spritz R.A. (2002) Apparent genotype-phenotype correlation in childhood, adolescent, and adult Chediak-Higashi syndrome. *Am J Med Genet* **108**, 16-22.

Katunuma N. & Kominami E. (1995) Structure, properties, mechanisms, and assays of cysteine protease inhibitors: cystatins and E-64 derivatives. *Methods Enzymol* **251**, 382-97.

Katz M.L., Gao C.L., Prabhakaram M., Shibuya H., Liu P.C. & Johnson G.S. (1997) Immunochemical localization of the Batten disease (CLN3) protein in retina. *Invest Ophthalmol Vis Sci* **38**, 2375-86.

Katz M.L., Khan S., Awano T., Shahid S.A., Siakotos A.N. & Johnson G.S. (2005) A mutation in the CLN8 gene in English Setter dogs with neuronal ceroid-lipofuscinosis. *Biochem Biophys Res Commun* **327**, 541-7.

Katz M.L., Shibuya H., Liu P.C., Kaur S., Gao C.L. & Johnson G.S. (1999) A mouse gene knockout model for juvenile ceroid-lipofuscinosis (Batten disease). *J Neurosci Res* **57**, 551-6.

Kawai M., Nakashima A., Ueno M., Ushimaru T., Aiba K., Doi H. & Uritani M. (2001) Fission yeast tor1 functions in response to various stresses including nitrogen starvation, high osmolarity, and high temperature. *Curr Genet* **39**, 166-74.

Khurana V. & Lindquist S. (2010) Modelling neurodegeneration in Saccharomyces cerevisiae: why cook with baker's yeast? *Nat Rev Neurosci* **11**, 436-49.

Kida E., Kaczmarski W., Golabek A.A., Kaczmarski A., Michalewski M. & Wisniewski K.E. (1999) Analysis of intracellular distribution and trafficking of the CLN3 protein in fusion with the green fluorescent protein in vitro. *Mol Genet Metab* **66**, 265-71.

Kilpatrick G.J., Bunce K.T. & Tyers M.B. (1990) 5-HT3 receptors. *Med Res Rev* **10**, 441-75.

Kim J.Y. & Park I.K. (2000) The flavin coenzymes: a new class of group I intron inhibitors. *Biochim Biophys Acta* **1475**, 61-6.

Kim S.J., Zhang Z., Hitomi E., Lee Y.C. & Mukherjee A.B. (2006) Endoplasmic reticulum stress-induced caspase-4 activation mediates apoptosis and neurodegeneration in INCL. *Hum Mol Genet* **15**, 1826-34.

Kim Y., Ramirez-Montealegre D. & Pearce D.A. (2003) A role in vacuolar arginine transport for yeast Btn1p and for human CLN3, the protein defective in Batten disease. *Proc Natl Acad Sci U S A* **100**, 15458-62.

Kiselyov K., Yamaguchi S., Lyons C.W. & Muallem S. (2010) Aberrant Ca2+ handling in lysosomal storage disorders. *Cell Calcium* **47**, 103-11.

Kita A., Sugiura R., Shoji H., He Y., Deng L., Lu Y., Sio S.O., Takegawa K., Sakaue M., Shuntoh H. & Kuno T. (2004) Loss of Apm1, the micro1 subunit of the clathrin-associated adaptor-protein-1 complex, causes distinct phenotypes and synthetic lethality with calcineurin deletion in fission yeast. *Mol Biol Cell* **15**, 2920-31.

Kitaguchi T., Wisniewski K.E., Maslinski S., Maslinska D., Wisniewski T.M. & Kim K.S. (1990) Beta-protein immunoreactivity in brains of patients with neuronal ceroid lipofuscinosis: ultrastructural and biochemical demonstration. *Neurosci Lett* **112**, 155-60.

Kitzmuller C., Haines R.L., Codlin S., Cutler D.F. & Mole S.E. (2008) A function retained by the common mutant CLN3 protein is responsible for the late onset of juvenile neuronal ceroid lipofuscinosis. *Hum Mol Genet* **17**, 303-12.

Klee C.B., Crouch T.H. & Krinks M.H. (1979) Calcineurin: a calcium- and calmodulin-binding protein of the nervous system. *Proc Natl Acad Sci U S A* **76**, 6270-3.

Klionsky D.J., Herman P.K. & Emr S.D. (1990) The fungal vacuole: composition, function, and biogenesis. *Microbiol Rev* **54**, 266-92.

Ko D.C., Binkley J., Sidow A. & Scott M.P. (2003) The integrity of a cholesterol-binding pocket in Niemann-Pick C2 protein is necessary to control lysosome cholesterol levels. *Proc Natl Acad Sci U S A* **100**, 2518-25.

Kohan R., Cismondi I.A., Oller-Ramirez A.M., Guelbert N., Anzolini T.V., Alonso G., Mole S.E., de Kremer D.R. & de Halac N.I. (2011) Therapeutic approaches to the challenge of neuronal ceroid lipofuscinoses. *Curr Pharm Biotechnol* **12**, 867-83.

Koike M., Nakanishi H., Saftig P., Ezaki J., Isahara K., Ohsawa Y., Schulz-Schaeffer W., Watanabe T., Waguri S., Kametaka S., Shibata M., Yamamoto K., Kominami E., Peters C., von Figura K. & Uchiyama Y. (2000) Cathepsin D deficiency induces lysosomal storage with ceroid lipofuscin in mouse CNS neurons. *J Neurosci* **20**, 6898-906.

Komatsu K., Inazuki K., Hosoya J. & Satoh S. (1986) Beneficial effect of new thiol protease inhibitors, epoxide derivatives, on dystrophic mice. *Exp Neurol* **91**, 23-9.

Korey C.A. & MacDonald M.E. (2003) An over-expression system for characterizing Ppt1 function in Drosophila. *BMC Neurosci* **4**, 30.

Kouranti I., McLean J.R., Feoktistova A., Liang P., Johnson A.E., Roberts-Galbraith R.H. & Gould K.L. (2010) A global census of fission yeast deubiquitinating enzyme localization and interaction networks reveals distinct compartmentalization profiles and overlapping functions in endocytosis and polarity. *PLoS Biol* **8**.

Kousi M., Lehesjoki A.E. & Mole S.E. (2012) Update of the mutation spectrum and clinical correlations of over 360 mutations in eight genes that underlie the neuronal ceroid lipofuscinoses. *Hum Mutat* **33**, 42-63.

Kousi M., Siintola E., Dvorakova L., Vlaskova H., Turnbull J., Topcu M., Yuksel D., Gokben S., Minassian B.A., Elleder M., Mole S.E. & Lehesjoki A.E. (2009) Mutations in CLN7/MFSD8 are a common cause of variant late-infantile neuronal ceroid lipofuscinosis. *Brain* **132**, 810-9.

Kramer H. & Phistry M. (1996) Mutations in the Drosophila hook gene inhibit endocytosis of the boss transmembrane ligand into multivesicular bodies. *J Cell Biol* **133**, 1205-15.

Kramer H. & Phistry M. (1999) Genetic analysis of hook, a gene required for endocytic trafficking in drosophila. *Genetics* **151**, 675-84.

Kremmidiotis G., Lensink I.L., Bilton R.L., Woollatt E., Chataway T.K., Sutherland G.R. & Callen D.F. (1999) The Batten disease gene product (CLN3p) is a Golgi integral membrane protein. *Hum Mol Genet* **8**, 523-31.

Kyttälä A., Ihrke G., Vesa J., Schell M.J. & Luzio J.P. (2004) Two motifs target Batten disease protein CLN3 to lysosomes in transfected nonneuronal and neuronal cells. *Mol Biol Cell* **15**, 1313-23.

Kyttälä A., Lahtinen U., Braulke T. & Hofmann S.L. (2006) Functional biology of the neuronal ceroid lipofuscinoses (NCL) proteins. *Biochim Biophys Acta* **1762**, 920-33.

Lane S.C., Jolly R.D., Schmechel D.E., Alroy J. & Boustany R.M. (1996) Apoptosis as the mechanism of neurodegeneration in Batten's disease. *J Neurochem* **67**, 677-83.

Larkin H., Ribeiro M.G. & Lavoie C. (2013) Topology and membrane anchoring of the lysosomal storage disease-related protein CLN5. *Hum Mutat* **34**, 1688-97.

Laurent-Matha V., Derocq D., Prebois C., Katunuma N. & Liaudet-Coopman E. (2006) Processing of human cathepsin D is independent of its catalytic function and auto-activation: involvement of cathepsins L and B. *J Biochem* **139**, 363-71.

Lemons R.M. & Thoene J.G. (1991) Mediated calcium transport by isolated human fibroblast lysosomes. *J Biol Chem* **266**, 14378-82.

Liao G., Yao Y., Liu J., Yu Z., Cheung S., Xie A., Liang X. & Bi X. (2007) Cholesterol accumulation is associated with lysosomal dysfunction and autophagic stress in Npc1 -/- mouse brain. *Am J Pathol* **171**, 962-75.

Lloyd-Evans E., Morgan A.J., He X., Smith D.A., Elliot-Smith E., Sillence D.J., Churchill G.C., Schuchman E.H., Galione A. & Platt F.M. (2008) Niemann-Pick disease type C1 is a sphingosine storage disease that causes deregulation of lysosomal calcium. *Nat Med* **14**, 1247-55.

Lloyd-Evans E. & Platt F.M. (2011) Lysosomal Ca(2+) homeostasis: role in pathogenesis of lysosomal storage diseases. *Cell Calcium* **50**, 200-5.

Lojewski X., Staropoli J.F., Biswas-Legrand S., Simas A.M., Haliw L., Selig M.K., Coppel S.H., Goss K.A., Petcherski A., Chandrachud U., Sheridan S.D., Lucente D., Sims K.B., Gusella J.F., Sondhi D., Crystal R.G., Reinhardt P., Sterneckert J., Scholer H., Haggarty S.J., Storch A., Hermann A. & Cotman S.L. (2014) Human iPSC models of neuronal ceroid lipofuscinosis capture distinct effects of TPP1 and CLN3 mutations on the endocytic pathway. *Hum Mol Genet* **23**, 2005-22.

Lonka L., Kyttala A., Ranta S., Jalanko A. & Lehesjoki A.E. (2000) The neuronal ceroid lipofuscinosis CLN8 membrane protein is a resident of the endoplasmic reticulum. *Hum Mol Genet* **9**, 1691-7.

Low C.P. & Yang H. (2008) Programmed cell death in fission yeast Schizosaccharomyces pombe. *Biochim Biophys Acta* **1783**, 1335-49.

Luiro K., Kopra O., Blom T., Gentile M., Mitchison H.M., Hovatta I., Tornquist K. & Jalanko A. (2006) Batten disease (JNCL) is linked to disturbances in mitochondrial, cytoskeletal, and synaptic compartments. *J Neurosci Res* **84**, 1124-38.

Luiro K., Kopra O., Lehtovirta M. & Jalanko A. (2001) CLN3 protein is targeted to neuronal synapses but excluded from synaptic vesicles: new clues to Batten disease. *Hum Mol Genet* **10**, 2123-31.

Luiro K., Yliannala K., Ahtiainen L., Maunu H., Jarvela I., Kyttala A. & Jalanko A. (2004) Interconnections of CLN3, Hook1 and Rab proteins link Batten disease to defects in the endocytic pathway. *Hum Mol Genet* **13**, 3017-27.

Lummis S.C. & Baker J. (1997) Radioligand binding and photoaffinity labelling studies show a direct interaction of phenothiazines at 5-HT3 receptors. *Neuropharmacology* **36**, 665-70.

Margraf L.R., Boriack R.L., Routheut A.A., Cuppen I., Alhilali L., Bennett C.J. & Bennett M.J. (1999) Tissue expression and subcellular localization of CLN3, the Batten disease protein. *Mol Genet Metab* **66**, 283-9.

Matsumoto K., Mizoue K., Kitamura K., Tse W.C., Huber C.P. & Ishida T. (1999) Structural basis of inhibition of cysteine proteases by E-64 and its derivatives. *Biopolymers* **51**, 99-107.

Melville S.A., Wilson C.L., Chiang C.S., Studdert V.P., Lingaas F. & Wilton A.N. (2005) A mutation in canine CLN5 causes neuronal ceroid lipofuscinosis in Border collie dogs. *Genomics* **86**, 287-94.

Metcalf D.J., Calvi A.A., Seaman M., Mitchison H.M. & Cutler D.F. (2008) Loss of the Batten disease gene CLN3 prevents exit from the TGN of the mannose 6-phosphate receptor. *Traffic* **9**, 1905-14.

Mikawa T., Kanoh J. & Ishikawa F. (2010) Fission yeast Vps1 and Atg8 contribute to oxidative stress resistance. *Genes Cells*.

Mitchison H.M., Bernard D.J., Greene N.D., Cooper J.D., Junaid M.A., Pullarkat R.K., de Vos N., Breuning M.H., Owens J.W., Mobley W.C., Gardiner R.M., Lake B.D., Taschner P.E. & Nussbaum R.L. (1999) Targeted disruption of the Cln3 gene provides a mouse model for Batten disease. The Batten Mouse Model Consortium [corrected]. *Neurobiol Dis* **6**, 321-34.

Mitchison H.M., Hofmann S.L., Becerra C.H., Munroe P.B., Lake B.D., Crow Y.J., Stephenson J.B., Williams R.E., Hofman I.L., Taschner P.E., Martin J.J., Philippart M., Andermann E., Andermann F., Mole S.E., Gardiner R.M. & O'Rawe A.M. (1998) Mutations in the palmitoyl-protein thioesterase gene (PPT; CLN1) causing juvenile neuronal ceroid lipofuscinosis with granular osmiophilic deposits. *Hum Mol Genet* **7**, 291-7.

Mizunuma M., Hirata D., Miyahara K., Tsuchiya E. & Miyakawa T. (1998) Role of calcineurin and Mpk1 in regulating the onset of mitosis in budding yeast. *Nature* **392**, 303-6.

Moertel C.G., Reitemeier R.J. & Gage R.P. (1963) A CONTROLLED CLINICAL EVALUATION OF ANTIEMETIC DRUGS. *Jama* **186**, 116-8.

Mole S.E., Michaux G., Codlin S., Wheeler R.B., Sharp J.D. & Cutler D.F. (2004) CLN6, which is associated with a lysosomal storage disease, is an endoplasmic reticulum protein. *Exp Cell Res* **298**, 399-406.

Mole S.E., Mitchison H.M. & Munroe P.B. (1999) Molecular basis of the neuronal ceroid lipofuscinoses: mutations in CLN1, CLN2, CLN3, and CLN5. *Hum Mutat* **14**, 199-215.

Mole S.E., Williams R.E. & Goebel H.H. (2005) Correlations between genotype, ultrastructural morphology and clinical phenotype in the neuronal ceroid lipofuscinoses. *Neurogenetics* **6**, 107-26.

Mole S.E., Williams R.E. & Goebel H.H. (2011) The neuronal ceroid lipofuscinoses (Batten disease).

Moore S.J., Buckley D.J., MacMillan A., Marshall H.D., Steele L., Ray P.N., Nawaz Z., Baskin B., Frecker M., Carr S.M., Ives E. & Parfrey P.S. (2008) The clinical and

genetic epidemiology of neuronal ceroid lipofuscinosis in Newfoundland. *Clin Genet* **74**, 213-22.

Moreno S., Klar A. & Nurse P. (1991) Molecular genetic analysis of fission yeast Schizosaccharomyces pombe. *Methods Enzymol* **194**, 795-823.

Morimoto M., Tanabe F., Kasai H. & Ito M. (2007) Effect of a thiol proteinase inhibitor, E-64-d, on susceptibility to infection with Staphylococcus aureus in Chediak-Higashi syndrome (beige) mice. *Int Immunopharmacol* **7**, 973-80.

Mulet J.M., Martin D.E., Loewith R. & Hall M.N. (2006) Mutual antagonism of target of rapamycin and calcineurin signaling. *J Biol Chem* **281**, 33000-7.

Munroe P.B., Mitchison H.M., O'Rawe A.M., Anderson J.W., Boustany R.-M., Lerner T.J., Taschner P.E.M., Vos N.d., Breuning M.H., Gardiner R.M. & Mole S.E. (1997) Spectrum of Mutations in the Batten Disease Gene, CLN3. *The American Journal of Human Genetics* **61**, 310-6.

Myllykangas L., Tyynela J., Page-McCaw A., Rubin G.M., Haltia M.J. & Feany M.B. (2005) Cathepsin D-deficient Drosophila recapitulate the key features of neuronal ceroid lipofuscinoses. *Neurobiol Dis* **19**, 194-9.

Narayan S.B., Rakheja D., Pastor J.V., Rosenblatt K., Greene S.R., Yang J., Wolf B.A. & Bennett M.J. (2006a) Over-expression of CLN3P, the Batten disease protein, inhibits PANDER-induced apoptosis in neuroblastoma cells: further evidence that CLN3P has anti-apoptotic properties. *Mol Genet Metab* **88**, 178-83.

Narayan S.B., Rakheja D., Tan L., Pastor J.V. & Bennett M.J. (2006b) CLN3P, the Batten's disease protein, is a novel palmitoyl-protein Delta-9 desaturase. *Ann Neurol* **60**, 570-7.

Naureckiene S., Sleat D.E., Lackland H., Fensom A., Vanier M.T., Wattiaux R., Jadot M. & Lobel P. (2000) Identification of HE1 as the second gene of Niemann-Pick C disease. *Science* **290**, 2298-301.

Nijssen P.C., Brusse E., Leyten A.C., Martin J.J., Teepen J.L. & Roos R.A. (2002) Autosomal dominant adult neuronal ceroid lipofuscinosis: parkinsonism due to both striatal and nigral dysfunction. *Mov Disord* **17**, 482-7.

Norman R.M. & Wood N. (1941) Congenital form of amaurotic family idiocy. *J Neurol Psych* **4**, 175-90.

Noskova L., Stranecky V., Hartmannova H., Pristoupilova A., Baresova V., Ivanek R., Hulkova H., Jahnova H., van der Zee J., Staropoli J.F., Sims K.B., Tyynela J., Van Broeckhoven C., Nijssen P.C., Mole S.E., Elleder M. & Kmoch S. (2011) Mutations in DNAJC5, encoding cysteine-string protein alpha, cause autosomal-dominant adult-onset neuronal ceroid lipofuscinosis. *Am J Hum Genet* **89**, 241-52.

Nugent T., Mole S.E. & Jones D. (2008) The transmembrane topology of Batten disease protein CLN3 determined by consensus computational prediction constrained by experimental data. *FEBS Letters* **582**, 1019-24.

Palmer D.N., Fearnley I.M., Walker J.E., Hall N.A., Lake B.D., Wolfe L.S., Haltia M., Martinus R.D. & Jolly R.D. (1992) Mitochondrial ATP synthase subunit c storage in the ceroid-lipofuscinoses (Batten disease). *Am J Med Genet* **42**, 561-7.

Pao S.S., Paulsen I.T. & Saier M.H., Jr. (1998) Major facilitator superfamily. *Microbiol Mol Biol Rev* **62**, 1-34.

Pearce D.A., Carr C.J., Das B. & Sherman F. (1999a) Phenotypic reversal of the btn1 defects in yeast by chloroquine: a yeast model for Batten disease. *Proc Natl Acad Sci U S A* **96**, 11341-5.

Pearce D.A., Ferea T., Nosel S.A., Das B. & Sherman F. (1999b) Action of BTN1, the yeast orthologue of the gene mutated in Batten disease. *Nat Genet* **22**, 55-8.

Pearce D.A. & Sherman F. (1997) BTN1, a yeast gene corresponding to the human gene responsible for Batten's disease, is not essential for viability, mitochondrial function, or degradation of mitochondrial ATP synthase. *Yeast* **13**, 691-7.

Pearce D.A. & Sherman F. (1998) A yeast model for the study of Batten disease. *Proc Natl Acad Sci U S A* **95**, 6915-8.

Pears M.R., Codlin S., Haines R.L., White I.J., Mortishire-Smith R., Mole S.E. & Griffin J.L. (2010) Deletion of btn1, an orthologue of CLN3, increases glycolysis and perturbs amino acid metabolism in the fission yeast model of Batten disease. *Molecular BioSystems*, 1093-102.

Pei Z., Calmels T.P., Creutz C.E. & Sebti S.M. (1995) Yeast cysteine proteinase gene ycp1 induces resistance to bleomycin in mammalian cells. *Mol Pharmacol* **48**, 676-81.

Pentchev P.G., Comly M.E., Kruth H.S., Vanier M.T., Wenger D.A., Patel S. & Brady R.O. (1985) A defect in cholesterol esterification in Niemann-Pick disease (type C) patients. *Proc Natl Acad Sci U S A* **82**, 8247-51.

Persaud-Sawin D.A., VanDongen A. & Boustany R.M. (2002) Motifs within the CLN3 protein: modulation of cell growth rates and apoptosis. *Hum Mol Genet* **11**, 2129-42.

Petkau T.L., Neal S.J., Milnerwood A., Mew A., Hill A.M., Orban P., Gregg J., Lu G., Feldman H.H., Mackenzie I.R., Raymond L.A. & Leavitt B.R. (2012) Synaptic dysfunction in progranulin-deficient mice. *Neurobiol Dis* **45**, 711-22.

Pilitsis J.G. & Kimelberg H.K. (1998) Adenosine receptor mediated stimulation of intracellular calcium in acutely isolated astrocytes. *Brain Res* **798**, 294-303.

Pohl S., Mitchison H.M., Kohlschutter A., van Diggelen O., Braulke T. & Storch S. (2007) Increased expression of lysosomal acid phosphatase in CLN3-defective cells and mouse brain tissue. *J Neurochem* **103**, 2177-88.

Porter M.Y., Turmaine M. & Mole S.E. (2005) Identification and characterization of Caenorhabditis elegans palmitoyl protein thioesterase1. *J Neurosci Res* **79**, 836-48.

Price A., Seals D., Wickner W. & Ungermann C. (2000) The docking stage of yeast vacuole fusion requires the transfer of proteins from a cis-SNARE complex to a Rab/Ypt protein. *J Cell Biol* **148**, 1231-8.

Pullarkat R.K. & Morris G.N. (1997) Farnesylation of Batten disease CLN3 protein. *Neuropediatrics* **28**, 42-4.

Puranam K.L., Guo W.X., Qian W.H., Nikbakht K. & Boustany R.M. (1999) CLN3 defines a novel antiapoptotic pathway operative in neurodegeneration and mediated by ceramide. *Mol Genet Metab* **66**, 294-308.

Rakheja D., Narayan S.B., Pastor J.V. & Bennett M.J. (2004) CLN3P, the Batten disease protein, localizes to membrane lipid rafts (detergent-resistant membranes). *Biochem Biophys Res Commun* **317**, 988-91.

Ramadan H., Al-Din A.S., Ismail A., Balen F., Varma A., Twomey A., Watts R., Jackson M., Anderson G., Green E. & Mole S.E. (2007) Adult neuronal ceroid lipofuscinosis caused by deficiency in palmitoyl protein thioesterase 1. *Neurology* **68**, 387-8.

Ramirez-Montealegre D. & Pearce D.A. (2005) Defective lysosomal arginine transport in juvenile Batten disease. *Hum Mol Genet* **14**, 3759-73.

Ranta S., Zhang Y., Ross B., Lonka L., Takkunen E., Messer A., Sharp J., Wheeler R., Kusumi K., Mole S., Liu W., Soares M.B., Bonaldo M.F., Hirvasniemi A., de la Chapelle A., Gilliam T.C. & Lehesjoki A.E. (1999) The neuronal ceroid lipofuscinoses in human EPMR and mnd mutant mice are associated with mutations in CLN8. *Nat Genet* **23**, 233-6.

Ratajczak E., Petcherski A., Ramos-Moreno J. & Ruonala M.O. (2014) FRET-assisted determination of CLN3 membrane topology. *PLoS One* **9**, e102593.

Rawlings N.D. & Barrett A.J. (1995) Families of aspartic peptidases, and those of unknown catalytic mechanism. *Methods Enzymol* **248**, 105-20.

Redwood S.M., Liu B.C., Weiss R.E., Hodge D.E. & Droller M.J. (1992) Abrogation of the invasion of human bladder tumor cells by using protease inhibitor(s). *Cancer* **69**, 1212-9.

Robinow C.F. (1977) The Number of Chromosomes in SCHIZOSACCHAROMYCES POMBE: Light Microscopy of Stained Preparations. *Genetics* **87**, 491-7.

Samarel A.M., Ferguson A.G., Decker R.S. & Lesch M. (1989) Effects of cysteine protease inhibitors on rabbit cathepsin D maturation. *Am J Physiol* **257**, C1069-79.

Santavuori P. (1982) Clinical findings in 69 patients with infantile neuronal ceroid lipofuscinosis. In: *Ceroid Lipofuscinoses (Batten disease)* (eds. by Armstrong D, Koppang N & Rider A), pp. 23-34. Elsevier, Amsterdam.

Santavuori P., Haltia M., Rapola J. & Raitta C. (1973) Infantile type of so-called neuronal ceroid-lipofuscinosis. 1. A clinical study of 15 patients. *J Neurol Sci* **18**, 257-67.

Sarin A., Adams D.H. & Henkart P.A. (1993) Protease inhibitors selectively block T cell receptor-triggered programmed cell death in a murine T cell hybridoma and activated peripheral T cells. *J Exp Med* **178**, 1693-700.

Sato A., Tanabe F., Ito M., Ishida E. & Shigeta S. (1990) Thiol proteinase inhibitors reverse the increased protein kinase C down-regulation and concanavalin A cap formation in polymorphonuclear leukocytes from Chediak-Higashi syndrome (beige) mouse. *J Leukoc Biol* **48**, 377-81.

Savukoski M., Klockars T., Holmberg V., Santavuori P., Lander E.S. & Peltonen L. (1998) CLN5, a novel gene encoding a putative transmembrane protein mutated in Finnish variant late infantile neuronal ceroid lipofuscinosis. *Nat Genet* **19**, 286-8.

Schmiedt M.L., Bessa C., Heine C., Ribeiro M.G., Jalanko A. & Kyttala A. (2010) The neuronal ceroid lipofuscinosis protein CLN5: new insights into cellular maturation, transport, and consequences of mutations. *Hum Mutat* **31**, 356-65.

Schultz M.L., Tecedor L., Stein C.S., Stamnes M.A. & Davidson B.L. (2014) CLN3 deficient cells display defects in the ARF1-Cdc42 pathway and actin-dependent events. *PLoS One* **9**, e96647.

Seehafer S.S. & Pearce D.A. (2006) You say lipofuscin, we say ceroid: defining autofluorescent storage material. *Neurobiol Aging* **27**, 576-88.

Settembre C., Zoncu R., Medina D.L., Vetrini F., Erdin S., Erdin S., Huynh T., Ferron M., Karsenty G., Vellard M.C., Facchinetti V., Sabatini D.M. & Ballabio A. (2012) A lysosome-to-nucleus signalling mechanism senses and regulates the lysosome via mTOR and TFEB. *EMBO J* **31**, 1095-108.

Shitamukai A., Hirata D., Sonobe S. & Miyakawa T. (2004) Evidence for antagonistic regulation of cell growth by the calcineurin and high osmolarity glycerol pathways in Saccharomyces cerevisiae. *J Biol Chem* **279**, 3651-61.

Siesjo B.K., Ingvar M. & Wieloch T. (1986) Cellular and molecular events underlying epileptic brain damage. *Ann N Y Acad Sci* **462**, 207-23.

Siintola E., Partanen S., Stromme P., Haapanen A., Haltia M., Maehlen J., Lehesjoki A.E. & Tyynela J. (2006) Cathepsin D deficiency underlies congenital human neuronal ceroid-lipofuscinosis. *Brain* **129**, 1438-45.

Siintola E., Topcu M., Aula N., Lohi H., Minassian B.A., Paterson A.D., Liu X.Q., Wilson C., Lahtinen U., Anttonen A.K. & Lehesjoki A.E. (2007) The novel neuronal ceroid lipofuscinosis gene MFSD8 encodes a putative lysosomal transporter. *Am J Hum Genet* **81**, 136-46.

Siintola E., Topcu M., Kohlschutter A., Salonen T., Joensuu T., Anttonen A.K. & Lehesjoki A.E. (2005) Two novel CLN6 mutations in variant late-infantile neuronal ceroid lipofuscinosis patients of Turkish origin. *Clin Genet* **68**, 167-73.

Simanjuntak Y., Liang J.J., Lee Y.L. & Lin Y.L. (2014) Repurposing of Prochlorperazine for Use Against Dengue Virus Infection. *J Infect Dis*.

Skaper S.D., Debetto P. & Giusti P. (2009) P2X(7) Receptors in Neurological and Cardiovascular Disorders. *Cardiovasc Psychiatry Neurol* **2009**, 861324.

Sleat D.E., Ding L., Wang S., Zhao C., Wang Y., Xin W., Zheng H., Moore D.F., Sims K.B. & Lobel P. (2009) Mass spectrometry-based protein profiling to determine the cause of lysosomal storage diseases of unknown etiology. *Mol Cell Proteomics* **8**, 1708-18.

Sleat D.E., Donnelly R.J., Lackland H., Liu C.G., Sohar I., Pullarkat R.K. & Lobel P. (1997) Association of mutations in a lysosomal protein with classical late-infantile neuronal ceroid lipofuscinosis. *Science* **277**, 1802-5.

Sleat D.E., El-Banna M., Sohar I., Kim K.H., Dobrenis K., Walkley S.U. & Lobel P. (2008) Residual levels of tripeptidyl-peptidase I activity dramatically ameliorate disease in late-infantile neuronal ceroid lipofuscinosis. *Mol Genet Metab* **94**, 222-33.

Sleat D.E., Sohar I., Pullarkat P.S., Lobel P. & Pullarkat R.K. (1998) Specific alterations in levels of mannose 6-phosphorylated glycoproteins in different neuronal ceroid lipofuscinoses. *Biochem J* **334**, 547-51.

Smith K.R., Dahl H.H., Canafoglia L., Andermann E., Damiano J., Morbin M., Bruni A.C., Giaccone G., Cossette P., Saftig P., Grotzinger J., Schwake M., Andermann F., Staropoli J.F., Sims K.B., Mole S.E., Franceschetti S., Alexander N.A., Cooper J.D., Chapman H.A., Carpenter S., Berkovic S.F. & Bahlo M. (2013) Cathepsin F mutations cause Type B Kufs disease, an adult-onset neuronal ceroid lipofuscinosis. *Hum Mol Genet* **22**, 1417-23.

Smith K.R., Damiano J., Franceschetti S., Carpenter S., Canafoglia L., Morbin M., Rossi G., Pareyson D., Mole S.E., Staropoli J.F., Sims K.B., Lewis J., Lin W.L., Dickson D.W., Dahl H.H., Bahlo M. & Berkovic S.F. (2012) Strikingly different clinicopathological phenotypes determined by progranulin-mutation dosage. *Am J Hum Genet* **90**, 1102-7.

Smythe E. & Ayscough K.R. (2006) Actin regulation in endocytosis. *J Cell Sci* **119**, 4589-98.

Sreedharan S.K., Verma C., Caves L.S., Brocklehurst S.M., Gharbia S.E., Shah H.N. & Brocklehurst K. (1996) Demonstration that 1-trans-epoxysuccinyl-L-leucylamido-(4-guanidino) butane (E-64) is one of the most effective low Mr inhibitors of trypsin-catalysed hydrolysis. Characterization by kinetic analysis and by energy minimization and molecular dynamics simulation of the E-64-beta-trypsin complex. *Biochem J* **316 (Pt 3)**, 777-86.

Steinfeld R., Heim P., von Gregory H., Meyer K., Ullrich K., Goebel H.H. & Kohlschutter A. (2002) Late infantile neuronal ceroid lipofuscinosis: quantitative description of the clinical course in patients with CLN2 mutations. *Am J Med Genet* **112**, 347-54.

Steinfeld R., Reinhardt K., Schreiber K., Hillebrand M., Kraetzner R., Bruck W., Saftig P. & Gartner J. (2006) Cathepsin D deficiency is associated with a human neurodegenerative disorder. *Am J Hum Genet* **78**, 988-98.

Steinfeld R., Steinke H.B., Isbrandt D., Kohlschutter A. & Gartner J. (2004) Mutations in classical late infantile neuronal ceroid lipofuscinosis disrupt transport of tripeptidyl-peptidase I to lysosomes. *Hum Mol Genet* **13**, 2483-91.

Storch S., Pohl S., Quitsch A., Falley K. & Braulke T. (2007) C-terminal prenylation of the CLN3 membrane glycoprotein is required for efficient endosomal sorting to lysosomes. *Traffic* **8**, 431-44.

Styrt B., Pollack C.R. & Klempner M.S. (1988) An abnormal calcium uptake pump in Chediak-Higashi neutrophil lysosomes. *J Leukoc Biol* **44**, 130-5.

Su L.J., Auluck P.K., Outeiro T.F., Yeger-Lotem E., Kritzer J.A., Tardiff D.F., Strathearn K.E., Liu F., Cao S., Hamamichi S., Hill K.J., Caldwell K.A., Bell G.W., Fraenkel E., Cooper A.A., Caldwell G.A., McCaffery J.M., Rochet J.C. & Lindquist S. (2010) Compounds from an unbiased chemical screen reverse both ER-to-Golgi trafficking defects and mitochondrial dysfunction in Parkinson's disease models. *Dis Model Mech* **3**, 194-208.

Sugita H., Ishiura S., Suzuki K. & Imahori K. (1980) Inhibition of epoxide derivatives on chicken calcium-activated neutral protease (CANP) in vitro and in vivo. *J Biochem* **87**, 339-41.

Sulzer D., Mosharov E., Talloczy Z., Zucca F.A., Simon J.D. & Zecca L. (2008) Neuronal pigmented autophagic vacuoles: lipofuscin, neuromelanin, and ceroid as macroautophagic responses during aging and disease. *J Neurochem* **106**, 24-36.

Sun L.L., Li M., Suo F., Liu X.M., Shen E.Z., Yang B., Dong M.Q., He W.Z. & Du L.L. (2013) Global analysis of fission yeast mating genes reveals new autophagy factors. *PLoS Genet* **9**, e1003715.

Tammen I., Houweling P.J., Frugier T., Mitchell N.L., Kay G.W., Cavanagh J.A., Cook R.W., Raadsma H.W. & Palmer D.N. (2006) A missense mutation (c.184C>T) in ovine CLN6 causes neuronal ceroid lipofuscinosis in Merino sheep whereas affected South Hampshire sheep have reduced levels of CLN6 mRNA. *Biochim Biophys Acta* **1762**, 898-905.

Tanabe F., Cui S.H. & Ito M. (2000) Abnormal down-regulation of PKC is responsible for giant granule formation in fibroblasts from CHS (beige) mice--a thiol proteinase inhibitor, E-64-d, prevents giant granule formation in beige fibroblasts. *J Leukoc Biol* **67**, 749-55.

Tanabe F., Kasai H., He L., Kin T., Fujikado T., Kumamoto T., Hara T., Iwata T. & Ito M. (2009) Improvement of deficient natural killer activity and delayed bactericidal activity by a thiol proteinase inhibitor, E-64-d, in leukocytes from Chediak-Higashi syndrome patients in vitro. *Int Immunopharmacol* **9**, 366-70.

Tanabe F., Nakajima T. & Ito M. (2013) The thiol proteinase inhibitor E-64-d ameliorates amyloid-beta-induced reduction of sAPPalpha secretion by reversing ceramide-induced protein kinase C down-regulation in SH-SY5Y neuroblastoma cells. *Biochem Biophys Res Commun* **441**, 256-61.

Tanen D.A., Miller S., French T. & Riffenburgh R.H. (2003) Intravenous sodium valproate versus prochlorperazine for the emergency department treatment of acute migraine headaches: a prospective, randomized, double-blind trial. *Ann Emerg Med* **41**, 847-53.

Tatebe H., Morigasaki S., Murayama S., Zeng C.T. & Shiozaki K. (2010) Rab-family GTPase regulates TOR complex 2 signaling in fission yeast. *Curr Biol* **20**, 1975-82.

Tecedor L., Stein C.S., Schultz M.L., Farwanah H., Sandhoff K. & Davidson B.L. (2013) CLN3 loss disturbs membrane microdomain properties and protein transport in brain endothelial cells. *J Neurosci* **33**, 18065-79.

Topçu M., Tan H., Yalnizoglu D., Usubutun A., Saatci I., Aynaci M., Anlar B., Topaloglu H., Turanli G., Kose G. & Aysun S. (2004) Evaluation of 36 patients from Turkey with neuronal ceroid lipofuscinosis: clinical, neurophysiological, neuroradiological and histopathologic studies. *Turk J Pediatr* **46**, 1-10.

Tribouillard-Tanvier D., Beringue V., Desban N., Gug F., Bach S., Voisset C., Galons H., Laude H., Vilette D. & Blondel M. (2008) Antihypertensive drug guanabenz is active in vivo against both yeast and mammalian prions. *PLoS One* **3**, e1981.

Tuxworth R.I., Chen H., Vivancos V., Carvajal N., Huang X. & Tear G. (2011) The Batten disease gene CLN3 is required for the response to oxidative stress. *Hum Mol Genet* **20**, 2037-47.

Tuxworth R.I., Vivancos V., O'Hare M.B. & Tear G. (2009) Interactions between the juvenile Batten disease gene, CLN3, and the Notch and JNK signalling pathways. *Hum Mol Genet* **18**, 667-78.

Tyynelä J., Palmer D.N., Baumann M. & Haltia M. (1993) Storage of saposins A and D in infantile neuronal ceroid-lipofuscinosis. *FEBS Lett* **330**, 8-12.

Tyynelä J., Sohar I., Sleat D.E., Gin R.M., Donnelly R.J., Baumann M., Haltia M. & Lobel P. (2000) A mutation in the ovine cathepsin D gene causes a congenital lysosomal storage disease with profound neurodegeneration. *EMBO J* **19**, 2786-92.

Uusi-Rauva K., Luiro K., Tanhuanpaa K., Kopra O., Martin-Vasallo P., Kyttala A. & Jalanko A. (2008) Novel interactions of CLN3 protein link Batten disease to dysregulation of fodrin-Na+, K+ ATPase complex. *Exp Cell Res* **314**, 2895-905.

Uvebrant P. & Hagberg B. (1997) Neuronal ceroid lipofuscinoses in Scandinavia. Epidemiology and clinical pictures. *Neuropediatrics* **28**, 6-8.

van Diggelen O.P., Keulemans J.L., Kleijer W.J., Thobois S., Tilikete C. & Voznyi Y.V. (2001) Pre- and postnatal enzyme analysis for infantile, late infantile and adult neuronal ceroid lipofuscinosis (CLN1 and CLN2). *Eur J Paediatr Neurol* **5 Suppl A**, 189-92.

Vance J.E. (2006) Lipid imbalance in the neurological disorder, Niemann-Pick C disease. *FEBS Lett* **580**, 5518-24.

Vanier M.T. & Millat G. (2003) Niemann-Pick disease type C. *Clin Genet* **64**, 269-81.

Vantaggiato C., Redaelli F., Falcone S., Perrotta C., Tonelli A., Bondioni S., Morbin M., Riva D., Saletti V., Bonaglia M.C., Giorda R., Bresolin N., Clementi E. & Bassi M.T. (2009) A novel CLN8 mutation in late-infantile-onset neuronal ceroid lipofuscinosis (LINCL) reveals aspects of CLN8 neurobiological function. *Hum Mutat* **30**, 1104-16.

Varughese K.I., Ahmed F.R., Carey P.R., Hasnain S., Huber C.P. & Storer A.C. (1989) Crystal structure of a papain-E-64 complex. *Biochemistry* **28**, 1330-2.

Vellodi A. (2005) Lysosomal storage disorders. *Br J Haematol* **128**, 413-31.

Vesa J., Chin M.H., Oelgeschlager K., Isosomppi J., DellAngelica E.C., Jalanko A. & Peltonen L. (2002) Neuronal ceroid lipofuscinoses are connected at molecular level: interaction of CLN5 protein with CLN2 and CLN3. *Mol Biol Cell* **13**, 2410-20.

Vesa J., Hellsten E., Verkruyse L.A., Camp L.A., Rapola J., Santavuori P., Hofmann S.L. & Peltonen L. (1995) Mutations in the palmitoyl protein thioesterase gene causing infantile neuronal ceroid lipofuscinosis. *Nature* **376**, 584-7.

Vidal-Donet J.M., Carcel-Trullols J., Casanova B., Aguado C. & Knecht E. (2013) Alterations in ROS activity and lysosomal pH account for distinct patterns of macroautophagy in LINCL and JNCL fibroblasts. *PLoS One* **8**, e55526.

Vilaca R., Silva E., Nadais A., Teixeira V., Matmati N., Gaifem J., Hannun Y.A., Sa Miranda M.C. & Costa V. (2014) Sphingolipid signalling mediates mitochondrial dysfunctions and reduced chronological lifespan in the yeast model of Niemann-Pick type C1. *Mol Microbiol* **91**, 438-51.

Vitavska O., Wieczorek H. & Merzendorfer H. (2003) A novel role for subunit C in mediating binding of the H+-V-ATPase to the actin cytoskeleton. *J Biol Chem* **278**, 18499-505.

Vitiello S.P., Wolfe D.M. & Pearce D.A. (2007) Absence of Btn1p in the yeast model for juvenile Batten disease may cause arginine to become toxic to yeast cells. *Hum Mol Genet* **16**, 1007-16.

Wadhawan M., Singh N. & Rathaur S. (2014) Inhibition of cathepsin B by E-64 induces oxidative stress and apoptosis in filarial parasite. *PLoS One* **9**, e93161.

Walenta J.H., Didier A.J., Liu X. & Kramer H. (2001) The Golgi-associated hook3 protein is a member of a novel family of microtubule-binding proteins. *J Cell Biol* **152**, 923-34.

Walkley S.U. (1998) Cellular pathology of lysosomal storage disorders. *Brain Pathol* **8**, 175-93.

Wang F., Wang H., Tuan H.F., Nguyen D.H., Sun V., Keser V., Bowne S.J., Sullivan L.S., Luo H., Zhao L., Wang X., Zaneveld J.E., Salvo J.S., Siddiqui S., Mao L., Wheaton D.K., Birch D.G., Branham K.E., Heckenlively J.R., Wen C., Flagg K., Ferreyra H., Pei J., Khan A., Ren H., Wang K., Lopez I., Qamar R., Zenteno

J.C., Ayala-Ramirez R., Buentello-Volante B., Fu Q., Simpson D.A., Li Y., Sui R., Silvestri G., Daiger S.P., Koenekoop R.K., Zhang K. & Chen R. (2014) Next generation sequencing-based molecular diagnosis of retinitis pigmentosa: identification of a novel genotype-phenotype correlation and clinical refinements. *Hum Genet* **133**, 331-45.

Wang H., Tang X., Liu J., Trautmann S., Balasundaram D., McCollum D. & Balasubramanian M.K. (2002) The multiprotein exocyst complex is essential for cell separation in Schizosaccharomyces pombe. *Mol Biol Cell* **13**, 515-29.

Wang M.L., Motamed M., Infante R.E., Abi-Mosleh L., Kwon H.J., Brown M.S. & Goldstein J.L. (2010) Identification of surface residues on Niemann-Pick C2 essential for hydrophobic handoff of cholesterol to NPC1 in lysosomes. *Cell Metab* **12**, 166-73.

Warnock A., Tan L., Li C., An Haack K., Narayan S.B. & Bennett M.J. (2013) Amlodipine prevents apoptotic cell death by correction of elevated intracellular calcium in a primary neuronal model of Batten disease (CLN3 disease). *Biochem Biophys Res Commun* **436**, 645-9.

Warrier V., Vieira M. & Mole S.E. (2013) Genetic basis and phenotypic correlations of the neuronal ceroid lipofusinoses. *Biochim Biophys Acta* **1832**, 1827-30.

Wheeler R.B., Sharp J.D., Schultz R.A., Joslin J.M., Williams R.E. & Mole S.E. (2002) The gene mutated in variant late-infantile neuronal ceroid lipofuscinosis (CLN6) and in nclf mutant mice encodes a novel predicted transmembrane protein. *Am J Hum Genet* **70**, 537-42.

Wisniewski K.E., Zhong N., Kaczmarski W., Kaczmarski A., Kida E., Brown W.T., Schwarz K.O., Lazzarini A.M., Rubin A.J., Stenroos E.S., Johnson W.G. & Wisniewski T.M. (1998) Compound heterozygous genotype is associated with protracted juvenile neuronal ceroid lipofuscinosis. *Ann Neurol* **43**, 106-10.

Wood V., Gwilliam R., Rajandream M.A., Lyne M., Lyne R., Stewart A., Sgouros J., Peat N., Hayles J., Baker S., Basham D., Bowman S., Brooks K., Brown D., Brown S., Chillingworth T., Churcher C., Collins M., Connor R., Cronin A., Davis P., Feltwell T., Fraser A., Gentles S., Goble A., Hamlin N., Harris D., Hidalgo J., Hodgson G., Holroyd S., Hornsby T., Howarth S., Huckle E.J., Hunt S., Jagels K., James K., Jones L., Jones M., Leather S., McDonald S., McLean J., Mooney P., Moule S., Mungall K., Murphy L., Niblett D., Odell C., Oliver K., O'Neil S., Pearson D., Quail M.A., Rabbinowitsch E., Rutherford K., Rutter S., Saunders D., Seeger K., Sharp S., Skelton J., Simmonds M., Squares R., Squares S., Stevens K., Taylor K., Taylor R.G., Tivey A., Walsh S., Warren T., Whitehead S., Woodward J., Volckaert G., Aert R., Robben J., Grymonprez B., Weltjens I., Vanstreels E., Rieger M., Schafer M., Muller-Auer S., Gabel C., Fuchs M., Dusterhoft A., Fritzc C., Holzer E., Moestl D., Hilbert H., Borzym K., Langer I., Beck A., Lehrach H., Reinhardt R., Pohl T.M., Eger P., Zimmermann W., Wedler H., Wambutt R., Purnelle B., Goffeau A., Cadieu E., Dreano S., Gloux S., Lelaure V., Mottier S., Galibert F., Aves S.J., Xiang Z., Hunt C., Moore K., Hurst S.M., Lucas M., Rochet M., Gaillardin C., Tallada V.A., Garzon A., Thode G., Daga R.R., Cruzado L., Jimenez J., Sanchez M., del Rey F., Benito J., Dominguez A., Revuelta J.L., Moreno S., Armstrong J., Forsburg S.L., Cerutti L., Lowe T., McCombie W.R., Paulsen I., Potashkin J., Shpakovski G.V., Ussery D.,

Barrell B.G. & Nurse P. (2002) The genome sequence of Schizosaccharomyces pombe. *Nature* **415**, 871-80.

Wu D., Liu J., Wu B., Tu B., Zhu W. & Luo J. (2014) The Batten disease gene CLN3 confers resistance to endoplasmic reticulum stress induced by tunicamycin. *Biochem Biophys Res Commun* **447**, 115-20.

Xin W., Mullen T.E., Kiely R., Min J., Feng X., Cao Y., O'Malley L., Shen Y., Chu-Shore C., Mole S.E., Goebel H.H. & Sims K. (2010) CLN5 mutations are frequent in juvenile and late-onset non-Finnish patients with NCL. *Neurology* **74**, 565-71.

Yamagata K., Hakata K., Maeda A., Mochizuki C., Matsufuji H., Chino M. & Yamori Y. (2007) Adenosine induces expression of glial cell line-derived neurotrophic factor (GDNF) in primary rat astrocytes. *Neurosci Res* **59**, 467-74.

Yashiroda Y., Okamoto R., Hatsugai K., Takemoto Y., Goshima N., Saito T., Hamamoto M., Sugimoto Y., Osada H., Seimiya H. & Yoshida M. (2010) A novel yeast cell-based screen identifies flavone as a tankyrase inhibitor. *Biochem Biophys Res Commun* **394**, 569-73.

Yoshida T., Toda T. & Yanagida M. (1994) A calcineurin-like gene ppb1+ in fission yeast: mutant defects in cytokinesis, cell polarity, mating and spindle pole body positioning. *J Cell Sci* **107 (Pt 7)**, 1725-35.

Yoshifuji H., Umehara H., Maruyama H., Itoh M., Tanaka M., Kawabata D., Fujii T. & Mimori T. (2005) Amelioration of experimental arthritis by a calpain-inhibitory compound: regulation of cytokine production by E-64-d in vivo and in vitro. *Int Immunol* **17**, 1327-36.

Yu C.E., Bird T.D., Bekris L.M., Montine T.J., Leverenz J.B., Steinbart E., Galloway N.M., Feldman H., Woltjer R., Miller C.A., Wood E.M., Grossman M., McCluskey L., Clark C.M., Neumann M., Danek A., Galasko D.R., Arnold S.E., Chen-Plotkin A., Karydas A., Miller B.L., Trojanowski J.Q., Lee V.M., Schellenberg G.D. & Van Deerlin V.M. (2010) The spectrum of mutations in progranulin: a collaborative study screening 545 cases of neurodegeneration. *Arch Neurol* **67**, 161-70.

Yu X.H., Jiang N., Yao P.B., Zheng X.L., Cayabyab F.S. & Tang C.K. (2014) NPC1, intracellular cholesterol trafficking and atherosclerosis. *Clin Chim Acta* **429**, 69-75.

Yuasa T., Hayashi T., Ikai N., Katayama T., Aoki K., Obara T., Toyoda Y., Maruyama T., Kitagawa D., Takahashi K., Nagao K., Nakaseko Y. & Yanagida M. (2004) An interactive gene network for securin-separase, condensin, cohesin, Dis1/Mtc1 and histones constructed by mass transformation. *Genes Cells* **9**, 1069-82.